

Distributed-Elementary-Source
Self-regularized Dyadic Green's
Functions for Modeling the Massloading
Effect in Micro-acoustic Devices

Hardik A. Vagh

(Doctor of Philosophy)

2011

RMIT University

Distributed-Elementary-Source
Self-regularized Dyadic Green's
Functions for Modeling the Massloading
Effect in Micro-acoustic Devices

Hardik A. Vagh

M.Sc. (Applied Physics)

August 2011

A thesis submitted in fulfillment of the requirement
for the degree of Doctor of Philosophy

School of Electrical and Computer Engineering

RMIT University

Melbourne, Australia

Declaration

I certify that except where due acknowledgement has been made, the work is that of the author alone; the work has not been submitted previously, in whole or in part, to qualify for any other academic award; the content of the thesis is the result of work which has been carried out since the official commencement date of the approved research program; and, any editorial work, paid or unpaid, carried out by a third party is acknowledged.

Hardik A. Vagh

Acknowledgement

I would like to thank the following people and organizations for their assistance in my research and in writing this thesis:

- My senior supervisor Prof. Alireza Baghai-Wadji for his continual support, advice and constructive feedback during my time with the RMIT University.
- A/Prof. Anthony Holland, Prof. Hashimoto, Dr. Glenn Mathews and Andrew Smith. Specially, Dr. Glenn Mathews and Andrew Smith for their expertise in various modeling techniques and healthy discussion regarding same.
- Australian Research Council (ARC) for the grant: LP0775463.
- Generous support granted by Dr. Glenn Mathews at RMIT University, Dr. Markus Mayer and Dr. Karl Wagner at EPCOS AG (Munich) and Mr. Stephane Chamaly at EPCOS Pty (Singapore) are gratefully appreciated
- Past and present friends for their friendship, advice and enjoyment: Murat,

Mariza, Istique, Paul, Zhe, Roslan, Muhamad and all the Table Tennis players.

- Special thanks to my parents Mr. Amratlal and Mrs. Rashmiben and my sister Mrs. Khushali and her in-law Mr. Sanjay, my extended family as well as all my other friends for their support and encouragement. A heartfelt thanks to my dear wife, Mrs. Harsha Vagh, for her continual support, optimism and understanding during the final stages of this thesis.

Abstract

A Surface-Integral-Modeling technique has been developed to solve time-harmonic boundary value problems in acoustics. The thesis focuses on describing the methodology and testing the consistency of the method. The technique establishes and utilizes the concept of Distributed-Elementary-Source Self-regularized Dyadic Green's functions in order to analyze fully-anisotropic elastic media used in micro-acoustic devices. A given device geometry is divided into rectangular subsections and subsequently detached from the original solid body. The individual subsections are regarded as stand-alone problems and characterized independently. Consecutively, a LIBRARY of precalculated Dyadic Green's Functions is generated for each isolated subsection. The content of the LIBRARY along with the proposed Sufficiency principle and Exhaustion principle, fully suffice to solve arbitrary physically-realizable boundary conditions for a given anisotropic device. A major advantage of precalculating Green's functions is the ability to reduce the usage of computational resources by recycling accurately precomputed numerical data. An additional data compression has been achieved by evaluating

the Green's functions and their spatial derivatives on bounding surfaces of the introduced isolated subsections. The underlying ideas have been explained in terms of four test examples in two- and three-dimensions. The computed results are verified against the results obtained by commercially available Finite Element Simulation package.

Contents

Contents	vii
List of Figures	xv
List of Tables	xxi
1 Introduction	1
1.1 Massloading Effect in SAW-devices	1
1.1.1 Introduction to Modeling of Micro-acoustic Devices: A Brief Literature Review	3
1.2 On the Notions of Self-regularized Dyadic Green's Function Tech- nique	10
1.2.1 Preliminary Considerations	13

1.2.2	Geometrical Discretization and Basic Cuboids	13
1.3	Boundary Value Problems Defining Two Test Cuboid	17
1.3.1	BVP for Test Cuboid I	17
1.3.2	BVP for Test Cuboid II	18
1.4	Outline of the Proposed Solution for Test Cuboid I: Construction of DES SR DGFs	19
1.4.1	Transformation of Functions and Differential Operators from Local to Master Co-ordinate System	20
1.4.2	Basis- and Testing Functions	21
1.4.3	Physics-based Model-Order-Reduction	25
1.5	Outline of the Proposed Solution for the Test Structure II	27
1.5.1	Sufficiency Principle	27
1.5.2	The Principle of Exhaustion	29
1.5.3	Application of the Sufficiency- and Exhaustion Principles	30
1.6	Thesis Organization	34

1.6.1	Chapter 2: Distributed-Elementary-Source Self-regularized Dyadic Green's Functions for Modeling the Massloading Effect in Acoustic Devices: 2D Isotropic Problems . . .	35
1.6.2	Chapter 3: 2D Elastodynamic Simulation of Fully - anisotropic Elastic Media Using Self - regularized Dyadic Greens Functions	35
1.6.3	Chapter 4: 3D Elastodynamic Simulation of An-isotropic/Isotropic Interface Problems in Elastic Media	36
1.7	Computational Platforms Utilized in Numerical Calculations . . .	37
1.8	List of Publications	38
2	Distributed-Elementary-Source Self-regularized Dyadic Green's Functions for Modeling the Massloading Effect in Acoustic Devices: 2D Isotropic Problems	39
2.1	Introduction	39
2.2	Preparatory Considerations	45
2.2.1	Weak-Galerkin Formulation in 3D	45
2.2.2	Partitioning into Quadrangles	50

2.3	Statement of The Problem	51
2.4	Proposed Methodology	52
2.4.1	Weak Galerkin Formulation in 2D	52
2.4.2	Discretization of Eq. (2.16) as Applied to the Master Square	53
2.5	The Concept of Distributed Elementary Sources and $\mathcal{GF}s$	58
2.5.1	Distributed Elementary Sources	58
2.5.2	Proposed $\mathcal{GF}s$ and Solution to Two-port/One-port Inter- face Problem	59
2.6	Results and Discussions	63
2.6.1	Numerical Verification and Comparison with ANSYS: Eigen- value Problem	63
2.6.2	Application of Proposed $\mathcal{GF}s$: Enforced Problem	71
2.7	Conclusion	73
2.8	Appendix	75
2.8.1	Affine Transformation to Master Coordinate System	75

2.8.2	Normalization of Jacobi-Polynomials	76
2.8.3	Construction of Basis Functions	78
3	2D Elastodynamic Simulation of Fully-anisotropic Elastic Media Using Self-regularized Dyadic Greens Functions	83
3.1	Introduction	83
3.2	Statement of the Problem	90
3.3	Construction of the Proposed Distributed-Elementary-Source Self- regularized Dyadic Green's Functions	92
3.3.1	Partitioning of Simulation Domain	92
3.3.2	Governing PDEs and their Equivalent Self-regularized Surface- integral Equations	95
3.3.3	Distributed-Elementary-Sources and the Associated Self- regularized Dyadic Green's Functions	98
3.4	Interpretation and Solution Strategy for Various Boundary Condi- tions	105

3.4.1	Algorithm for Solving Inhomogeneous Neumann Boundary Conditions	106
3.4.2	Algorithm for Solving Inhomogeneous Dirichlet Boundary Conditions	109
3.5	Tearing and connecting subsystems: problem description	112
3.5.1	Solution Algorithm for Interface Problem	116
3.6	Numerical Results and Discussion	120
3.6.1	Verification of Dirichlet Boundary Condition on Test Bound- ary	122
3.6.2	Verification of Solution for Multi-quadrangles	123
3.6.3	Solution of Multi-quadrangle Composite Problems With Varying Material Constitutions	124
3.7	Concluding Remarks	127
4	3D Elastodynamic Simulation of Anisotropic/Isotropic Interface Problems in Elastic Media	131
4.1	Introduction	131

4.2	Theory and Principles Utilized for Tearing and Interconnecting Isotropic and Anisotropic Cuboids	139
4.2.1	Distributed-Elementary-Source Self-regularized Dyadic Green's functions ($\mathcal{G}\mathcal{F}$) versus Dirac delta-function excitation of the media	140
4.3	Statement of the Problem	142
4.3.1	Partitioning a Given Structure into an Adequate Number of Hexahedrons and Problem Description	142
4.3.2	Partitioning into Hexahedrons	143
4.4	Distributed-Elementary-Source Self-regularized Dyadic Green's Func- tions	144
4.4.1	Description of Weak-Galerkin Formulation	144
4.4.2	Discretization of Eq. (4.17)	148
4.4.3	Distributed Elementary Sources and Associated Green's Functions	152

4.4.4	Algorithm for Solving Inhomogeneous Neumann Boundary Conditions: Implementation of Sufficiency- and Exhaustion Principles	157
4.4.5	Construction and Optimization of LIBRARY	159
4.5	Result and Discussion	162
4.5.1	Numerical Comparison with ANSYS: Eigenvalue Problem .	162
4.5.2	Application of Superposition and Exhaustion Principle by Utilizing \mathcal{GF} s: Enforced Problems	165
4.6	Conclusion	171
4.7	Summary	172
	References	177

List of Figures

1.1	A typical artistic view of a SAW device geometry	6
1.2	Example showing the section of the device geometry	8
1.3	Basic Cuboid-I as one-port problems, where springs suggests time harmonistic nature of the problem. The surface attached to the spring should symbolize the distributive nature of sources. The surfaces of the cuboid, where no sources are applied, indicate stress-free boundaries	14
1.4	Basic Cuboid-I and Basic Cuboid-II separated by equivalent forces. The surface attached to the spring should symbolize the distribu- tive nature of sources. The surfaces of the cuboid, where no sources are applied, indicate stress-free boundaries	15
1.5	Example of a system matrix showing the sparseness in the matrix for an isotropic material	23

2.1	Co-ordinate of an arbitrarily-located cuboid with the volume Ω and surfaces S_i^\pm ($i = 1, 2, 3$)	44
2.2	Partitioning the cuboid given in Fig. 2.1 into two hexahedrons “ a ” and “ b ”	48
2.3	A composite 2D structure with a distributed excitation source acting on the bottom surface of quadrangle “ a ,” with the remaining surfaces being stress free	50
2.4	An example showing the separation of the composite structure shown in Fig. 2.3 into two solid bodies by introducing equivalent traction forces on the interface. In this problem body “ a ” is considered as a two-port quadrangle, while body “ b ” is a one-port quadrangle	54
2.5	Distributive Elementary Sources: $b_0(\xi)$ (upper left), $b_1(\xi)$ (lower left), $b_2(\xi)$ (upper right) and $b_3(\xi)$ (lower right)	56
2.6	A comparison between eigenfrequencies obtained by the proposed method and the numerical results obtained by FEM package ANSYS	64
2.7	Displacement $u_1(\xi, \zeta)$, as a response to the force $b_0(\xi)$ acting at $\zeta = -1.0$	65

2.8	Associated stress distribution $T_{31}(\xi, \zeta)$ in response to the force $b_0(\xi)$ acting at $\zeta = -1.0$	66
2.9	Displacement $u_1(\xi, \zeta)$, (in the figure, $v(\xi, \zeta)$) as a response to the force $b_1(\xi)$ acting at $\zeta = -1.0$	67
2.10	Associated stress distribution $T_{31}(\xi, \zeta)$ in response to the force $b_1(\xi)$ acting at $\zeta = -1.0$	68
2.11	Matched displacement $u_1(x, z)$ (in the figure, $v(\xi, \zeta)$) for first DES applied at $z = -1.0$	69
2.12	Corresponding matched stress component $T_{31}(x, z)$ derived from the matched displacement components	70
3.1	A simplified artistic view of typical SAW device geometry	91
3.2	Example showing the cross-section of the device geometry	91
3.3	Discretization of 2D fully-anisotropic test problem	92
3.4	Distributive Elementary Sources: $b_0(x)$ (upper left), $b_1(x)$ (lower left), $b_2(x)$ (upper, right) and $b_3(x)$ (lower right)	101
3.5	Discretization of 2D multi-quadrangle test problem with all the quadrangles exhibiting same material properties	108

3.6	Dirichlet boundary condition solved with the help of principle of Exhaustion and Sufficiency principle utilizing pre-computed \mathcal{GF} s .	113
3.7	Displacement component $u_1(x, z)$ showing interconnection between multi-quadrangles modelled utilizing \mathcal{GF} s	114
3.8	Displacement component u_1 for the model problem solved using ANSYS (a FEM based Software package)	115
3.9	Displacement component $u_3(x, z)$ showing interconnection between multi-quadrangles modelled utilizing \mathcal{GF} s	121
3.10	Displacement component u_3 for the model problem solved using ANSYS (a FEM based Software package)	122
3.11	Fully-anisotropic elastodynamic problem showing interconnection between quadrangles with different types of material properties modelled utilizing proposed \mathcal{GF} s method	125
4.1	A L-shaped joint with interface between anisotropic and isotropic medium	135
4.2	Example showing the partitioning of the L-shaped joint	136
4.3	An arbitrarily located cuboid	139

4.4	A comparison between eigenfrequencies obtained by the proposed method and the numerical results obtained by FEM package ANSYS	151
4.5	Displacement component $u_1(x, y, z)$ for a 3D elastodynamic problem after solving the interface conditions between anisotropic and isotropic cuboids	152
4.6	Displacement component $u_2(x, y, z)$ for a 3D elastodynamic problem after solving the interface conditions between anisotropic and isotropic cuboids	153
4.7	Displacement component $u_3(x, y, z)$ derived for three cuboids and placed side by side after determining the equivalent forces at the interfaces	154
4.8	A complex wall-shaped enclosure structure	163
4.9	Displacement component $u_1(x, y, z)$ for the wall-shaped enclosure computed with the help of proposed \mathcal{GF} s method	164
4.10	Displacement component $u_2(x, y, z)$ for the wall-shaped enclosure computed with the help of proposed \mathcal{GF} s method	165
4.11	Displacement component $u_3(x, y, z)$ for the wall-shaped enclosure computed with the help of proposed \mathcal{GF} s method	166

List of Tables

1.1	Categorization of basic cuboids. The numbers characterizing Basic cuboids depend on the number of sides permitted for exchanging energy with environment	11
2.1	Main Symbols and abbreviations used in the chapter	43
3.1	Main symbols and abbreviations used in this manuscript	87
3.2	On the boundary conditions: interpretation and solution strategy	129
3.3	Materials and its properties utilized in numerical examples	130
4.1	Materials and its properties utilized in numerical examples. The units of ρ and C are 10^3kg/m^3 and 10^{10}N/m^2 respectively	160

Chapter 1

Introduction

1.1 Massloading Effect in SAW-devices

Simulation of the massloading effect continues to be of great interest and paramount significance in micro-acoustic devices community. Efforts in miniaturizing devices, stringent constraints in the design, along with challenges for protecting individual components from the influence of the neighboring elements, have all added substantially to the relevance of the massloading phenomenon. The massloading effect is a major higher order effect. It is a phenomenon which is understood as altering the acoustic impedance of propagating surface- or bulk waves by the mass- and the elasticity property of metallic electrodes. Thereby, waves propagating along the substrate surface, or within the substrate, interact electrically and acoustically with electrodes which are deposited in large numbers on the plane surface of a piezoelectric substrate, before getting scattered into

various types of coupled surface- and bulk waves. Examples for the piezoelectric substrates are LiNbO₃, LiTaO₃ or Quartz, which typically support several hundreds to a few thousands metallic electrodes made of, in majority of cases, aluminium or, in some cases, of much heavier gold. The massloading effect may decisively deteriorate the device performance or be exploited advantageously in signal forming, shaping and processing devices. To account for the massloading effect we need to solve a boundary value problem subject to fairly complex boundary conditions. A routine complexity analysis would reveal that in modern devices the number of unknowns in computations may easily exceed tens of millions. Traditional simulations based on the almighty Finite Element Method (FEM) and the elegant Boundary Element Method (BEM) or a hybridization of both, are quite general tools in terms of the geometry of electrodes, the substrate and their material constitutions. These methods however, lack a most desirable property - the flexibility in producing pre-calculated data, so that the data can be stored in libraries for frequent future usage in device design cycles. Ordinarily, pre-calculating data is regarded to be particularly challenging as stress distributions on the bounding surfaces of the metallic electrodes are not only dependent on various topological and material parameters, but are also strongly frequency-dependent. The pre-calculation of such primary data and storing them for future use, is an important feature of this work. Furthermore, measure for drastically reducing the number of of unknowns and ideas for accelerating computation will be discussed.

1.1.1 Introduction to Modeling of Micro-acoustic Devices: A Brief Literature Review

Since early 70s, many analytical, semi-analytical and numerical techniques have been proposed for the analysis of piezoelectric structural devices. We here mainly limit ourselves to the techniques adopted by ultrasonics community. Modeling and simulation of micro-acoustic devices such as Surface Acoustic Wave (SAW) and Bulk Acoustic Wave (BAW) devices are generally considered to be a challenging task. The complexities in modeling is due to inherent features such as multi-physics phenomena and multi-scale sub-structures. Various methods have been adapted, from a wide range of scientific and engineering fields to solve the involved Boundary Value Problems (BVPs). Most prominent methods are:

- Perturbation Techniques
- Coupling of Modes
- Variational Techniques
- Finite Element Method
- Finite Difference Method
- Boundary Element Method (Method of Moments)
- Combined Finite Element/Boundary Element Method

These techniques have served, in one way or another, the SAW- and BAW community significantly. During late 60's and early 70's the solution strategy was revolving around perturbation analysis, variational techniques, finite difference methods and equivalent circuit types of analysis. Perturbation analysis, being an analytical method, was concerned with small changes in solution, caused due to small changes in physical parameters of the problem. Considering such as minor changes in resonant frequencies or propagation velocities, the perturbation theory was providing satisfactory results [1, 2]. However, in describing major higher-order effects, e.g. the massloading, where the exact solutions are not available, the Perturbation theory fails to impress. This is where variational techniques, being numerical in nature, had upper hand. In the variation techniques, in order to calculate the desired physical quantity, a test or trial solution is estimated providing the minimum error. Such direct approximation techniques of variation calculus have been introduced for the analysis of electroelastic vibration problems [3, 4]. The numerical computation in variation methods is quite involved and rigorous, compared to the Perturbation analysis [1, 5]. The equivalent circuit analysis found its traces in modern Coupling-of-modes, which are utilized for various resonator and SAW filter analysis. Both, equivalent circuit analysis and Coupling-of-modes, have their own advantages and disadvantages [6, 7].

Boundary Element Method and Green's Functions Based Techniques

The Boundary Element Method (BEM) is a method in which the boundary of the region under consideration is sub-divided and then the problem is solved with the help of weighted residual technique; hence being referred to as the 'Boundary Element Method.' Brebbia and Dominguez [8] introduced and discussed the usage of different types of boundary elements, namely constant and linear variation for potential problems. Milsom et. al. [9] applied the method to the coupled electromagnetic and acoustic fields under quasi-static approximation. They were able to analyze SAW transducers with a few electrodes deposited on the plane surface of a piezoelectric semi-space. They included in their analysis generation of bulk waves but neglected all other higher order effects including the mass-loading phenomenon. In most applications of BEM 2D piezoelectric models were considered. This is accomplished by considering electrodes with infinitely long aperture length and thus neglecting transversal effects. The second- and higher-order effects such as massloading, conductivity of electrodes and other effects due to diffraction and scattering of the surface waves were also ignored. The major disadvantage of the method was the amount of computational storage space and time required for solving the involved integrals, and the system of coupled linear equations. However, BEM has only been widely accepted in the SAW community since early 90s.

Generally, considering a semi-infinite of finite substrate, electrical and mechanical

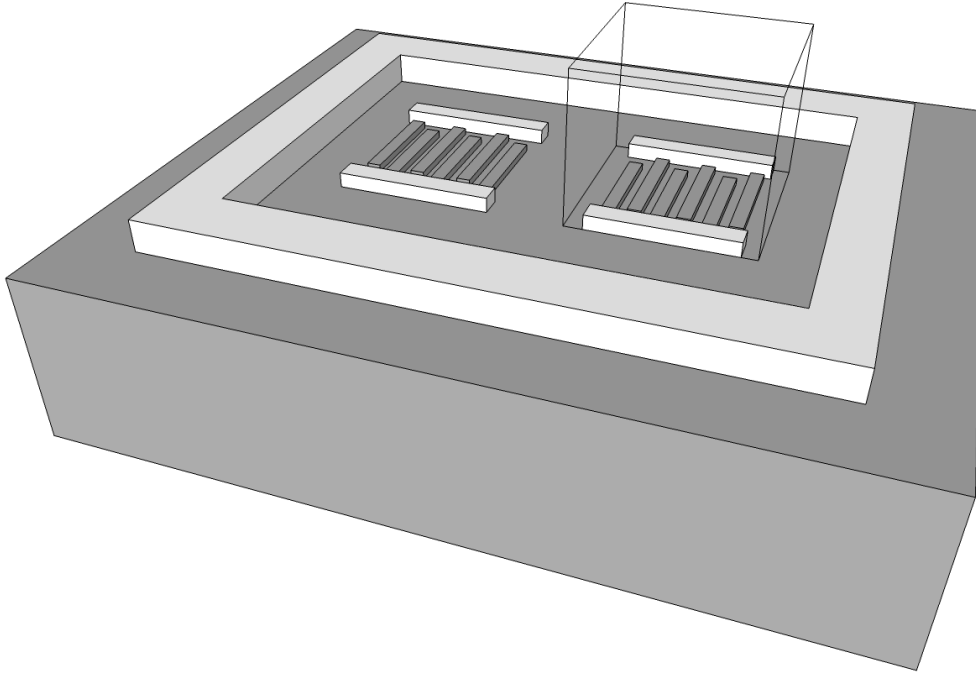


Figure 1.1: A typical artistic view of a SAW device geometry

responses to delta functions type of excitations (point-and line-source charges and forces) are referred to as the (dyadic) Green's function. These Green's functions play a key role in any BEM implementation. In case of electrostatic problems one can solve the problem analytically. However, in general quasi-static piezoelectric problems, under the assumption of harmonic time-dependence ($e^{-j\omega t}$), the Green's functions can only be calculated numerically. Most often the Green's functions constructed under the afore-mentioned delta function excitations possess singularities. Consequently, the double convolution surface integrals, involving the Green's functions as their kernels are as a rule notoriously difficult to calculate numerically. These are but a few reasons why an efficient modeling of wave propagation in SAW devices is highly challenging even in 2D models. Many

proposals have been made for the construction of Green's functions in infinite and semi-infinite media [8, 10, 11, 12]. Mid 80's the SAW community was facing challenges by necessity of accounting of the Bulk Acoustic Waves (BAW) in addition to SAW. The rigorousness and efficiency of the analysis methods in terms of computational time became inevitable as complex-structured devices demanded increasingly higher precision level. Few attempts were made using BEM (or as it is alternatively called Method-of-Moments) along with Green's functions technique and Ritz-Galerkin method to fully account for bulk- surface waves interaction (Wagner & Visintini, Wagner et. al. [13, 14]). Furthermore, the Method-of-Moments (MoM) was applied to model 2D and 3D elemental charge distribution in leaky acoustic wave devices [15]. The paper demonstrated the derivation of spectral-domain Green's functions using Floquet Theorem for characterizing periodic problems. Were, the singularities of Green's functions were isolated and treated separately. The asymptotic behavior of Green's functions are also treated explicitly at infinity and at origin [15, 16, 17]. The massloading has been considered as a higher-order effect, which requires attention due to the technological advances in utilizing different types of electrodes with comparatively larger dimensions to achieve a desired reflectivity and interaction with acoustic fields. A brief survey of the method was presented by Baghai-Wadji and Ringhofer [18], the paper also introduces to the idea which is core to this chapter; the interaction between the two acoustic elements manifests itself through an energy exchange in such a way that the boundary- and interface conditions are satisfied.

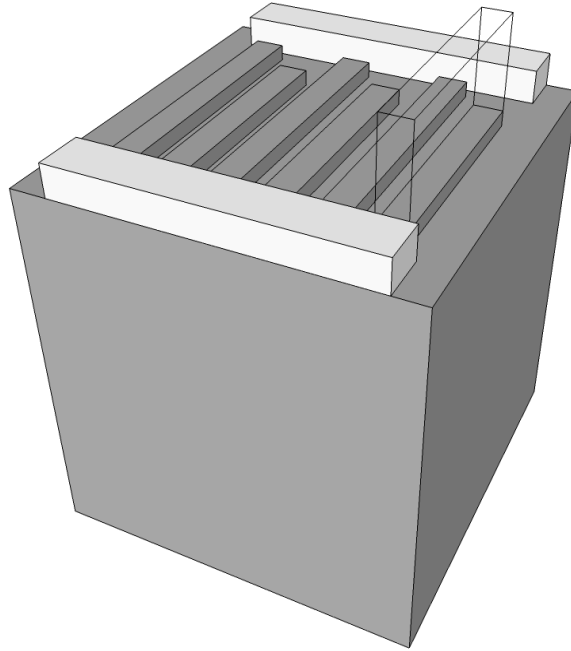


Figure 1.2: Example showing the section of the device geometry

Finite Element Method and Related Advanced Techniques

There are a number of advantages in considering Finite Element Method (FEM) as a primary analysis techniques [19]. The advances of FEM modeling, during the last decade have been presented in [20] and references therein. One of the advantages of the FEM is the capability of handling complex geometries with ease not just in 2D but also in 3D piezoelectric media [21]. However, FEM applied to a realistic model of a complete 3D SAW device is still farfetched. For an accurate analysis of the dominant mode of surface acoustic wave propagation in plate-like finite piezoelectric solids, Wang J. and Jingbo L.[22] has developed a 2D theory utilizing an exponential expansion of displacements and electrical potential in the

thickness direction, essentially, creating a theory similar to popular plate theory of Mindlin [23]. Additionally, in FEM the structural geometry is subdivided or meshed to form finite elements, where the system of coupled equations is solved over each elements and assembled. Generally, increasing the number of these mesh elements increases the accuracy of the total solution. For a typical 3D radio frequency resonator, considering ten elements per wavelengths will blow up the number of discretization necessary to the order of 10^{10} . Handling such enormous number of data is a huge task, even with the current advancements in computational technologies [24]. These concerns forced the analysis to look for other formalisms free from meshing, such as, Mesh-free Methods [25, 26], and Element-free Galerkin Methods [27, 28]. These methods improved the convergence of the solutions. However, the proposed methods were still computationally expensive, which limited the scope of their applicability. Domain Decomposition methods [29, 30], Interface Element Methods [31, 32], Dynamic Substructuring methods [33, 34, 35, 36], Multidomain Spectral Methods [37], were among few other methods, which provide the solutions to the problems in various engineering fields. The central idea of these methods is substructuring the media and solving each sub-domain individually and thus reducing the computational time for each domain. The domains are then assembled using conventional techniques such as Lagrange multiplier, penalty parameter, conservative coupling approach, Moving Least-squares Interpolate Technique [30, 35, 36].

Hybridization of FEM/BEM Techniques

Both FEM and BEM exhibit their own characteristic advantages and disadvantages. Constant efforts have been made to hybridize the two methods such that one can benefit from the advantages of both methods simultaneously. The combination of FEM/BEM is achieved by merging BEM formulation using semi-infinite Green's functions and FEM computation of the mechanical behavior of each metallic electrode [38, 39, 40, 41]. Analysis of the reflectivity of the arbitrarily-shaped electrodes considering the massloading effect was also possible through the combination of periodic Green's functions with simulation of massive electrodes utilizing FEM [38, 42].

1.2 On the Notions of Self-regularized Dyadic Green's Function Technique

There has been numerous attempts in order to circumvent the drawbacks associated with the afore-mentioned methods. While, FEM adapted hybrid versions such as mixed FEM/BEM techniques, BEM is still thriving on various Green's functions techniques. Generally, BEM is considered to be a most powerful analysis technique. However, BEM is accompanied by a number of drawbacks: 1) Problem-specific Green's functions are sought where the underlying integral formulation leads to the singularities, which are not easy to handle. (The Green's

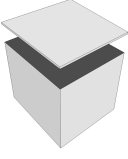


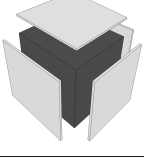
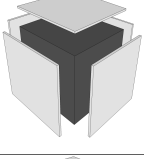
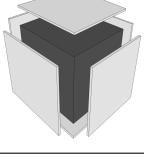
<i>Cuboid type</i>	<i>Name</i>	<i>Type of problem</i>
	Basic cuboid-I	One-port problem
	Basic cuboid-II	Two-port problem
	Basic cuboid-III	Three-port problem
	Basic cuboid-IV	Four-port problem
	Basic cuboid-V	Five-port problem
	Basic cuboid-VI	Six-port problem

Table 1.1: Categorization of basic cuboids. The numbers characterizing Basic cuboids depend on the number of sides permitted for exchanging energy with environment

functions also become singular whilst calculating the interaction of an element on the boundary with itself, self-action.) 2) The numerical calculations of Fourier-type integrals which are oscillating are in general complicated. This is in particular the case when mutual interaction of two nearby elements are computed. 3) In BEM, the system matrices are *dense* as oppose to *banded matrices* appearing in FEM, thus resulting in more computational time in solving the system of equations.

The Self-regularized Dyadic Green's Functions technique proposed in this work makes sure that no singularities arise in computations in the first place. The device geometry is subdivided into appropriate number of cuboids (3D solid figure bounded by six rectangular faces) and then solved individually. For solving each cuboids, employed basis- and test functions, constitute a set of smooth functions. The smoothness property ensures that the derivatives of the analysis-and synthesis functions are smooth and easily calculable. The integrals are derived in closed-form with virtually no additional computational time. The distributed nature of the analyzing- and synthesizing functions results in the fact that there is no singularities in integrands. Furthermore, the associated system matrices involving orthonormal basis functions, are *sparse matrices*, a fact which reduces not only the computational storage space but also the computational time. Details of the proposed technique are presented next by considering 3D one-port and two-port problems.

1.2.1 Preliminary Considerations

The proposed method of Self-regularized Dyadic Green's functions is conceptually a sophisticated process. We shall make a number of assumptions, merely to ease the description of our method. However, we fully take into account the massloading to make the problem relevant to SAW- and BAW device community. We will consider a purely mechanical problem, assuming that the electrodes and all the other sub-structures are mechanically excited by sources which oscillate time harmonically at a given frequency ω . We subdivide the geometry into sections. For each section we construct the Distributed-Elementary-Source (DES) Self-regularized (SR) Dyadic Green's Functions (DGFs), abbreviated as $\mathcal{GF}s$. We assemble the sub-sections following the matching process (solving interface problem). This recipe is introduced further, where we also describe the tools that are core to the $\mathcal{GF}s$ method.

1.2.2 Geometrical Discretization and Basic Cuboids

One of the key features of the proposed Self-regularized Dyadic Green's function method is the way we partition the geometry. Let us consider the geometry of a typical SAW device as shown in Fig. 1.1. The geometry consists of the substrate structure loaded with electrodes and busbars surrounded by absorbing wall structure. Focusing on the section of Fig. 1.1 allows us to narrate the

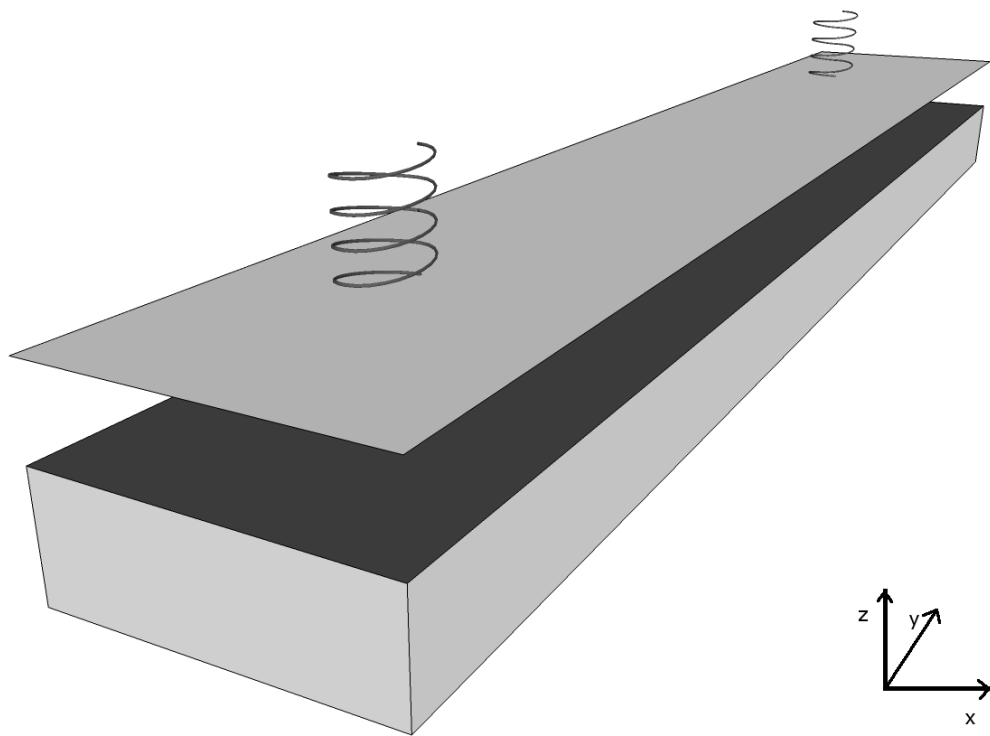


Figure 1.3: Basic Cuboid-I as one-port problems, where springs suggests time harmonic nature of the problem. The surface attached to the spring should symbolize the distributive nature of sources. The surfaces of the cuboid, where no sources are applied, indicate stress-free boundaries

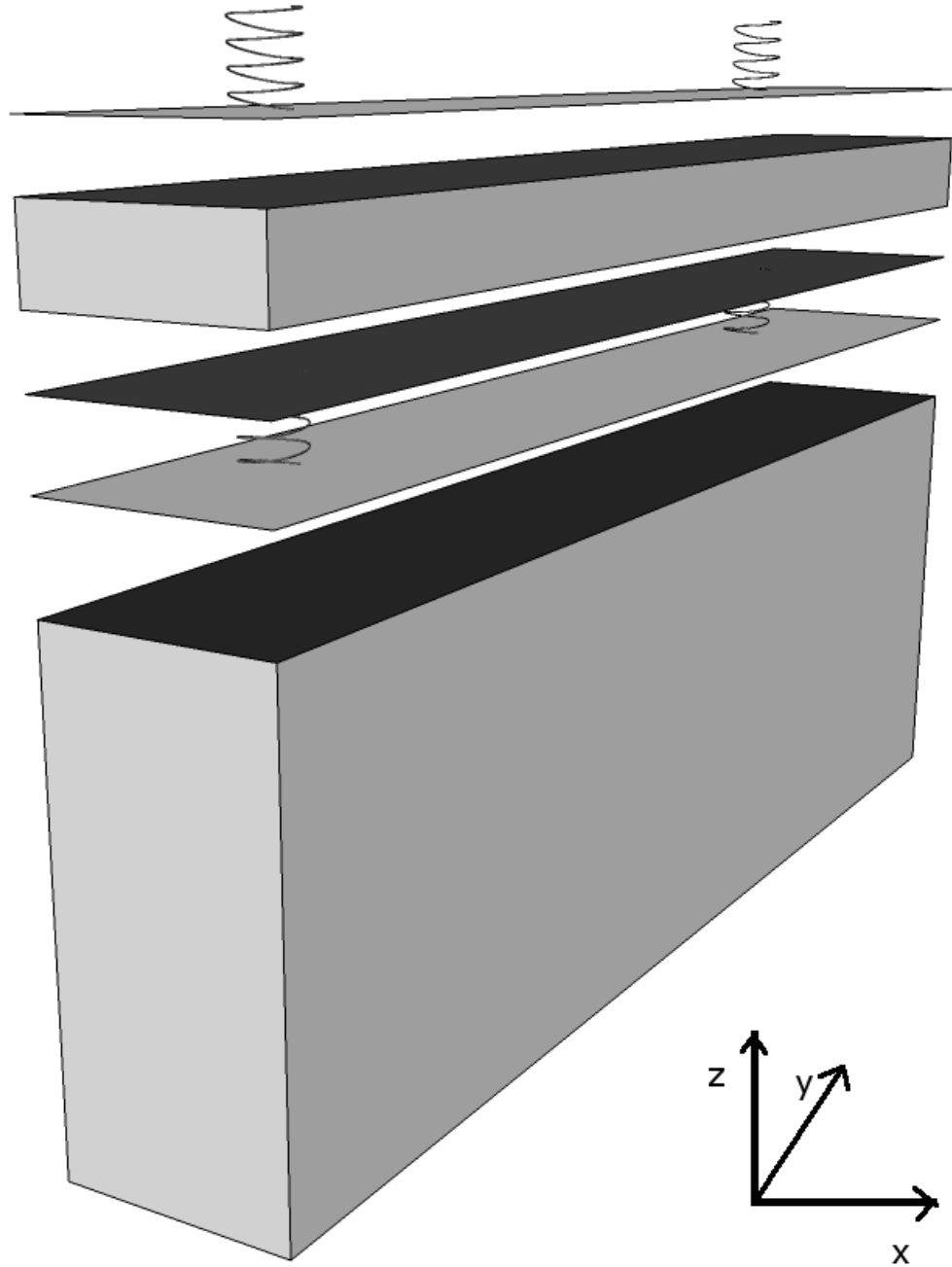


Figure 1.4: Basic Cuboid-I and Basic Cuboid-II separated by equivalent forces. The surface attached to the spring should symbolize the distributive nature of sources. The surfaces of the cuboid, where no sources are applied, indicate stress-free boundaries

discretization process (Fig. 1.2): We subdivide the device geometry of the massive structure into an adequate number of cuboids. Thereby, one electrode or the entire busbar may be represented by one mesh-less cuboid. We appropriately refer to these cuboids as mesh-less since no further discretization (meshing) of geometry is required as oppose to the FEM and BEM. This property allows us to consider the entire electrode section as one basic cuboid. We categorize each cuboid depending on the number of adjacent cuboids attached. For example, a cuboid is called Basic Cuboid-I; Fig. 1.3, because only one port of the hexahedron is allowed to exchange energy with the adjacent cuboid or environment. All the electrodes in Fig. 1.2 are one-port cuboids, and hence Basic Cuboid-I, provided they are not excited by any external sources. Obviously, if the same cuboid exchanges energy with one adjacent side, and simultaneously with environment through a different side makes the problem a two-port cuboid, and thus Basic Cuboid-II. Consequently, device structure is a compilation of such basic cuboids of different types (refer Table 1.1). Therefore, cuboids of particular types need to be characterized and solved individually. Thereby, since each each cuboid is mesh-less, it is necessary that the supports of the opted basis- and testing functions occupies the entire domain of the cuboids.

1.3 Boundary Value Problems Defining Two Test Cuboid

In this chapter, two types of Boundary Value Problems are introduced: one- and two port problems. We present a unified solution strategy to typical one- and two port problems arising in the proposed method. Furthermore, it is shown that more complex BVPs of interest can be reduced to the solution scheme developed here.

1.3.1 BVP for Test Cuboid I

The equation of motion for the test cuboid I, sketched in Fig. 1.3 is given by the governing equation

$$\underline{\underline{\nabla}}^t \mathbf{T} = -\rho_I \omega^2 \mathbf{u}, \quad \text{in } \Omega, \quad (1.1)$$

and the inhomogeneous Neumann boundary condition:

$$\boldsymbol{\tau}_3|_{TestBoundary} = F \quad (1.2)$$

Our objective is the construction of Green's functions associated with the one-port problem formulated in Eqs. (1.1) and (1.2). A time-harmonic oscillation according to $e^{-j\omega t}$ has been assumed throughout the work. For a detailed discussion of the properties of the differential operator $\underline{\underline{\nabla}}$ and the constituent 6×3 matrices \mathbf{N}_n ($n = 1, 3$) the reader is referred to the discussion in [11]. Here, \mathbf{u}

is the mechanical displacement vector, and \mathbf{T} stands for the stress tensor. The stresses $\boldsymbol{\tau}_n$ ($n = 1, 3$) are defined as follows: $\boldsymbol{\tau}_n = \mathbf{N}_n^t \mathbf{T} = \mathbf{N}_n^t \mathbf{C} \underline{\underline{\nabla}} \mathbf{u}$

1.3.2 BVP for Test Cuboid II

The test cuboid II (Fig. 1.4) involves two cuboids occupying the volumina, Ω_a and Ω_b , representing one electrode and the substrate hexahedron, respectively, having a common interface. Additionally, cuboid “a” is subject to external forces operating at frequency ω . Thus the BVP characterizing the “ab”-composite structure is given by:

$$\underline{\underline{\nabla}}^t \mathbf{T}_a = -\rho\omega^2 \mathbf{u}_a, \quad \text{in } \Omega_a \quad (1.3a)$$

and

$$\underline{\underline{\nabla}}^{tr} \mathbf{T}_b = -\rho\omega^2 \mathbf{u}_b, \quad \text{in } \Omega_b \quad (1.3b)$$

By definition Ω_a is a two-port cuboid, whereas, Ω_b is a one-port cuboid. The boundary- and interface conditions are given by

$$\boldsymbol{\tau}_3^a|_{TestBoundary} = \mathbf{F}, \quad (1.4)$$

along with

$$\boldsymbol{\tau}_3^a|_{Interface} = \boldsymbol{\tau}_3^b|_{Interface} \quad (1.5a)$$

and

$$\mathbf{u}_a|_{interface} = \mathbf{u}_b|_{Interface}. \quad (1.5b)$$

At the interface between “*a*” and “*b*,” we shall introduce equivalent forces and separate the bodies for independent analysis. The boundary sections other than the interface and the test boundary are assumed to be stress free.

1.4 Outline of the Proposed Solution for Test Cuboid I: Construction of DES SR DGFs

We follow the standard Galerkin scheme to solve the BVP given by Eqs. (1.1) and (1.2) for the test cuboid I (Fig. 1.3). The solution comprises of the following steps: 1) Expand the unknown functions in the problem in terms of a finite number of appropriately selected basis functions; 2) carry out the standard rolling over of the derivative operator; 3) apply Gauss’ divergence theorem to transform volume integrals into their equivalent surface integrals; 4) transform the resulting coupled system of equations to the master co-ordinate system, where the basis functions, their derivatives and integrals are pre-defined. The latter step requires the transformation of derivatives and integrals, expressed in the original domain; a task which is discussed next.

1.4.1 Transformation of Functions and Differential Operators from Local to Master Co-ordinate System

Consider the function $g(x, y, z)$. Subject the Cartesian co-ordinates x, y and z to the single-valued transformations $x = x(\xi)$, $y = y(\eta)$ and $z = z(\zeta)$. Then, we can write:

$$\begin{aligned} g(x, y, z) &= g(x(\xi), y(\eta), z(\zeta)) \\ &= h(\xi, \eta, \zeta) \end{aligned} \quad (1.6)$$

Furthermore, applying the chain rule the following relationship can be established:

$$\begin{aligned} \frac{\partial g(x, y, z)}{\partial x} &= \frac{\partial \xi}{\partial x} \frac{\partial h(\xi, \eta, \zeta)}{\partial \xi} + \frac{\partial \eta}{\partial x} \frac{\partial h(\xi, \eta, \zeta)}{\partial \eta} + \frac{\partial \zeta}{\partial x} \frac{\partial h(\xi, \eta, \zeta)}{\partial \zeta} \\ \frac{\partial g(x, y, z)}{\partial y} &= \frac{\partial \xi}{\partial y} \frac{\partial b(\xi, \eta, \zeta)}{\partial \xi} + \frac{\partial \eta}{\partial y} \frac{\partial b(\xi, \eta, \zeta)}{\partial \eta} + \frac{\partial \zeta}{\partial y} \frac{\partial b(\xi, \eta, \zeta)}{\partial \zeta} \\ \frac{\partial g(x, y, z)}{\partial z} &= \frac{\partial \xi}{\partial z} \frac{\partial b(\xi, \eta, \zeta)}{\partial \xi} + \frac{\partial \eta}{\partial z} \frac{\partial b(\xi, \eta, \zeta)}{\partial \eta} + \frac{\partial \zeta}{\partial z} \frac{\partial b(\xi, \eta, \zeta)}{\partial \zeta} \end{aligned} \quad (1.7)$$

In the particular case of linear transformations,

$$\begin{aligned} x(\xi) &= a_1 + a_2\xi \\ y(\eta) &= b_1 + b_2\eta \\ z(\zeta) &= c_1 + c_2\zeta \end{aligned} \quad (1.8)$$

the Eq. (1.7) can be cast in the following simple matrix representation:

$$\begin{bmatrix} \frac{\partial g(x,y,z)}{\partial x} \\ \frac{\partial g(x,y,z)}{\partial y} \\ \frac{\partial g(x,y,z)}{\partial z} \end{bmatrix} = \begin{bmatrix} \frac{1}{a_2} & 0 & 0 \\ 0 & \frac{1}{b_2} & 0 \\ 0 & 0 & \frac{1}{c_2} \end{bmatrix} \begin{bmatrix} \frac{\partial h(\xi,\eta,\zeta)}{\partial \xi} \\ \frac{\partial h(\xi,\eta,\zeta)}{\partial \eta} \\ \frac{\partial h(\xi,\eta,\zeta)}{\partial \zeta} \end{bmatrix} \quad (1.9)$$

In addition, Auld's differential operator $\underline{\nabla}$ in three dimensions transforms as follows (refer to [11]):

$$\begin{aligned} \underline{\nabla} &= \mathbf{N}_1 \partial_x + \mathbf{N}_2 \partial_y + \mathbf{N}_3 \partial_z \\ &= \mathbf{N}_1 \left[\frac{1}{a_2} \partial_\xi \right] + \mathbf{N}_2 \left[\frac{1}{b_2} \partial_\eta \right] + \mathbf{N}_3 \left[\frac{1}{c_2} \partial_\zeta \right] \\ &= \underline{\tilde{\nabla}} \end{aligned} \quad (1.10)$$

Additionally, we have

$$\int_{\Omega} dx dy dz g(x, y, z) = a_2 b_2 c_2 \int_{\mathbb{D}} d\xi d\eta d\zeta h(\xi, \eta, \zeta). \quad (1.11)$$

Here, the “ \mathbb{D} ” symbolizes the volume $-1 \leq \xi, \eta, \zeta \leq +1$.

1.4.2 Basis- and Testing Functions

We take the polynomials $b_l(\xi)$, $b_m(\eta)$ and $b_n(\zeta)$ to be orthonormalized Legendre polynomials on the interval $[-1,1]$. We employ these 1D basis functions to form a set of 3D $B_i(\xi, \eta, \zeta)$ basis functions: $B_i(\xi, \eta, \zeta) = B_{l \odot m \odot n}(\xi, \eta, \zeta) = b_l(\xi) b_m(\eta) b_n(\zeta)$, with $l = 0, \dots, L$, $m = 0, \dots, M$, $n = 0, \dots, N$ and $i = 0, \dots, L \times M \times N$. Obviously, due to the resulting factorized form, the

calculation of the derivatives of $B_i(\xi, \eta, \zeta)$ with respect to any of the independent variables ξ, η and ζ can be reduced to calculation of the derivatives of 1D functions. A similar conclusion can be made for the calculation of the integrals, which arise in implementations. The integrals, carried out over the domain $-1 \leq \xi, \eta, \zeta \leq +1$, are obtained in closed-form and tabulated. The distributed nature of the basis functions results in the property that no singularities arise in the process of calculating Green's functions. Furthermore, since the derivatives and integrals are calculated in closed-form in 1D, there is hardly any additional computation time required to calculate the derivatives and integrals involving 3D polynomials.

As an example consider the i^{th} component of the displacement vector \mathbf{u} being approximated in terms of a linear superposition of the constructed basis functions $B_j(\xi, \eta, \zeta)$:

$$u_i(\xi, \eta, \zeta) \approx \sum_{j=0}^{L \times M \times N} u_j^{(i)} B_j(\xi, \eta, \zeta), \quad (1.12)$$

where, $i = 1, 2, 3$. The test functions, which are required in the implementation of the standard Galerkin method are chosen from the set of composite basis functions $B_j(\xi, \eta, \zeta)$. Correspondingly, the force functions, defined on the boundary surface, can be synthesized a linear combination of 2D basis functions. As an example, assuming the force function $F(\xi, \eta)$, defined on the square $(\xi, \eta) \in [-1, 1] \times [-1, 1]$,

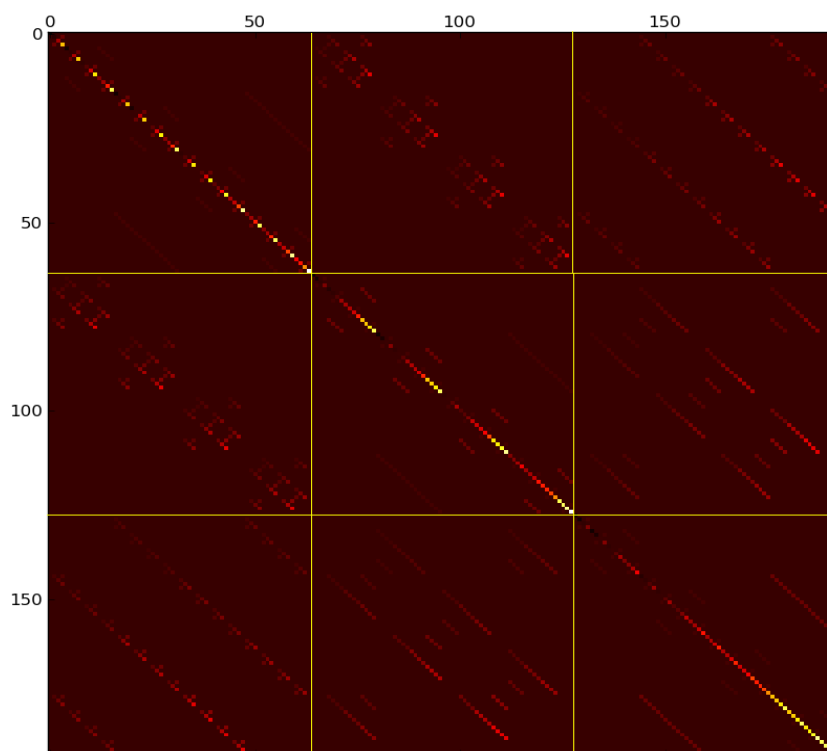


Figure 1.5: Example of a system matrix showing the sparseness in the matrix for an isotropic material

can be approximated by

$$F(\xi, \eta) \approx \sum_{j=0}^{L \times M} \alpha_j B_j(\xi, \eta). \quad (1.13)$$

(Strictly speaking we should have introduced no symbol other than $B_j(\xi, \eta)$ to denote $b_l(\xi)b_m(\eta)$. However, since there is no danger for confusion, the same symbol was used.) Solving the involved system of coupled equations results in the components of the displacement vector, and thus the solution to the underlying BVP.

The implementation of the Galerkin scheme is straightforward. However, for varying source functions one needs to solve the system of equation anew, a process, which can be exhaustive computationally. This bottleneck can be remedied by utilizing the pre-calculated DES SR Dyadic Green's Functions. By definition, our Green's functions are responses (displacement functions) to elementary excitations defined on a section of the boundary surface, while keeping the remaining portion of the boundary to be stress free. In the case of one-port problem, the elementary sources are 2D basis functions, which are distributed over the considered surface of the test structure I. Successive application of the 2D basis functions, and solving the resulting system of equations, as described above, result in the associated displacement components, and thus to the required Green's functions, which will be collectively denoted by \mathcal{GF} s. The computed information defining \mathcal{GF} s is then stored for frequent future usage. Since any displacement distribution in response to an arbitrary excitation function can be modelled by the pre-computed Green's functions, we can write:

$$u_i(x, y, z) \approx \sum_{j=0}^{L \times M} \alpha_j^{(i)} \mathcal{GF}_j^{(i)}(x, y, z) \quad (1.14)$$

Remark: Before proceeding further it should be pointed out that, Eqs. (1.9) and (1.11) convey an important property, whose utilization may significantly reduce the computational cost. These equations show that, upon linear transformation, the integration and differentiation operators are not dependent on translation

coefficients, a_1, b_1 and c_1 , appearing in transformation Eq. (1.9). Thus, if the size of the basic cuboid does not change, it is not necessary to recalculate the system of equations. Instead, whenever required, use the same stored \mathcal{GF} s, by just translating them to the desired position. This essentially meaning, computing the \mathcal{GF} s for one test structure I, solves the problem for any hexahedron identical to the test cuboid I, regardless of its actual position in the device geometry. In addition to this most advantageous feature, the associated system matrix is sparse, evidence of which can be seen in Fig. 1.5.

1.4.3 Physics-based Model-Order-Reduction

Finally, before concluding this section it should be mentioned that both \mathcal{GF} s and their derivatives are defined on the entire simulation domain. The storage of these functions is necessary for repeated future usage. However, storing entire-domain solutions in their original form, as they stand, requires excessive amounts of storage space, rendering the retrieval of data an exceedingly slow process. Instead the calculated \mathcal{GF} s and their derivatives are evaluated (collapsed) on the boundary. This process effectively compresses the data set involved, without compromising the accuracy of the numerical results. In view of this most desirable feature of the proposed method, it will also be referred to as the physics-based Model-Order-Reduction (MOR) technique. The mentioned data compression becomes particularly significant when three dimensional building blocks are put together

to synthesize large number of cuboids, utilizing the Green's functions in reduced form.

LIBRARY of \mathcal{GF} s and the Concept of WORKING MEMORY: The assumed finite number of basis functions span a subspace of the Hilbert space; the computed \mathcal{GF} s carry sufficient information to describe any conceivable vibration of the considered canonical problems. The compressed \mathcal{GF} s and their derivative functions are stored in a storage space referred to as the LIBRARY. The stored \mathcal{GF} s are categorized depending on the type of the material characterizing a given cuboid, size of cuboid and the operating frequency. The created LIBRARY contains the \mathcal{GF} s for standard materials used in the micro-acoustic industry. The information in the LIBRARY enables both 2D and 3D device modeling and simulation. The LIBRARY is made accessible to authorized designers, who only need to focus on the design constraints, without being disrupted by the numerical and computational difficulties. In applications only those encoded \mathcal{GF} s are retrieved and copied into the WORKING MEMORY which is unconditionally necessary for modelling a given structure.

1.5 Outline of the Proposed Solution for the Test Structure II

The test cuboid II is a combination of basic cuboid I and Basic cuboid II. The discussion of the solution for these type of problems, sketched in Fig. 1.4, is rather complex. However, by restricting the discussion to scalar problems, the complexity can be reduced significantly. A strategic outline has been drawn in the following section. To convey the essence of the idea, it fully suffices to consider scalar-valued sources and responses and thus talk about scalar Green's functions only for this section.

1.5.1 Sufficiency Principle

Assume a certain force distribution $F(s)$, ($s \in [0, 1]$), operating at the given frequency ω , acts on the bounding surface Γ . The involvement of the frequency is extraordinarily important in practical simulations but has no relevance in the present discussion. It has been assumed that the boundary has been parameterized: we traverse the entire (closed) boundary by varying the parameter s from 0 to 1. The problem is the determination of the domain response function in terms of displacement to the force distribution $F(s)$. In particular, we are interested in the determination of the response of the medium $R(s)$, evaluated on domain's bounding surface. A second quantity of interest is the derivative of the

response function of the medium evaluated at the bounding surface, $DR(s)$. The rationale behind our interest in $R(s)$ and $DR(s)$ stems from the fact that if we wish to interface the current domain with adjacent sections, we only need to be equipped with the knowledge about $R(s)$ and $DR(s)$. Obviously, changing $F(s)$, the response functions $R(s)$ and $DR(s)$ will change accordingly. In our method we fully exploit the advantages innate to Green's functions. From a strategic point of view (computationally), we wish to pre-calculate relevant data and store them for future simulations. To this end we exploit the fact that $F(s)$ can be synthesized with sufficient accuracy from $(N + 1)$ distributed elementary (basis) functions $b_n(s)$ with $n \in \mathcal{N}_0$ and $\mathcal{N}_0 = 0, \dots, N$. Denote the individual responses of the medium to $b_n(s)$ by $G_n(s)$ and consecutively calculate their derivatives $DG_n(s)$. Not surprisingly, the letters G and D are meant to remind us of Green's functions and their derivatives, respectively. The mentioned synthesis is valid if we can assure that $b_n(s)$ ($n \in \mathcal{N}_0$) constitute a subset of a complete sequence of functions. Assume the latter sequence exists. Then, the following inferences are immediate: (i) $F(s)$ can be expressed in terms of $b_n(s)$ by introducing $(N + 1)$ expansion coefficients c_n ($n \in \mathcal{N}_0$). (ii) The responses $G_n(s)$ and $DG_n(s)$ to the individual $b_n(s)$ are already available, in the LIBRARY or calculable for a new simulation domain. Therefore, the responses of the medium to $F(s)$, i.e., $G(s)$ and $DG(s)$, can be obtained by a linear combination of $G_n(s)$ and $DG_n(s)$, respectively, adequately weighted by the coefficients c_n . The merit of the story is that if the excitation, i.e. $F(s)$ changes to, say, $\tilde{F}(s)$, we don't need to solve the

BVP from scratch. Instead, we just need to determine the expansion coefficients \tilde{c}_n of $\tilde{F}(s)$ by synthesizing $\tilde{F}(s)$ from the basis functions $b_n(s)$. The responses of the medium to $\tilde{F}(s)$ can readily be obtained by weighting the pre-calculated $G_n(s)$ and $DG_n(s)$ by the coefficients \tilde{c}_n and adding together the resulting terms.

1.5.2 The Principle of Exhaustion

In order to introduce this principle clearly a few comments are in place. (1) The pre-calculated Green's functions $G_n(s)$ and their derivatives $DG_n(s)$, both evaluated at the bounding surface, are scalar functions, which depend on one variable only. Thus they are completely expressible in terms of the set of basis functions $b_n(s)$. In fact by way of their construction, $G_n(s)$ and $DG_n(s)$ are already available in the desired form, each in terms of $(N + 1)$ numbers. This is of paramount significance in computations: the availability of a set of $2(N + 1)$ (pre-calculated) numbers fully characterizes the solution of our problem (at a given frequency). (2) To keep track of the pre-calculated functions $G_n(s)$ and $DG_n(s)$ and to further manipulate them we only need to take care of $2(N + 1)$ numbers. Since $(N + 1)$ independent excitations (independent numerical experiments) can be carried out, $2(N + 1) \times (N + 1)$ numbers fully characterize our BVP (again at a given frequency); these numbers exhaust the knowledge about our BVP (principle of exhaustion). (3) A further and very important fact is the following: As we can show, the relevant types of boundary conditions such as, homogeneous

and inhomogeneous Dirichlet, homogeneous and inhomogeneous Neumann, and interface conditions can be calculated utilizing the aforementioned $2(N + 1) \times (N + 1)$ numbers - a property which manifestly justifies the notion of exhaustion.

1.5.3 Application of the Sufficiency- and Exhaustion Principles

In order to deal with the interface conditions in the test structure II, let us first familiarize ourselves with the solution of a comparatively easier problem, namely, the Dirichlet boundary condition. As it turns out, solving interface condition is conceptually a minor modification of solving the Dirichlet boundary condition. Consider the equation of motion

$$\underline{\underline{\nabla}}^t \mathbf{T} = -\rho\omega^2 \mathbf{u}, \quad \text{in } \Omega, \quad (1.15)$$

and the Dirichlet boundary condition with \mathbf{U} being a known function, defined on the boundary:

$$\mathbf{u}|_{TestBoundary} = \mathbf{U} \quad (1.16)$$

It should be noted that while the displacement on Γ is known upon assumption, the stress on Γ is *a priori* unknown. Assume that each of the three component of the unknown stress distribution on the boundary can be synthesized using \mathcal{N}_0 appropriately chosen orthonormal basis functions, weighted by \mathcal{N}_0 expansion coefficients c_0, c_1, \dots, c_N . The task is reduced to determination of the expansion

coefficients such that the governing equation is satisfied in Ω and the displacement on the boundary matches (in weak sense) the given displacement function. To this end utilizing our constructed LIBRARY we proceed as follows. We excite the (Ω, Γ) -medium by the force (basis) function $b_n(s)$, acting on Γ . Since $b_n(s)$ is an elementary function, the response of the medium will be referred to as the Green's function associated with $b_n(s)$. The Green's Function evaluated on the boundary Γ , i.e., $G_n(s)$, has been, however, pre-calculated and thus can be copied from the LIBRARY into the WORKING MEMORY. It should be noted that the Green's function $G_n(s)$, being a function defined on Γ , can be expressed in terms of $b_i(s), i \in \mathcal{N}_0$:

$$G_n(s) = \sum_{i=0}^N g_{ni} b_i(s) \quad (1.17)$$

By saying that the Green's function $G_n(s)$ is stored in the LIBRARY, it is meant that the coefficients $g_{ni}, i \in \mathcal{N}_0$ have been stored in the LIBRARY. A further realization is that $G_n(s)$ is, upon construction, the displacement functions $u_n(s)$ evaluated on the boundary. Obviously, in virtue of linearity, exciting the medium by $c_n b_n(s)$, the corresponding displacement on Γ is $c_n G_n(s)$. Retrieving $G_n(s)$ for $n = 0, \dots, N$ from the LIBRARY, multiplying by c_0, \dots, c_N , and adding, we obtain the displacement on Γ :

$$u(s)|_{\Gamma} = \sum_{n=0}^N c_n G_n(s) \quad (1.18)$$

The reader may ask why this peculiar way of expanding the displacement on the boundary $u(s)$ in terms of $G_n(s)$, rather than the more intuitive way of expansion

in terms of the basis functions $b_n(s)$, say, $\tilde{u}(s)|_\Gamma = \sum_{n=0}^N \tilde{c}_n b_n(s)$; after all $u(s)$ is a function defined on Γ and can thus be expressed in terms of basis functions to any arbitrary accuracy, as we expressed the stress on Γ in terms of $b_n(s)$. A little reflection shows that $u(s)|_\Gamma = \sum_{n=0}^N c_n G_n(s)$ is such that its continuation into the Ω is unique and at the same time fulfills the governing equations.

Thus the computational task is reduced to the determination of the unknowns $c_n, n \in \mathcal{N}_0$. To this end we use the fact that the displacement on Γ is a given function, i.e. $U(s)$. Setting $\sum_{n=0}^N c_n G_n(s) = U(s)$, and using Eq. (1.17) leads to:

$$\sum_{n=0}^N c_n \sum_{i=0}^N g_{ni} b_i(s) = U(s) \quad (1.19)$$

On the other hand since $U(s)$ is known, we have $U(s) = \sum_{k=0}^N \alpha_k b_k(s)$ with known α_k . Substituting the latter equation into Eq. (1.19); multiplying both the sides by $b_j(s)$ and integrating over Γ and using orthonormality condition for the basis functions we obtain

$$\sum_{n=0}^N c_n \sum_{i=0}^N g_{ni} \delta_{ij} = \alpha_j, \quad (1.20)$$

which is equivalent with

$$\sum_{n=0}^N c_n g_{nj} = \alpha_j. \quad (1.21)$$

Proceeding similarly with the remaining basis functions we obtain \mathcal{N}_0 equations for the determination of \mathcal{N}_0 unknowns c_n . Thus, with the available coefficient matrix $[g_{nj}]$ and, consequently, its inverse $[g_{nj}]^{-1}$ the unknown expansion coefficients

c_n can be determined:

$$[c_n] = [g_{nj}]^{-1}[\alpha_j]. \quad (1.22)$$

Note that effectively the computational cost for solving the Dirichlet problems is negligible and is reduced to solving \mathcal{N}_0 equations. More precisely, given $U(s)$, we merely need to compute \mathcal{N}_0 inner-products $\alpha_j = \langle b_j | U \rangle$ and multiply the resulting vector $[\alpha_j]$ from the left by the pre-calculated inverse matrix $[g_{nj}]^{-1}$.

Remark: Above, to simplify the discussion, we made a few tacit assumptions which need to be clarified. (1) We assumed that the force- and displacement functions are scalar. (2) Furthermore, we assumed that the support of the basis functions comprises the entire boundary Γ . Having explained the trust of the method, the discussions in the following chapters will demonstrate how the above constrained can be relaxed, respectively, removed. As the reader can expect the solution procedure is straight forward, however, considerably more complex. However, the application of the above recipe remains valid.

Copy the Distributed-Elementary-Source Self-regularized Dyadic Green's Functions (\mathcal{GF} s) from the LIBRARY into the WORKING MEMORY individually for each cuboids. Utilize the \mathcal{GF} s employing the Sufficiency- and Exhaustion Principles, to match the solutions at the interfaces. This completes the solution of the BVPs with interface conditions.

1.6 Thesis Organization

The presentation in this chapter profiles a brief introduction to the proposed method of \mathcal{GF} s technique. The method offers a number of novelties and advantages compared with the standard techniques. The novelties and advantages will be discussed in the forthcoming chapters in greater detail. Thereby, each chapter has been adapted from the corresponding submitted journal paper to make a coherent whole. The chapters should also reflect the progress of thoughts as they developed in the course of the thesis as well as the incremental complexity in the types of problems addressed. Necessarily, the chapters contain sections which are repeated more than once. However, the repetitions are kept in the chapters to maintain the similarity between the chapters and the submitted papers, as far as tolerable, also to reinforce the introduced concepts in addressing the problems (2D and 3D). The reader who is only interested in gaining an overall understanding of the proposed methodology, may wish to skip the repetitions, or similar variations. The chapters are organized, depending on the choice of material (isotropic or anisotropic), and the dimensionality of domain (2D or 3D), as follows:

1.6.1 Chapter 2: Distributed-Elementary-Source Self-regularized Dyadic Green's Functions for Modeling the Massloading Effect in Acoustic Devices: 2D Isotropic Problems

A concept for the simulation of two dimensional isotropic models of massive electrodes in micro-acoustic devices has been presented. The method is based on a mesh-less analysis of the underlying boundary value problem. An efficient procedure for the calculation of the involved dyadic Greens functions has been introduced. Major advantage of the proposed method is in the ability of pre-calculating and storing relevant data for the characterization of individual substructures. The latter property is by construction amenable to parallel computing. A glimpse of the numerical results and carefully drafted figures facilitate the discussion of the underlying ideas.

1.6.2 Chapter 3: 2D Elastodynamic Simulation of Fully - anisotropic Elastic Media Using Self - regularized Dyadic Greens Functions

The presentation begins with the geometrical sub-sectioning of the simulation domain and discussing the types of Basic cuboids involved. Next a weak formulation is presented for two dimensional rectangularly-shaped basic rectangles. The discussion then focuses on explaining the involved Distributed-Elementary-Source

Self-regularized Dyadic Greens Functions (\mathcal{GF} s). The \mathcal{GF} s are then applied to test problems emphasizing different types of boundary conditions. The numerical results obtained show the successful application of the proposed \mathcal{GF} s to a multi-domain test cuboid, by comparing the numerical results against the data obtained from a commercially available FEM simulation package. Utilizing the \mathcal{GF} s from the generated LIBRARY, the chapter concludes with an analysis of the interface problem involving fully-anisotropic cuboids.

1.6.3 Chapter 4: 3D Elastodynamic Simulation of Anisotropic/Isotropic Interface Problems in Elastic Media

A three dimensional problem of ideally-bonded fully-anisotropic interacting elastic media, subject to harmonically time-varying loading at one edge has been analyzed. The underlying boundary value problem is considered as a group of boundary integral equations each characterized by an associated independent boundary value problem. The introduced subsystems are then excited individually by distributed elementary forces rather than standard localized Dirac delta functions. The corresponding Distributed-Elementary-Source Self-regularized Dyadic Green's functions are consecutively calculated and stored. The principle of Exhaustion and the Sufficiency principle along with the stored dyadic Green's functions enable the satisfaction of displacement- and stress continuity over the interfaces. Furthermore, generalizations have been made, allowing interaction with

much larger variety of material types and in particular, interactions between isotropic and anisotropic subsystems. The developed technique offers the prospect of assembling complex device geometries from pre-calculated canonical structures and thus suggests a genuine shift in computational engineering.

1.7 Computational Platforms Utilized in Numerical Calculations

To compute the test problems in the following chapters, a number of computational platform were utilized. Moreover, all the calculations were carried out on a standard dual-core PC, running at 1.86 GHz with 2Gb of RAM. For the fundamental studies, MAPLETM was used to calculate and plot the solutions, which is a symbolic interpreted mathematical package. For the more rigorous analysis and numerical implementations, the scripting language ‘Python’ was utilized. In addition, open-source libraries such as Scipy, Numpy, and Pysparse were utilized, which are fundamental and specialized packages needed for scientific computing with Python. For visual display of 1D basis functions, the open-source python package Matplotlib was employed. For displaying the results in two- and three dimensional, a freeware version of Paraview was used, which is a visualization program based on the Visualization toolkit (VTK).

1.8 List of Publications

1. Hardik Vagh and Alireza Baghai-Wadji . 3d Mass-loading Effects Of Metallic Electrodes With Ultra-high Aspect Ratios In Saw Devices, IEEE International Ultrasonic Symposium, 11-14 October, 2010, San Diego, California, United States.
2. Hardik Vagh and Alireza Baghai-Wadji . On The Construction Of Problem-specific Basis Functions For Modelling The Massloading Effects In Micro-acoustic Devices, International Symposium on Integrated Circuits, 14-16 December, 2009, Singapore.
3. Hardik Vagh, Alireza Baghai-Wadji and Stephane Chamaly. Ab-initio Meshless Modelling Of Three Dimensional Massloading Effects In Saw And Baw Devices, IEEE International Ultrasonic Symposium, 20-23 September, 2009, Italy.
4. Hardik A. Vagh and Alireza Baghai-Wadji, A Scheme To Calculate Higher-order Homogenization As Applied To Micro-acoustic Boundary Value Problems, SPIE Conference, December 2008, RMIT University, Melbourne.
5. Vagh H. A. and Baghai-Wadji A. R. Recipes For Efficient Higher-order Multiscale Asymptotic Analysis Ultrawideband and Ultrashort Impulse Signals, 15-19 September, 2008, Ukraine.

Chapter 2

Distributed-Elementary-Source Self-regularized Dyadic Green's Functions for Modeling the Massloading Effect in Acoustic Devices: 2D Isotropic Problems

2.1 Introduction

Simulation of the massloading effect in surface acoustic wave (SAW) and bulk acoustic wave (BAW) devices has been of paramount interest and significance in the micro-acoustic device community ([7, 39, 43] and the references therein). Traditional calculations, based on the Finite Element Method (FEM), Boundary Element Method (BEM) or a combination of both, lack the desired ability in

precalculating and storing data in a LIBRARY for frequent future usage in device design cycles. Ordinarily, the idea of identifying pre-calculable data is regarded as a challenging task because stress distributions on the bounding surfaces of the metallic electrodes, used in micro-acoustic devices, are strongly frequency dependent. In addition to our desire of having more efficient numerical techniques, inherent limitations of FEM and BEM also need to be addressed: While BEM easily applies to open-boundary problems and provides comparatively accurate results, it is not suitable for solving problems related to strongly varying material inhomogeneities. On the other hand, despite the fact that FEM straightforwardly accommodates material inhomogeneities, its application to open-boundary problems is plagued by compromising achievable accuracies. (In general, the accuracy achievable by FEM is inferior to that obtainable by BEM.) Part of these and related difficulties can be remedied by hybridizing FEM and BEM at the cost of higher computational requirements. Alternatively, in order to improve the accuracy of the solutions, new mesh-less methods such as Element-free Galerkin Method, Mesh-less local Petrov-Galerkin Method, Point Interpolation Method, etc. have generated considerable interest along with hp-Finite Element Methods [19, 26, 28, 44]. Further complications arising in BEM are due to the existence of the strong- and hyper strong singularities in the involved Green's functions and their spatial derivatives [11]. Computationally, the origin of these singularities can be traced back to the utilization of idealized localized sources. In our technique we employ smoothly distributed sources and test the resulting residua by

means of distributed and smooth functions, thus eliminating most of the mentioned problems in one stroke.

The presentation in this chapter limits itself to the “proof of concept.” The method promises to be powerful enough to tackle complex problems which typically arise in SAW- and BAW devices. At the same time, the technique being semi-numerical in its nature, is sufficiently simple to elucidate “thought” experiments, underpinning the construction of the associated Dyadic Green’s Functions (DGFs). In order to emphasize the distinct way of constructing inherently Self-regularized (SR) DGFs, we graphically and computationally illustrate the relevant steps involved. We shall underline this important feature in our method, by referring to the constructed Green’s functions, Distributed-Elementary-Source Self-regularized Dyadic Green’s Functions (DES SR DGFs). To save space we shall use \mathcal{GF} s when referring to DES SR DGFs. Utilizing our pre-computed \mathcal{GF} s for suitably-chosen structural sub-domains, we are then well positioned to introduce a procedure for matching the constituent substructures of a given complex domain: A metallic electrode positioned on a piezoelectric substrate in SAW- and BAW devices manifests its influence by generating stress distributions at the electrode/substrate interface. (To focus on the introduced technique, the electric charges on the bounding surfaces of the electrodes have been ignored in this chapter. The effect of electric charges can be included in the analysis by the method presented in Ref. [10].) Viewed in this way, electrodes determining the device

characteristics, can be replaced by their stress footprints on the substrate surface. The resulting stress distributions can be regarded as sources for the excitation of acoustic waves in these devices. Indeed being in control of the stress distribution functions on the electrode/substrate interfaces, in addition to the electric charge distribution functions on the bounding surfaces of the electrodes, at a given frequency, we can manipulate excitation and scattering of acoustic waves in any desired way. Distant analogies to this description can be found in well-known methods such as domain decomposition, tearing and interconnecting methods, penalty-based finite element interface technology, etc.[30, 32, 33, 37]. However, this analogy is merely limited to the problem description, as will be clear in the course of our discussion. The introduced method utilizes entire-domain basis functions and exploits the property of orthogonality. The integrals and derivatives, required to solve the Boundary Value Problems (BVPs) of interest, are also calculated over the entire domain rather than at discrete nodes, allowing the method to fall into the category of mesh-free or element-free methods, leading to numerous advantages over standard FEM. These tools are employed in a sophisticated manner to pre-calculate and generate a LIBRARY of problem-related \mathcal{GF} s, which are computed by minimizing the associated residua (Galerkin Method).

In this chapter we demonstrate the implementation of our ideas as follows: A weak formulation will be presented first assuming three dimensional (3D) spatial dependence. We then restrict our discussion to 2D problems in order to thoroughly

Table 2.1: Main Symbols and abbreviations used in the chapter

<i>Symbols</i>	<i>Description</i>
$\overline{\nabla}$... Auld's divergence-type operator [11]
$\overline{\mathbf{C}}$... Stiffness matrix [1]
ρ	... Mass density
ω	... Operating frequency
\mathbf{u}	... Mechanical displacement vector
\mathbf{v}	... Test vector
\mathbf{T}	... Stress tensor
$F_{s,\parallel}^a(x)$... External force component parallel (\parallel) to the "southern" (s) boundary surface of quadrangle "a"
$(\cdot)^t$... Transposition operator
Ω	... Volume of the 3D medium
S	... Bounding surface of the 3D medium
A	... Area of the 2D medium
Γ	... Boundary line of 2D medium
\square	... $-1 \leq \xi \leq 1$ and $-1 \leq \zeta \leq 1$
\oint_S	... Closed surface integral
$\delta_{n,\bar{n}}$... Kronecker delta symbol
\mathcal{N}	... The set of numbers $1, \dots, N$
\mathcal{N}_0	... The set of numbers $0, 1, \dots, N$
$f \iff F$... F is a discrete representation of the continuum entity f
DES	... Distributed Elementary Source
SR	... Self-regularized
DGFs	... Dyadic Green's Functions
\mathfrak{F}_s	... DES SR DGFs

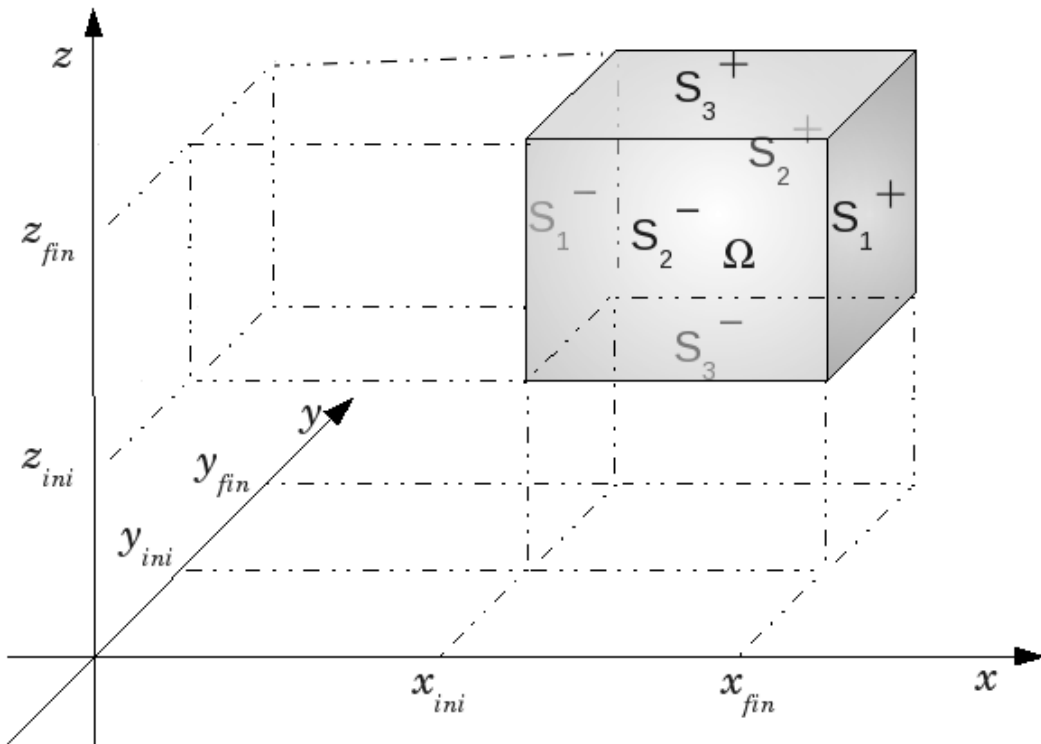


Figure 2.1: Co-ordinate of an arbitrarily-located cuboid with the volume Ω and surfaces S_i^\pm ($i = 1, 2, 3$)

communicate details of our method related to the process of “tearing” a domain into sub-domains, and the matching procedure. In this way, the enabling power of the introduced \mathcal{GF} s should become more clear. Next the superior properties of the utilized basis functions are described along with calculating their derivatives and integrals. The \mathcal{GF} s are then utilized to satisfy the interface conditions leading to the results and conclusion sections.

Convention: We shall take the x -axis to be in the horizontal direction, the y -axis pointing into this plane and the z -axis to be in the vertical direction. For 2D analysis, there will be no variation in the y -direction ($\partial y \equiv 0$).

2.2 Preparatory Considerations

2.2.1 Weak-Galerkin Formulation in 3D

Consider an isotropic homogeneous elastic cuboid as shown in Fig. 2.1. The elastic medium being characterized by the stiffness matrix \mathbf{C} and the constant mass density ρ , occupies the volume Ω with the boundary surface S . The equation of motion for this medium reads:

$$\underline{\underline{\nabla}}^t \mathbf{T} = -\rho\omega^2 \mathbf{u}, \quad \text{in } \Omega, \quad (2.1)$$

or, equivalently,

$$[\mathbf{N}_1^t \partial_x + \mathbf{N}_2^t \partial_y + \mathbf{N}_3^t \partial_z] \mathbf{T} = -\rho \omega^2 \mathbf{u}, \quad \text{in } \Omega. \quad (2.2)$$

The superscript t signifies transposition. A harmonic time-dependence according to $e^{-j\omega t}$ has been assumed. For a detailed discussion of the properties of the operator $\underline{\nabla}$ and the constituent 6×3 matrices \mathbf{N}_i ($i = 1, 2, 3$) we refer to the discussion in [11]. Here, \mathbf{u} is the mechanical displacement vector and \mathbf{T} stands for the stress tensor, which appears in our calculations as a column vector with six components T_i ($i = 1, \dots, 6$). Introducing stresses $\boldsymbol{\tau}_i$, ($i = 1, 2, 3$) according to

$$\boldsymbol{\tau}_i = \mathbf{N}_i^t \mathbf{T} = \mathbf{N}_i^t \mathbf{C} \underline{\nabla} \mathbf{u} \quad (2.3)$$

we can transform Eq. (2.2) into the following convenient form:

$$\partial_x \boldsymbol{\tau}_1 + \partial_y \boldsymbol{\tau}_2 + \partial_z \boldsymbol{\tau}_3 = -\rho \omega^2 \mathbf{u} \quad (2.4)$$

Here, $\boldsymbol{\tau}_i$ comprises the stress components T_{1i}, T_{2i}, T_{3i} which act on the surface with the outward unit normal vector \mathbf{n}_i . Multiplying both sides of Eq. (2.4) by the transpose of a 3×1 test vector \mathbf{v} (elementary weighting function representing any of the vectors $(v_1 \ 0 \ 0)^t$, $(0 \ v_2 \ 0)^t$, or $(0 \ 0 \ v_3)^t$) we obtain:

$$\mathbf{v}^t \partial_x \boldsymbol{\tau}_1 + \mathbf{v}^t \partial_y \boldsymbol{\tau}_2 + \mathbf{v}^t \partial_z \boldsymbol{\tau}_3 = -\rho \omega^2 \mathbf{v}^t \mathbf{u} \quad (2.5)$$

Obviously Eq. (2.5) is equivalent with:

$$\begin{aligned} & \partial_x(\mathbf{v}^t \boldsymbol{\tau}_1) - (\partial_x \mathbf{v}^t) \boldsymbol{\tau}_1 + \partial_y(\mathbf{v}^t \boldsymbol{\tau}_2) - (\partial_y \mathbf{v}^t) \boldsymbol{\tau}_2 \\ & + \partial_z(\mathbf{v}^t \boldsymbol{\tau}_3) - (\partial_z \mathbf{v}^t) \boldsymbol{\tau}_3 = -\rho\omega^2 \mathbf{v}^t \mathbf{u} \end{aligned} \quad (2.6)$$

Interpreting the scalar quantities $\mathbf{v}^t \boldsymbol{\tau}_i$ ($i = 1, 2, 3$) as the components of a 3×1 vector \mathbf{P} , the terms with a plus sign at the LHS of Eq. (2.6), taken collectively, constitute the divergence of \mathbf{P} :

$$\partial_x(\mathbf{v}^t \boldsymbol{\tau}_1) + \partial_y(\mathbf{v}^t \boldsymbol{\tau}_2) + \partial_z(\mathbf{v}^t \boldsymbol{\tau}_3) = \text{div} \mathbf{P} \quad (2.7)$$

In view of Eq. (2.7), and integrating both sides of Eq. (2.6) over the volume Ω , we obtain:

$$\begin{aligned} & - \int_{\Omega} d\Omega (\partial_x \mathbf{v}^t) \boldsymbol{\tau}_1 - \int_{\Omega} d\Omega (\partial_y \mathbf{v}^t) \boldsymbol{\tau}_2 - \int_{\Omega} d\Omega (\partial_z \mathbf{v}^t) \boldsymbol{\tau}_3 \\ & + \int_{\Omega} d\Omega \text{div} \mathbf{P} = -\rho\omega^2 \int_{\Omega} d\Omega \mathbf{v}^t \mathbf{u} \end{aligned} \quad (2.8)$$

Here, the divergence term deserves particular attention: Consider Gauss' Divergence theorem

$$\int_{\Omega} d\Omega \text{div} \mathbf{P} = \oint_{\mathcal{S}} d\mathcal{S} \mathbf{n}^t \mathbf{P}, \quad (2.9)$$

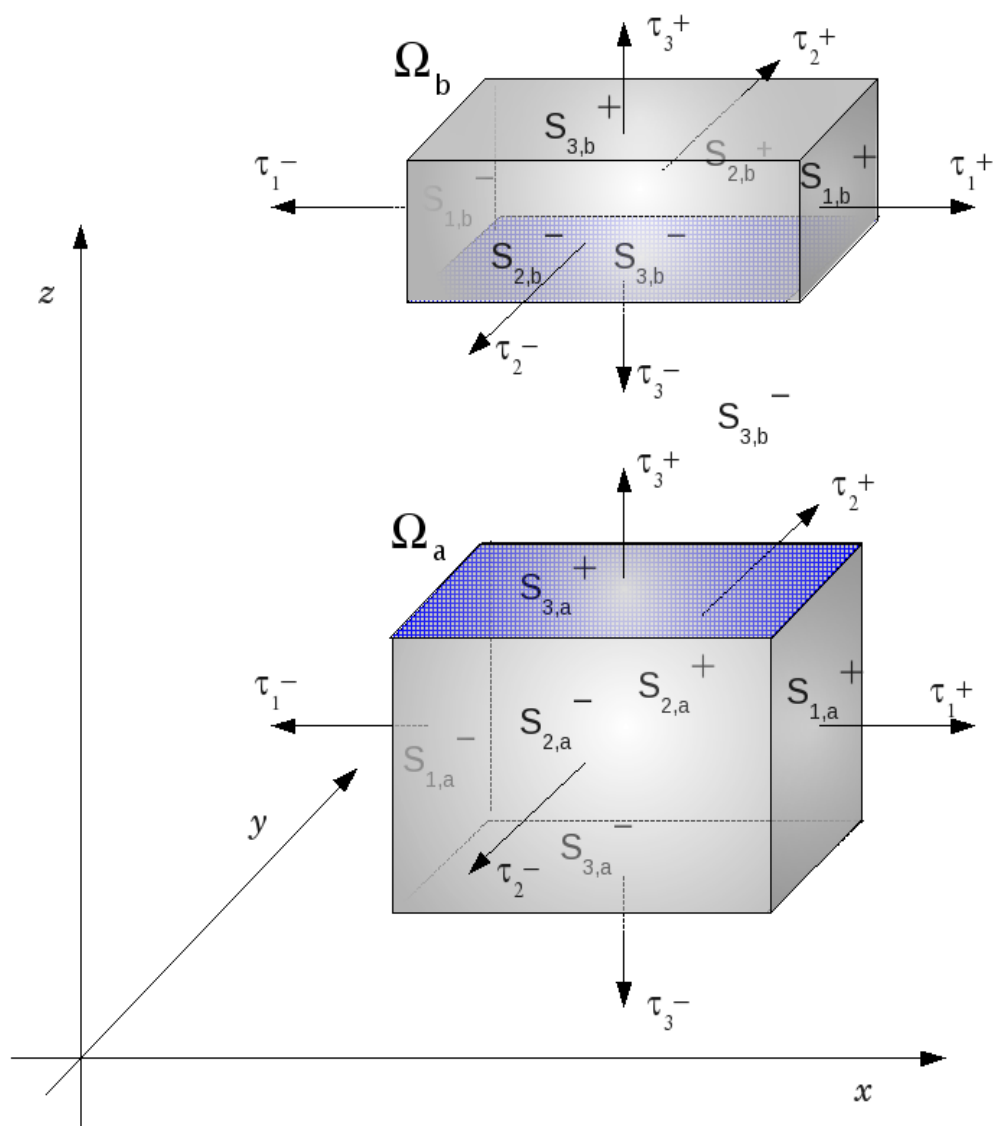


Figure 2.2: Partitioning the cuboid given in Fig. 2.1 into two hexahedrons “a” and “b”

with \mathbf{n} being the unit vector normal to the closed boundary S of the volume Ω pointing outwards (Fig. 2.1):

$$\begin{aligned}
\oint_S dS \mathbf{n}^t \mathbf{P} &= \int_{S_1^+} dydz \begin{bmatrix} 1 \\ 0 \\ 0 \end{bmatrix}^t \begin{bmatrix} P_1 \\ P_2 \\ P_3 \end{bmatrix} + \int_{S_1^-} dydz \begin{bmatrix} -1 \\ 0 \\ 0 \end{bmatrix}^t \begin{bmatrix} P_1 \\ P_2 \\ P_3 \end{bmatrix} \\
&+ \int_{S_2^+} dx dz \begin{bmatrix} 0 \\ 1 \\ 0 \end{bmatrix}^t \begin{bmatrix} P_1 \\ P_2 \\ P_3 \end{bmatrix} + \int_{S_2^-} dx dz \begin{bmatrix} 0 \\ -1 \\ 0 \end{bmatrix}^t \begin{bmatrix} P_1 \\ P_2 \\ P_3 \end{bmatrix} \\
&+ \int_{S_3^+} dx dy \begin{bmatrix} 0 \\ 0 \\ 1 \end{bmatrix}^t \begin{bmatrix} P_1 \\ P_2 \\ P_3 \end{bmatrix} + \int_{S_3^-} dx dy \begin{bmatrix} 0 \\ 0 \\ -1 \end{bmatrix}^t \begin{bmatrix} P_1 \\ P_2 \\ P_3 \end{bmatrix} \quad (2.10)
\end{aligned}$$

In view of the definitions $P_i = \mathbf{v}^t \boldsymbol{\tau}_i$ ($i = 1, 2, 3$), introduced above, Eq. (2.10) can be written in the following compact form:

$$\begin{aligned}
\oint_S dS \mathbf{n}^t \mathbf{P} &= \int_{S_1^+} dydz \mathbf{v}^t \boldsymbol{\tau}_1 - \int_{S_1^-} dydz \mathbf{v}^t \boldsymbol{\tau}_1 \\
&+ \int_{S_2^+} dx dz \mathbf{v}^t \boldsymbol{\tau}_2 - \int_{S_2^-} dx dz \mathbf{v}^t \boldsymbol{\tau}_2 \\
&+ \int_{S_3^+} dx dy \mathbf{v}^t \boldsymbol{\tau}_3 - \int_{S_3^-} dx dy \mathbf{v}^t \boldsymbol{\tau}_3 \quad (2.11)
\end{aligned}$$

With Eqs. (2.9) and (2.11), Eq. (2.8) reads:

$$\begin{aligned}
&- \int_{\Omega} d\Omega (\partial_x \mathbf{v}^t) \boldsymbol{\tau}_1 - \int_{\Omega} d\Omega (\partial_y \mathbf{v}^t) \boldsymbol{\tau}_2 - \int_{\Omega} d\Omega (\partial_z \mathbf{v}^t) \boldsymbol{\tau}_3 \\
&+ \int_{S_1^+} dydz \mathbf{v}^t \boldsymbol{\tau}_1 + \int_{S_2^+} dx dz \mathbf{v}^t \boldsymbol{\tau}_2 + \int_{S_3^+} dx dy \mathbf{v}^t \boldsymbol{\tau}_3 \\
&- \int_{S_1^-} dydz \mathbf{v}^t \boldsymbol{\tau}_1 - \int_{S_2^-} dx dz \mathbf{v}^t \boldsymbol{\tau}_2 - \int_{S_3^-} dx dy \mathbf{v}^t \boldsymbol{\tau}_3 \\
&= -\rho \omega^2 \int_{\Omega} d\Omega \mathbf{v}^t \mathbf{u} \quad (2.12)
\end{aligned}$$

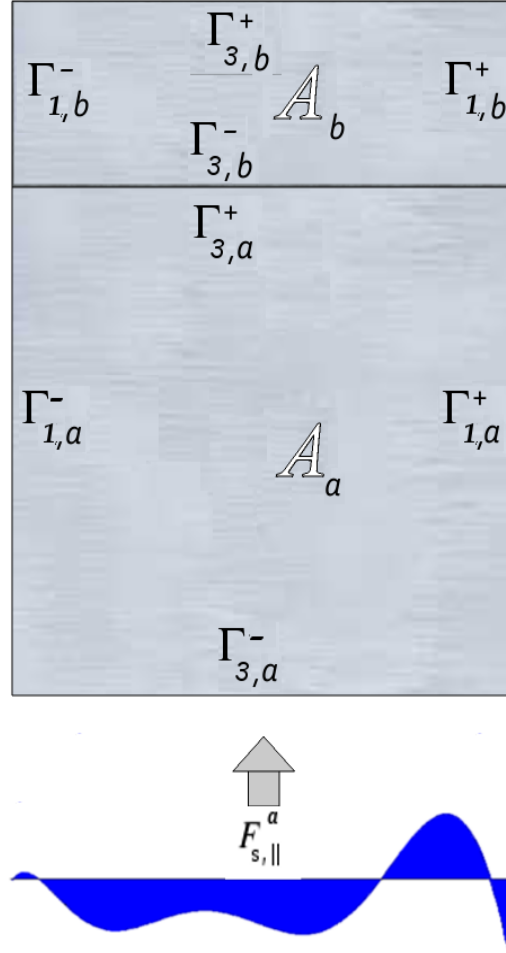


Figure 2.3: A composite 2D structure with a distributed excitation source acting on the bottom surface of quadrangle “ a ,” with the remaining surfaces being stress free

2.2.2 Partitioning into Quadrangles

As shown in Fig. 2.2 we partition Ω into Ω_a and Ω_b ($\Omega_a \cup \Omega_b = \Omega$ and $\Omega_a \cap \Omega_b = \emptyset$).

The two quadrangles a and b touch each other at the common interface $S_{3,a}^+ = S_{3,b}^-$ (Figure 2.2 shows the locations of $S_{3,a}^+$ and $S_{3,b}^-$.) Considering stress-free boundary

conditions on all the surfaces except $S_{3,a}^-$, $S_{3,a}^+$ and $S_{3,b}^-$, and in view of Eq. (2.12), we obtain the following simplified equation for characterizing the quadrangle “a”:

$$\begin{aligned}
& - \int_{\Omega_a} d\Omega_a(\partial_x \mathbf{v}^t) \boldsymbol{\tau}_1 - \int_{\Omega_a} d\Omega_a(\partial_y \mathbf{v}^t) \boldsymbol{\tau}_2 \\
& - \int_{\Omega_a} d\Omega_a(\partial_z \mathbf{v}^t) \boldsymbol{\tau}_3 - \int_{S_{3,a}^-} dx dy \mathbf{v}^t \boldsymbol{\tau}_3 \\
& + \int_{S_{3,a}^+} dx dy \mathbf{v}^t \boldsymbol{\tau}_3 = -\rho\omega^2 \int_{\Omega_a} d\Omega_a \mathbf{v}^t \mathbf{u}
\end{aligned} \tag{2.13}$$

Proceeding analogously, for the quadrangle “b” we have:

$$\begin{aligned}
& - \int_{\Omega_b} d\Omega_b(\partial_x \mathbf{v}^t) \boldsymbol{\tau}_1 - \int_{\Omega_b} d\Omega_b(\partial_y \mathbf{v}^t) \boldsymbol{\tau}_2 \\
& - \int_{\Omega_b} d\Omega_b(\partial_z \mathbf{v}^t) \boldsymbol{\tau}_3 - \int_{S_{3,b}^-} dx dy \mathbf{v}^t \boldsymbol{\tau}_3 \\
& = -\rho\omega^2 \int_{\Omega_b} d\Omega_b \mathbf{v}^t \mathbf{u}
\end{aligned} \tag{2.14}$$

These equations build the foundation for the discussion of \mathcal{GF} s and their utilization in solving BVPs we are interested in. We have implemented and thoroughly tested the applicability of Eqs. (2.13) and (2.14) to 3D problems. However, to ease the discussion, we shall reduce Eqs. (2.13) and (2.14) to 2D by considering problems in the (x, z) -plane. The next section is devoted to this task.

2.3 Statement of The Problem

Connecting a system of partitioned quadrangles by utilizing pre-calculated \mathcal{GF} s for individual quadrangles.

2.4 Proposed Methodology

2.4.1 Weak Galerkin Formulation in 2D

Suppressing y -derivatives ($\Omega_a \rightarrow A_a$), and replacing Ω_a by A_a and $S_{3,a}^\pm$ by $\Gamma_{3,a}^\pm$ (Fig. 2.3), Eq. 2.13 reduces to:

$$\begin{aligned} & - \int_{A_a} dA_a (\partial_x \mathbf{v}^t) \boldsymbol{\tau}_1 - \int_{A_a} dA_a (\partial_z \mathbf{v}^t) \boldsymbol{\tau}_3 \\ & - \int_{\Gamma_{3,a}^-} dx \mathbf{v}^t \boldsymbol{\tau}_3 + \int_{\Gamma_{3,a}^+} dx \mathbf{v}^t \boldsymbol{\tau}_3 = -\rho\omega^2 \int_{A_a} dA_a \mathbf{v}^t \mathbf{u} \end{aligned} \quad (2.15)$$

The boundary sections $\Gamma_{1,a}^+$, $\Gamma_{1,a}^-$, $\Gamma_{3,a}^+$ and $\Gamma_{3,a}^-$ represent surfaces facing “east,” “west,” “north,” and “south,” respectively (Fig. 2.3). Substituting the expression for $\boldsymbol{\tau}_1$ and $\boldsymbol{\tau}_3$ from Eq. (2.3) into the first two terms we have:

$$\begin{aligned} & - \int_{A_a} dA_a (\partial_x \mathbf{v}^t) \mathbf{N}_1^t \mathbf{C} \underline{\underline{\nabla}} \mathbf{u} - \int_{A_a} dA_a (\partial_z \mathbf{v}^t) \mathbf{N}_3^t \mathbf{C} \underline{\underline{\nabla}} \mathbf{u} \\ & - \int_{\Gamma_{3,a}^-} dx \mathbf{v}^t \boldsymbol{\tau}_3 + \int_{\Gamma_{3,a}^+} dx \mathbf{v}^t \boldsymbol{\tau}_3 = -\rho\omega^2 \int_{A_a} dA_a \mathbf{v}^t \mathbf{u} \end{aligned} \quad (2.16)$$

Here, the differential operator $\underline{\underline{\nabla}}$ reduced to two dimensions, has the explicit form:

$$\underline{\underline{\nabla}} = N_1 \partial x + N_3 \partial z. [11]$$

2.4.2 Discretization of Eq. (2.16) as Applied to the Master Square

Consider an arbitrarily-located rectangularly-shaped elastic body with sides being parallel to the (x, z) -coordinate axes. With reference to the discussion in Appendix 2.8.1, such a quadrangle can be transformed (translated) to the master square positioned at the center of the (ξ, ζ) -coordinate system, Eq. (2.16) becomes:

$$\begin{aligned}
& - \int_{\square} d\xi d\zeta a_2 c_2 \left[\frac{1}{a_2} \partial_{\xi} \tilde{\mathbf{v}}^t \right] \mathbf{N}_1^t \mathbf{C} \tilde{\underline{\underline{\mathbf{V}}}} \tilde{\mathbf{u}} - \int_{\tilde{\Gamma}_{3,a}^-} d\xi a_2 \tilde{\mathbf{v}}^t \tilde{\boldsymbol{\tau}}_3 \\
& - \int_{\square} d\xi d\zeta a_2 c_2 \left[\frac{1}{c_2} \partial_{\zeta} \tilde{\mathbf{v}}^t \right] \mathbf{N}_3^t \mathbf{C} \tilde{\underline{\underline{\mathbf{V}}}} \tilde{\mathbf{u}} + \int_{\tilde{\Gamma}_{3,a}^+} d\xi a_2 \tilde{\mathbf{v}}^t \tilde{\boldsymbol{\tau}}_3 \\
& = -\rho\omega^2 \int_{\square} d\xi d\zeta a_2 c_2 \tilde{\mathbf{v}}^t \tilde{\mathbf{u}}
\end{aligned} \tag{2.17}$$

Quantities carrying a tilde refer to the transformed variables in (ξ, ζ) -coordinate system. In particular, $\tilde{\mathbf{u}}$ stands for the displacement vector with the components $\tilde{u}_1(\xi, \zeta)$ and $\tilde{u}_3(\xi, \zeta)$:

$$\tilde{\mathbf{u}} = \begin{bmatrix} \tilde{u}_1(\xi, \zeta) \\ \tilde{u}_3(\xi, \zeta) \end{bmatrix} \tag{2.18}$$

The scalar functions $\tilde{u}_i(\xi, \zeta)$ ($i = 1, 3$) can be expressed in terms of the complete set of orthonormal basis functions $B_{l,n}(\xi, \zeta)$ (refer to Appendix 2.8.3 for details).

For $\tilde{u}_1(\xi, \zeta)$, e.g., by keeping a finite number of expansion terms, we have:

$$\tilde{u}_1(\xi, \zeta) \approx \sum_{l=0}^L \sum_{n=0}^N u_{l,n}^{(1)} B_{l,n}(\xi, \zeta) \tag{2.19}$$

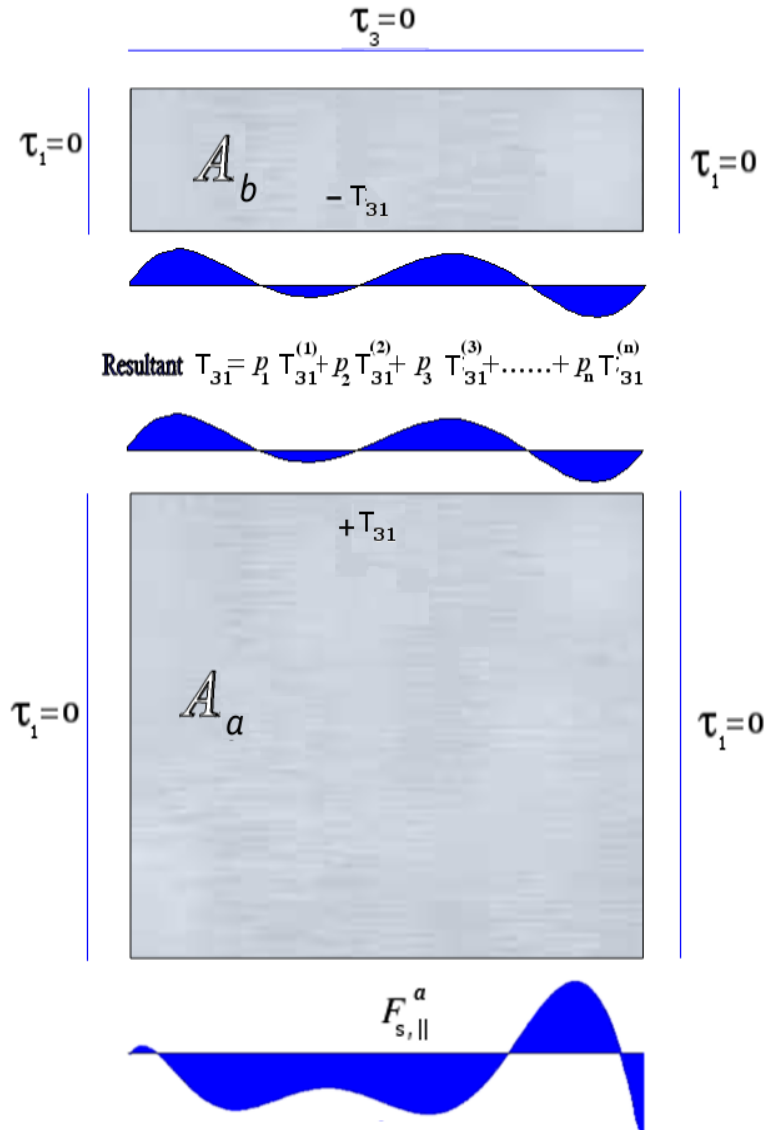


Figure 2.4: An example showing the separation of the composite structure shown in Fig. 2.3 into two solid bodies by introducing equivalent traction forces on the interface. In this problem body “a” is considered as a two-port quadrangle, while body “b” is a one-port quadrangle

For brevity, the spatial variables ξ and ζ in $B_{l,n}(\xi, \zeta)$ will be suppressed in the remaining discussion. A similar series expansion can be written for $\tilde{u}_3(\xi, \zeta)$. Employing matrix notation, and introducing the $2 \times [2 \times (L + 1) \times (N + 1)]$ matrix \mathbf{B} and $2 \times (L + 1) \times (N + 1)$ vector \mathbf{U} , we can write:

$$\tilde{\mathbf{u}} \approx \begin{bmatrix} \cdots & B_{l \odot n} & \cdots \\ \cdots & 0_{l \odot n} & \cdots \\ \cdots & 0_{l \odot n} & \cdots \\ \cdots & B_{l \odot n} & \cdots \end{bmatrix} \begin{bmatrix} \vdots \\ u_{l \odot n}^{(1)} \\ \vdots \\ \vdots \\ u_{l \odot n}^{(3)} \\ \vdots \end{bmatrix} \quad (2.20a)$$

$$= \mathbf{B}\mathbf{U} \quad (2.20b)$$

Here, the symbol $l \odot n$ refers to the arrangement of the indices in the following form: $[(0, 0), (0, 1), \dots, (0, N), (1, 0), \dots, (L, N)]$. The matrix \mathbf{B} accommodates the basis functions, and the vector \mathbf{U} comprises the unknown expansion coefficients, as indicated in the transition from Eq. (2.20a) to Eq. (2.20b).

On elaborating the integrals in Eq. (2.17), the first and third terms result in the “stiffness” matrix \mathbf{K} , whereas the term at the RHS leads to the “mass” matrix \mathbf{M} . Using Eq. (2.20b) and letting \mathbf{B} , represent (\iff) the known weighting function \mathbf{v} (with components v_1 and v_3), we obtain

$$\begin{aligned} a_2 c_2 \int_{\square} d\xi d\zeta \tilde{\mathbf{v}}^t \tilde{\mathbf{u}} &\iff a_2 c_2 \int_{\square} d\xi d\zeta \mathbf{B}^t \mathbf{B} \mathbf{U} \\ &= a_2 c_2 \mathbf{I} \mathbf{U} = \mathbf{M} \mathbf{U} \end{aligned} \quad (2.21)$$

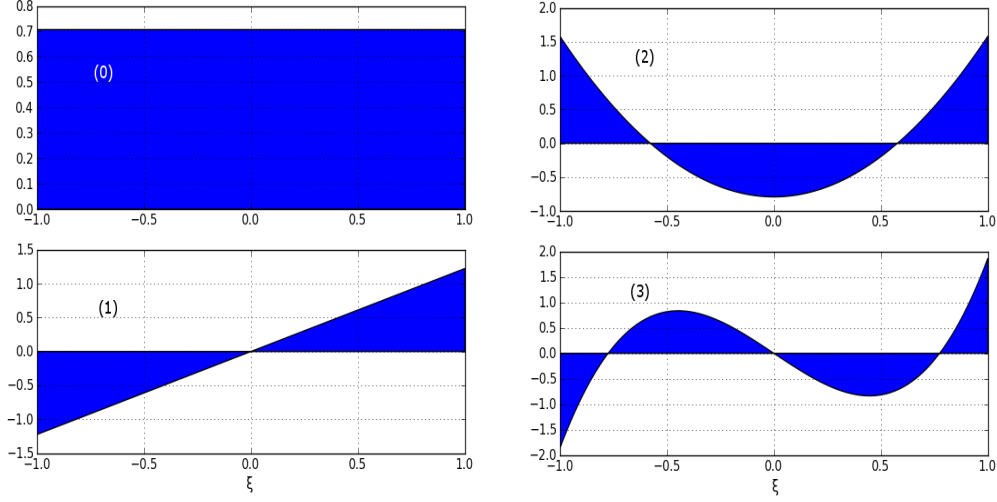


Figure 2.5: Distributive Elementary Sources: $b_0(\xi)$ (upper left), $b_1(\xi)$ (lower left), $b_2(\xi)$ (upper right) and $b_3(\xi)$ (lower right)

for the mass matrix \mathbf{M} . In the second transition, in Eq. (2.21), we used $\int_{\square} d\xi d\zeta \mathbf{B}^t \mathbf{B} = \mathbf{I}$, (with \mathbf{I} being the identity matrix of appropriate dimension) a fact which is the manifestation of orthonormality property of the basis functions (refer to Appendix 2.8.3). The $\tilde{\boldsymbol{\tau}}_3$ in the second integral at the LHS of Eq. (2.17) constitutes the imposed “traction force” vector which can be conveniently symbolized in the following manner:

$$\int_{\tilde{\Gamma}_{3,a}^-} d\xi a_2 \tilde{\mathbf{v}}^t \tilde{\boldsymbol{\tau}}_3 \iff \begin{bmatrix} \mathbf{F}_{31} \\ 0 \end{bmatrix}_{\tilde{\Gamma}_{3,a}^-} = \mathbf{F}_{3,a}^- \quad (2.22)$$

Note that 0-augmentation of the $(L+1) \times (N+1)$ vector, to $\mathbf{F}_{31}|_{\tilde{\Gamma}_{3,a}^-}$ is required since any general excitation force acting on any of the four boundary surfaces of the quadrangle “ a ” ought to be $2 \times (L+1) \times (N+1)$ dimensional.

Remark: In Eqs. (2.21) and (2.22) we encounter one- and two dimensional integrals of matrices, which we denote, for the sake of brevity, by $\int d\boldsymbol{\varkappa}\mathbf{A}$. In our formulation $\int d\boldsymbol{\varkappa}\mathbf{A}$ is interpreted as a matrix, the entries of which are the integrals of the respective matrix elements: $\int d\boldsymbol{\varkappa}\mathbf{A} = [\int d\boldsymbol{\varkappa}A_{i,j}]$. (For details of calculations refer to the Appendix 2.8.3.)

Summarizing our results Eq. (2.17), describing the quadrangle “a,” reads:

$$[\mathbf{K} - \rho\omega^2\mathbf{M}]_a U_a = -\mathbf{F}_{3,a}^- + \mathbf{F}_{3,a}^+ \quad (2.23)$$

The term $\mathbf{F}_{3,a}^+$ corresponds to the fourth term at the LHS in Eq. (2.17). A similar set of equations can be set up for the quadrangle “b” *mutatis mutandis*:

$$[\mathbf{K} - \rho\omega^2\mathbf{M}]_b U_b = -\mathbf{F}_{3,b}^- \quad (2.24)$$

Solving Eqs. (2.23) and (2.24) for the given set of distributed elementary source functions for each individual vector components of the traction force $\boldsymbol{\tau}_i$, results in the expansion coefficients U_a and U_b of the dyadic Green’s functions, (\mathcal{GF} s) which uniquely specify the quadrangles “a” and “b,” respectively.

2.5 The Concept of Distributed Elementary Sources and $\mathcal{GF}s$

Given a BVP, Green's functions are conventionally defined as responses of the medium to elementary excitations. Thereby, Dirac's delta function excitations are considered - a fact which has rendered Green's functions the name tag "impulse responses." Isolated localized excitation forces result in Green's functions which are generally but not always singular. The Green's function singularities can be strong or hyper strong a fact which hampers the accuracy of numerical results achievable. Consequently, considerable attention for the regularization of the singularities is required [11]. By utilizing distributed sources we eliminate this problem.

2.5.1 Distributed Elementary Sources

We assume distributed elementary sources (the components of the traction forces) to be any of the basis functions $b_n(\xi)$ $n \in \mathcal{N}_0$, with $b_n(\xi)$ being a polynomial of order n . The first four lowest order sources are shown in Fig. 2.5. For two-dimensional (factorized) basis-functions, e.g., $B_{l,n}(\xi, \zeta) = b_l(\xi)b_n(\zeta)$ evaluated at the boundary, we write, $B_{l,n}(\text{const}, \zeta) = \alpha_l b_n(\zeta)$ and $B_{l,n}(\xi, \text{const}) = \gamma_n b_l(\xi)$ with α_l being the value of $b_l(\xi = \text{const})$ and γ_n being the value for $b_n(\zeta = \text{const})$.

2.5.2 Proposed \mathcal{GF} s and Solution to Two-port/One-port Interface Problem

Before delving into the discussion of the numerical results it is imperative to clearly point out what is new in this chapter. This seems necessary not only to position our method relative to existing techniques but also to help the reader to have a better understanding of the proposed concept. The idea of domain decomposition and equivalent forces in FEM and other numerical techniques is common place. To convey the essence of differences between our work and conventional techniques in engineering applications, it fully suffices to limit ourselves to scalar-valued sources and the corresponding responses (scalar Green's functions). Further below, the idea will be extended to vector-valued quantities; consequently DGFs will enter into our discussion. The introduced methodology utilizes (i) the superposition principle along with (ii) the concept of exhaustion.

Application of Superposition and Exhaustion Principle by Utilizing \mathcal{GF} s

At this stage we are prepared to communicate the “punch” of our technique and explain clearly how it allows to carrying out computations with enhanced accuracy by simultaneously reducing the order of the complexity (physics-based model-order-reduction, a notion which will be addressed in detail elsewhere). Once again refer to the composite structure in Fig. 2.3. The external force func-

tion $F_{s,\parallel}^a(x)$ excites the structure at a given frequency. Our goal is the determination of the displacement functions $u_1(x, z)$ and $u_3(x, z)$ in the entire structure comprising the quadrangles “ a ” and “ b ,” under the boundary conditions that the surfaces facing east, west and north are stress-free. Figure 2.4 shows the composite structure being segmented into two quadrangles by introducing stress distributions $T_{31}(x)$ and $T_{33}(x)$ (only $T_{31}(x)$ has been shown in the figure). Note that while $F_{s,\parallel}^a(x)$ is known, $T_{31}(x)$ and $T_{33}(x)$ are *a priori* unknown. We recognize the problem “ a ” as a two-port problem since, it exchanges acoustic energy with environment over the s (southern) and n (northern) ports. This consideration also justifies the problem “ b ” to be called a one-port problem.

We introduce a few further abbreviations to ease the discussion. The force acting at the southern port of “ a ” can be oriented in the x -direction or in the z -direction, denoted, respectively, by $F_{s,\parallel}^a(x)$ and $F_{s,\perp}^a(x)$. In the current case $F_{s,\parallel}^a(x)$ is the only excitation force ($F_{s,\perp}^a(x) \equiv 0$). Similarly at the northern port of “ a ” we have, $F_{n,\parallel}^a(x)$ and $F_{n,\perp}^a(x)$. Note that in general each of the four force functions defines an independent physically realizable BVP. Furthermore, with the help of the “superposition principle” each of these four force functions can be synthesized from, say, $(N + 1)$ basis functions $b_0(x), \dots, b_N(x)$. For example, the southern port can be excited by $F_{s,\parallel}^a(x) = b_i(x)$, $i \in \mathcal{N}_0$, with all other boundaries being stress free. Consecutively, by operating the remaining forces on southern and northern ports, we obtain a total $4 \times (N + 1)$ independent excitation problems.

Note that all the excitations are well-behaved because of their distributive nature. The solution to each excitation problem can be fully described in terms of the resulting displacement functions $u_1^a(x, z)$ and $u_3^a(x, z)$, leading to a total of $2 \times 4 \times (N + 1)$ response functions (\mathcal{GF} s). Each of these functions can be evaluated at the southern and northern port ($z = \text{const.}$) resulting in $2 \times 2 \times 4 \times (N + 1)$ x -dependent functions. The power of our technique manifests itself in the fact that each of these \mathcal{GF} s evaluated at the ports can be expressed in terms of $(N + 1)$ basis functions. (Remember, these responses are after all functions of x , defined on a finite support, which upon agreement, support $(N + 1)$ basis functions). Thus a total of $(N + 1) \times 2 \times 2 \times 4 \times (N + 1)$ numbers characterize any conceivable vibration of the quadrangle “ a ” as a result of the forces acting at the southern and northern ports at a given frequency (principle of exhaustion applied to the two-port problems in 2D). Similarly, for quadrangle “ b ” (one-port problem), we can argue in following way. Here, we have two types of forces, $F_{s,\parallel}^b(x)$ and $F_{s,\perp}^b(x)$, each of which can be expressed in terms of $(N + 1)$ basis functions, leading to $2 \times (N + 1)$ independent experiments. Each experiment leads to two responses $u_1^b(x, z)$ and $u_3^b(x, z)$, producing a total of $2 \times 2 \times (N + 1)$ functions. These functions need to be evaluated at the southern port of “ b ” resulting in $1 \times 2 \times 2 \times (N + 1)$ functions depending on x . Since each function can be expressed in terms of $(N + 1)$ basis functions, a total of $(N + 1) \times 1 \times 2 \times 2 \times (N + 1)$ numbers fully characterize the acoustic vibrations of the quadrangle “ b ,” at a given frequency.

Refocusing on the quadrangle “a,” we summarize our results as follows: $F_{s,\parallel}^a(x)$ being a given function, can be expressed in terms of basis functions $b_i(x)$ $i \in \mathcal{N}_0$, resulting in $(N + 1)$ known expansion coefficients $\alpha_{s,\parallel}^a(i)$. The northern forces $F_{n,\parallel}^a(x)$ and $F_{n,\perp}^a(x)$ are not given. However, $F_{n,\parallel}^a(x)$ and $F_{n,\perp}^a(x)$, can each be expressed in terms of $(N + 1)$ basis functions, resulting in the unknown expansion coefficients $\alpha_{n,\parallel}^a(i)$ and $\alpha_{n,\perp}^a(i)$, $i \in \mathcal{N}_0$. In view of the fact that the responses to the DES (i.e. \mathcal{GF} s) at the southern and northern ports are already available and expressed in terms of the aforementioned $16 \times (N + 1)^2$ numbers, we can describe the vibrational behaviors of quadrangle “a” i.e. $u_1^a(x, z)$ and $u_3^a(x, z)$ evaluated at the northern port by means of $(N + 1)$ known expansion coefficients $\alpha_{s,\parallel}^a(i)$ and $2 \times (N + 1)$ unknown expansion coefficients $\alpha_{n,\parallel}^a(i)$ and $\alpha_{n,\perp}^a(i)$. For the determination of the $2 \times (N + 1)$ expansion coefficients $\alpha_{n,\parallel}^a(i)$ and $\alpha_{n,\perp}^a(i)$ we need to consider acoustic energy exchange between the quadrangles “a” and “b” by accounting for the interface conditions (in the weak sense). This brings quadrangle “b” into the picture. Assume arbitrary forces $F_{s,\parallel}^b(x)$ and $F_{s,\perp}^b(x)$ are acting on the southern port of “b.” These sources are *a priori* unknown, but obviously can be synthesized from $b_i(x)$ $i \in \mathcal{N}_0$ by introducing the $2 \times (N + 1)$ expansion coefficients $\alpha_{s,\parallel}^b(i)$ and $\alpha_{s,\perp}^b(i)$. Availability of the stored $4 \times (N + 1)^2$ responses of the quadrangle “b,” allows us to describe the vibrational behaviors in terms of $2 \times (N + 1)$ unknown coefficients $\alpha_{s,\parallel}^b(i)$ and $\alpha_{s,\perp}^b(i)$, $i \in \mathcal{N}_0$. Matching $u_1^b(x, z)$ and $u_3^b(x, z)$ with $u_1^a(x, z)$ and $u_3^a(x, z)$, respectively, at the interface, generates $2 \times (N + 1)$ equations for the determinations of the $2 \times (N + 1)$ unknown

expansion coefficients $\alpha_{\parallel}(i)$ and $\alpha_{\perp}(i)$ $i \in \mathcal{N}_0$, with $\alpha_{\parallel}(i) = \alpha_{n,\parallel}^a(i) = \alpha_{s,\parallel}^b(i)$ and $\alpha_{\perp}(i) = \alpha_{n,\perp}^a(i) = \alpha_{s,\perp}^b(i)$. This completes our discussion of determining the dynamics of composite structures in terms of their reduced (collapsed on the boundary) \mathcal{GF} s, which are pre-calculated and stored as simple arrays of numbers.

2.6 Results and Discussions

2.6.1 Numerical Verification and Comparison with ANSYS: Eigenvalue Problem

A 2D master square consisting of an isotropic material (Aluminum) was considered as simulation domain in order to conduct eigenfrequency analysis in Fig. 2.6. The comparison is a testimony for the accuracy and efficiency of the proposed method in terms of computational resources required. The results shown in Fig. 2.6 are encouraging. Advantages of the utilized basis functions are plenty. The “system” matrix is sparse due to the orthogonality of the basis functions leading to moderate storage space requirements. Determination of the eigen-pairs for the test structures we studied, show acceleration of computations by a factor of 10 compared with the results obtained by commercially available packages. Despite the advantages concerning reduced storage space, and faster computation times, the main feature of our method is the utility of the tabulated \mathcal{GF} s. The results in the next sections shed light on this important property.

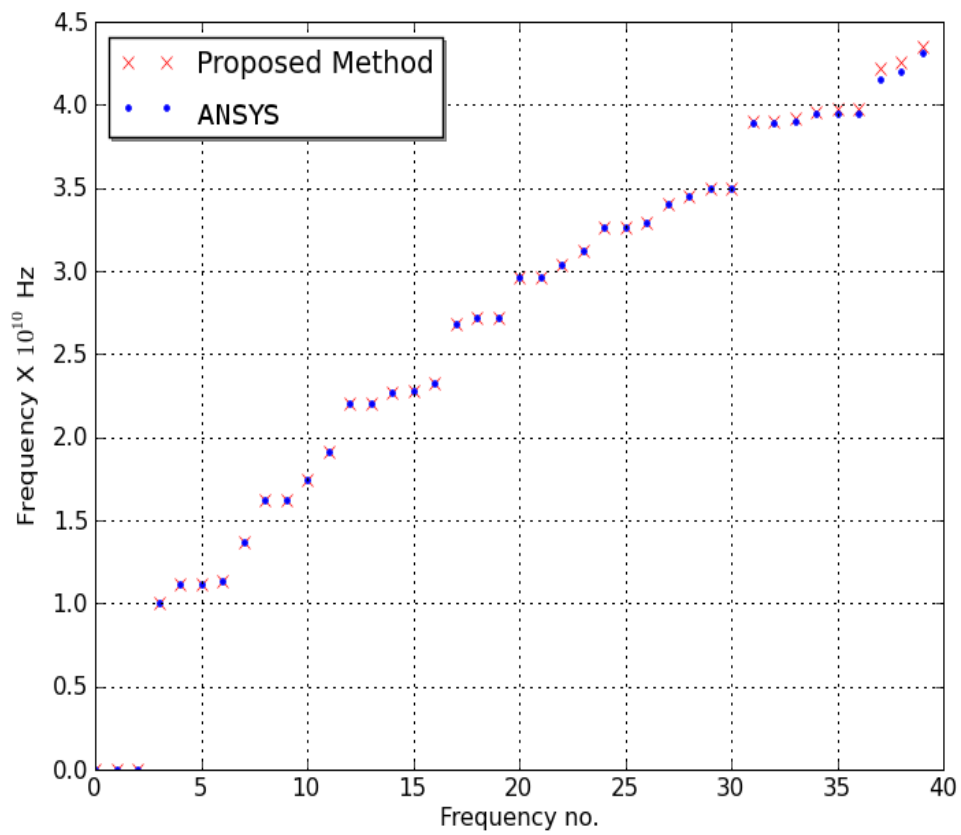


Figure 2.6: A comparison between eigenfrequencies obtained by the proposed method and the numerical results obtained by FEM package ANSYS

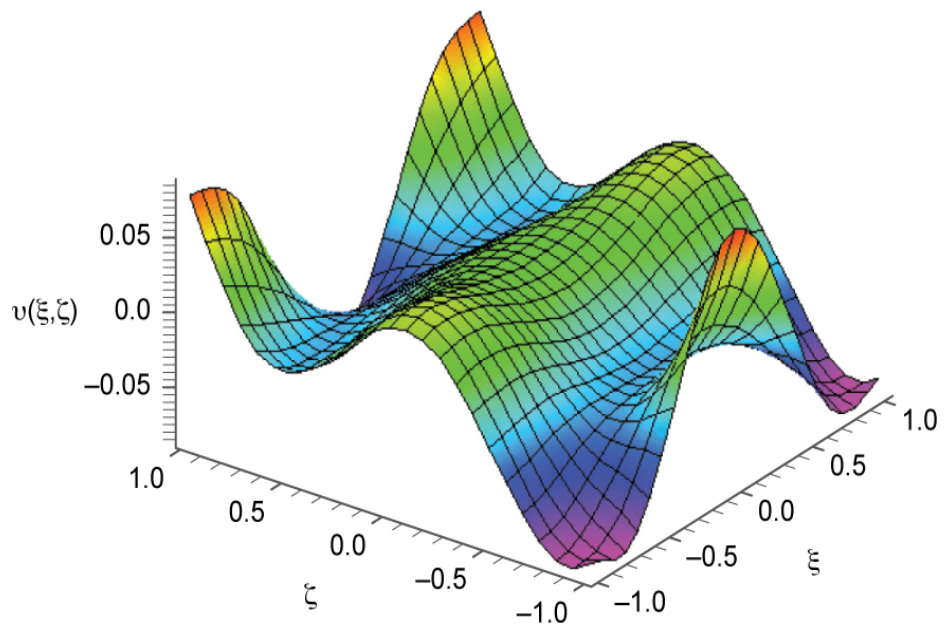


Figure 2.7: Displacement $u_1(\xi, \zeta)$, as a response to the force $b_0(\xi)$ acting at $\zeta = -1.0$

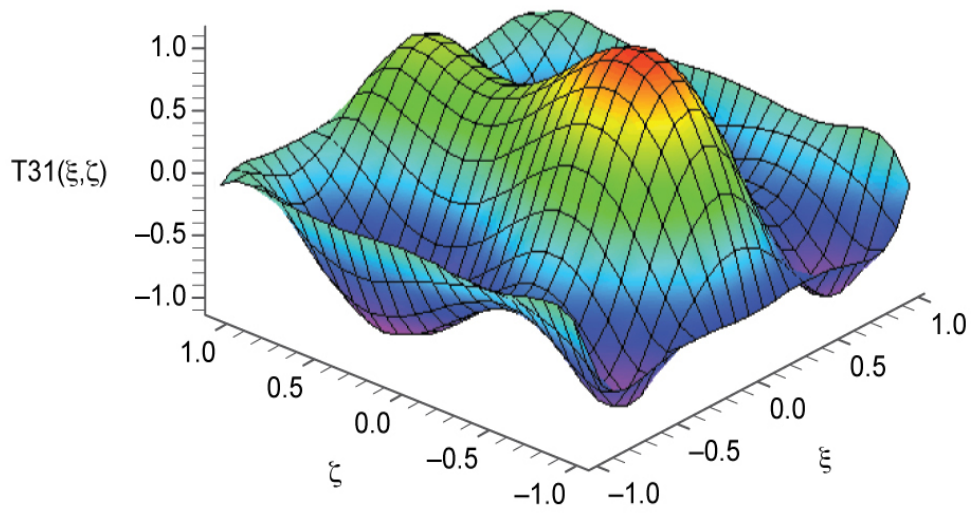


Figure 2.8: Associated stress distribution $T_{31}(\xi, \zeta)$ in response to the force $b_0(\xi)$ acting at $\zeta = -1.0$

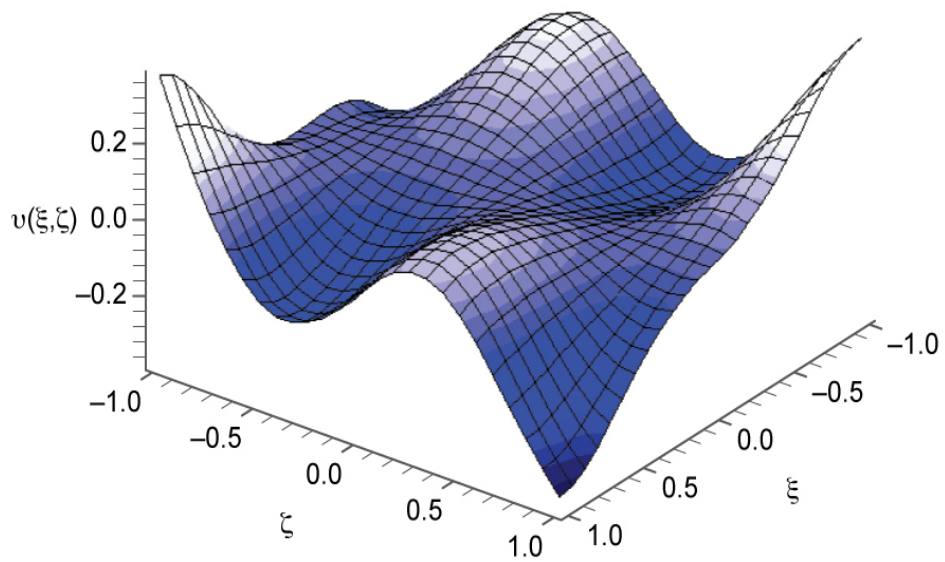


Figure 2.9: Displacement $u_1(\xi, \zeta)$, (in the figure, $v(\xi, \zeta)$) as a response to the force $b_1(\xi)$ acting at $\zeta = -1.0$

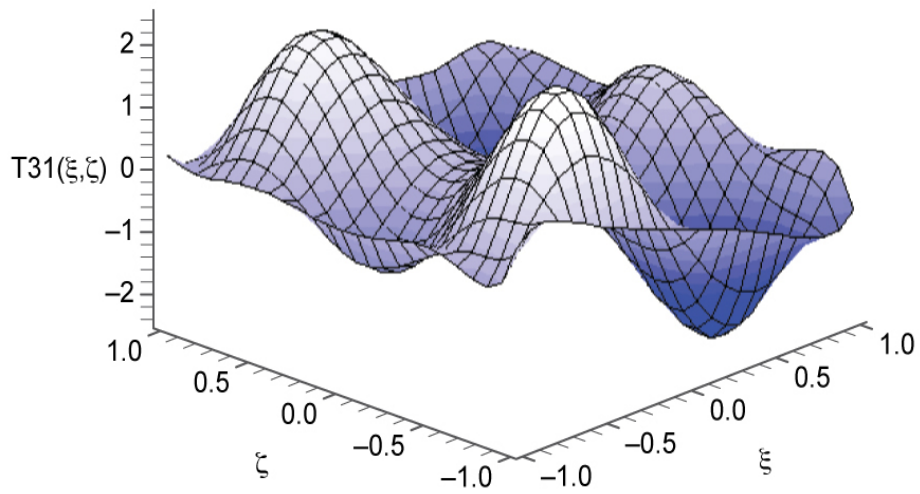


Figure 2.10: Associated stress distribution $T_{31}(\xi, \zeta)$ in response to the force $b_1(\xi)$ acting at $\zeta = -1.0$

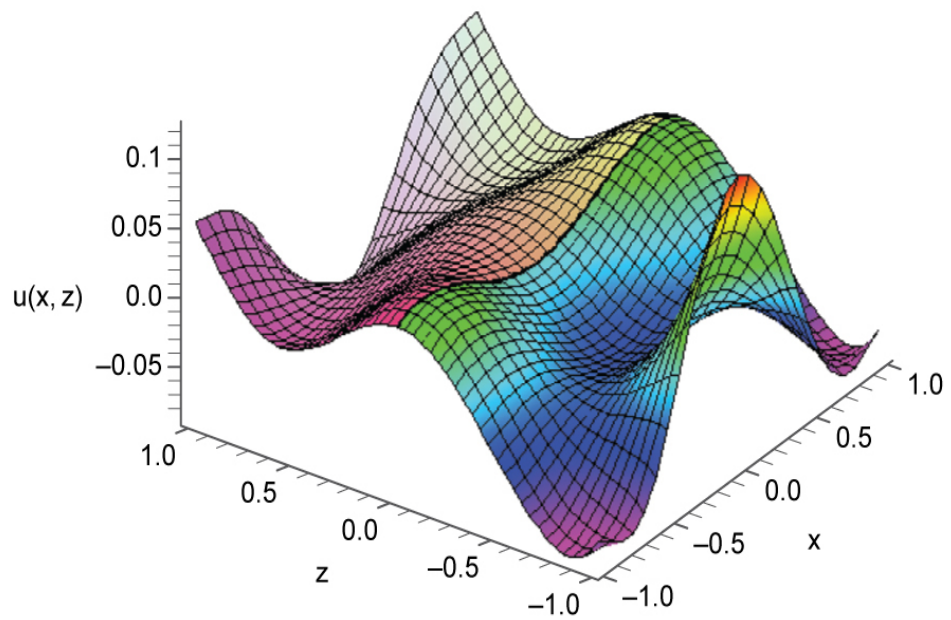


Figure 2.11: Matched displacement $u_1(x, z)$ (in the figure, $v(\xi, \zeta)$) for first DES applied at $z = -1.0$

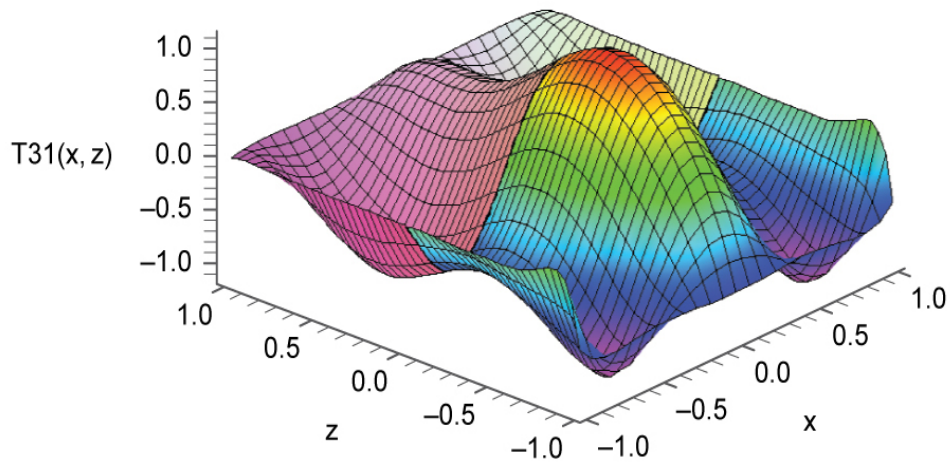


Figure 2.12: Corresponding matched stress component $T_{31}(x, z)$ derived from the matched displacement components

2.6.2 Application of Proposed \mathcal{GF} s: Enforced Problem

To demonstrate the applicability of the \mathcal{GF} s, consider the enforced problem as narrated in Fig. 2.4. The magnitude of the DESs are given in N/m^2 , with operating frequency being 2.01 GHz. The simulation domain models a massive elastic isotropic medium (aluminum), with the mass density $\rho = 2.77 \times 10^3 \text{kg/m}^3$ and the stiffness constants $C_{11} = 10.80 \times 10^{10} \text{N/m}^2$, $C_{44} = 2.85 \times 10^{10} \text{N/m}^2$ and $C_{12} = 5.10 \times 10^{10} \text{N/m}^2$.

Self-consistency Analysis of the Employed \mathcal{GF} s

Consider the master square in two dimensions extending from -1 to 1 in both ξ - and ζ - directions. We shall refer to the edge $\xi = -1$ the southern edge. In order to test the self-consistency of the developed and pre-calculated \mathcal{GF} s, we carried out a series of numerical experiments two of which are analyzed next.

1. *Experiment:* (i) Excite the southern edge by a force function $F_{s,\parallel}(\xi) = b_0(\xi)$, where $b_0(\xi)$ is as shown in Fig 2.5 (upper left) (ii) Compute the resulting displacements $u_1(\xi, \zeta)$ and $u_3(\xi, \zeta)$. Fig. 2.7 shows the function $u_1(\xi, \zeta)$. (iii) Calculate the associated stress distributions $T_{31}(\xi, \zeta)$ and $T_{33}(\xi, \zeta)$ from the computed $u_1(\xi, \zeta)$ and $u_3(\xi, \zeta)$. (iv) Evaluate the latter functions at the southern edge. (v) Examine how accurately the condition $T_{31}(\xi, -1) + F_{s,\parallel}(\xi) = 0$ and $T_{33}(\xi, -1) = 0$ are fulfilled. A glance at the Figs. 2.8 and 2.5 (upper left) shows that even a moderate

number of basis functions ensure the validity of the former condition, which is exemplified here.

2. *Experiment*: Figures 2.9 and 2.10 show the displacement- and stress distributions, respectively, for the case $F_{s,\parallel}(\xi) = b_1(\xi)$. As it is evident from Figs. 2.10 and 2.5 (lower left), the condition $T_{31}(\xi, -1) + F_{s,\parallel}(\xi) = 0$ is excellently satisfied.

Remark: In building our LIBRARY of \mathcal{GF} s, the consistency of the \mathcal{GF} s where tested for all elementary excitations relevant to our analysis.

Self-consistency Analysis of the Interface Problem

The following numerical experiment requires special attention due to its complexity. In this section we shall revisit the *First Experiment* from the previous section in order to reproduce the results depicted in Figs. 2.7 and 2.8 by utilizing a totally different procedure. (i) Consider the set up for the *First Experiment*. In particular note that $F_{s,\parallel}(x) = b_0(x)$. (ii) Subdivide the structure into two quadrangles (to get a better idea have a glance at Fig. 2.4). In our calculations, quadrangle “a” covers the area $-1 \leq x \leq 1$ and $-1 \leq z \leq 0$, and quadrangle “b” occupies the region $-1 \leq x \leq 1$ and $0 \leq z \leq 1$. This partitioning introduces the ‘fictitious’ interface $x = 0$. (iii) Consider quadrangle “a” as a two-port and quadrangle “b” as a one-port problem. (iv) Consecutively, transform each quadrangle into the master square and employ the LIBRARY of pre-calculated \mathcal{GF} s. (v) Utilizing the

methodology introduced in the body of solve the interface problem.

Figures 2.11 and 2.12, respectively, show the computed displacement- and stress functions. Obviously, these solutions should match those produced in Figs. 2.7 and 2.8. Excellent agreement achieved between the two solutions is an encouraging testimony for the validity of our proposed method.

Remark: A comprehensive series of numerical tests were carried out for composite structures involving isotropic/anisotropic- and anisotropic/anisotropic interfaces. Both 2D and 3D structures were considered. Invariably in all experiments we found encouraging results. Details of the latter experiments will be presented elsewhere. Here, it should be merely mentioned that the created LIBRARY is powerful enough to allow 2D and 3D mass-loading analysis in conventional, as well as, more exotic SAW and BAW structures.

2.7 Conclusion

We considered BVPs which typically arise in the analysis of the massloading problems in micro-acoustic devices. Letting appropriately-selected distributed forces act on the bounding surface of the medium under consideration, we introduced the notion of distributed-elementary-source self-regularized dyadic Green's functions denoted by \mathcal{GF} s. It was pointed out and numerically demonstrated that due to the employment of distributed sources, the resulting Green's functions are

automatically regularized. This property which results in well-conditioned system matrices is in contrast to conventionally constructed Green's functions which are ordinarily plagued with strong or hyper-strong singularities, requiring special attention for their regularization. We demonstrated that the information contents of \mathcal{GF} s and their spatial derivatives, evaluated at the boundary surface, can be efficiently and compactly stored in terms of a reasonable number of vectors, and conveniently retrieved for frequent future applications. Indeed the resulting long string of data "naturally" imposes itself as the DNA of the underlying BVPs. This analogy is further reinforced by the ability that the stored information (\mathcal{GF} s) fully suffices to solve all types of homogeneous and inhomogeneous boundary conditions (Dirichlet, Neumann) and interface condition. Utilizing pre-constructed basis functions we tested the applicability of the proposed technique against the professional software package ANSYS. An application of proposed \mathcal{GF} s to interface problem was also demonstrated.

Utilization of the constructed orthonormal polynomials enabled the calculation of derivatives and integrals in analytical form, making the computation efficient and amenable to parallel computing. Additional aspects of the proposed \mathcal{GF} s were also touched upon in recently published contributions [45, 46, 47]. A further favorable features of our technique will be elaborated in the forthcoming chapters.

2.8 Appendix

2.8.1 Affine Transformation to Master Coordinate System

Consider a function $g(x, z)$. Subjecting the Cartesian coordinates x and z to the transformations $x = x(\xi)$ and $z = z(\zeta)$, we can write

$$\begin{aligned} g(x, z) &= g(x(\xi), z(\zeta)) \\ &= b(\xi, \zeta). \end{aligned} \quad (2.25)$$

Additionally with the help of chain rule we have:

$$\begin{aligned} \frac{\partial g(x, z)}{\partial x} &= \frac{\partial \xi}{\partial x} \frac{\partial b(\xi, \zeta)}{\partial \xi} + \frac{\partial \zeta}{\partial x} \frac{\partial b(\xi, \zeta)}{\partial \zeta} \\ \frac{\partial g(x, z)}{\partial z} &= \frac{\partial \xi}{\partial z} \frac{\partial b(\xi, \zeta)}{\partial \xi} + \frac{\partial \zeta}{\partial z} \frac{\partial b(\xi, \zeta)}{\partial \zeta} \end{aligned} \quad (2.26)$$

In the case of linear transformations,

$$\begin{aligned} x(\xi) &= a_1 + a_2 \xi, \\ z(\zeta) &= c_1 + c_2 \zeta, \end{aligned} \quad (2.27)$$

the Eq. (2.26) can be cast in form:

$$\begin{bmatrix} \frac{\partial g(x, z)}{\partial x} \\ \frac{\partial g(x, z)}{\partial z} \end{bmatrix} = \begin{bmatrix} \frac{1}{a_2} & 0 \\ 0 & \frac{1}{c_2} \end{bmatrix} \begin{bmatrix} \frac{\partial b(\xi, \zeta)}{\partial \xi} \\ \frac{\partial b(\xi, \zeta)}{\partial \zeta} \end{bmatrix} \quad (2.28)$$

Consequently, Auld's operator $\underline{\underline{\nabla}}$ in 2D transforms as follows:

$$\begin{aligned}\underline{\underline{\nabla}} &= N_1 \partial x + N_3 \partial z \\ &= N_1 \left[\frac{1}{a_2} \partial_\xi \right] + N_3 \left[\frac{1}{c_2} \partial_\zeta \right] \\ &= \underline{\underline{\tilde{\nabla}}}\end{aligned}\tag{2.29}$$

Additionally, we have

$$\int_{A_1} dx dz = a_2 c_2 \int_{\square} d\xi d\zeta.\tag{2.30}$$

2.8.2 Normalization of Jacobi-Polynomials

Three types of orthogonal polynomials are dominant in the mathematical physics: Jacobi, Hermite and Laguerre. The Jacobi polynomials offer themselves as the natural choice for our problem since they are orthogonal on the finite interval $[-1,1]$. The Jacobi polynomials denoted by $P_n^{(\alpha,\beta)}(\varkappa)$, have been extensively used for mathematical analysis and implementation in spectral methods [48, 49, 50].

They are conveniently presented by the well-known Rodrigues formula:

$$\begin{aligned}P_n^{(\alpha,\beta)}(\varkappa) &= \frac{1}{2^n n!} (\varkappa - 1)^{-\alpha} (\varkappa + 1)^{-\beta} \\ &\quad \times \left(\frac{d}{d\varkappa} \right)^n \left[(\varkappa - 1)^{n+\alpha} (\varkappa + 1)^{n+\beta} \right]\end{aligned}\tag{2.31}$$

Here, the independent variable \varkappa represents any of the variables ξ, η or ζ in the Cartesian. The classical Jacobi polynomials associated with the parameters

$\alpha, \beta > -1$, are a sequence of polynomials $P_n^{(\alpha, \beta)}(\mathcal{X}) (n = 0, 1, 2, \dots)$, of degree n , satisfying the orthogonality relation

$$\int_{-1}^{+1} d\mathcal{X} g(\mathcal{X}) P_m^{(\alpha, \beta)}(\mathcal{X}) P_n^{(\alpha, \beta)}(\mathcal{X}) = \begin{cases} 0, & m \neq n, \\ h_n, & m = n, \end{cases}, \quad (2.32)$$

with the weighting function

$$g(\mathcal{X}) = (1 - \mathcal{X})^\alpha (1 + \mathcal{X})^\beta, \quad (2.33)$$

and

$$h_n = \frac{2^{\alpha+\beta+1} \Gamma(n + \alpha + 1) \Gamma(n + \beta + 1)}{(2n + \alpha + \beta + 1) n! \Gamma(n + \alpha + \beta + 1)}. \quad (2.34)$$

The Jacobi polynomials satisfy the recurrence relation

$$\begin{aligned} P_{n+1}^{(\alpha, \beta)}(\mathcal{X}) &= \frac{\alpha^2 - \beta^2 (2n + \alpha + \beta + 1) + (2n + \alpha + \beta)_3 \mathcal{X}}{2(n+1)(n + \alpha + \beta + 1)(2n + \alpha + \beta)} P_n^{(\alpha, \beta)}(\mathcal{X}) \\ &\quad - \frac{(n + \alpha)(n + \beta)(2n + \alpha + \beta + 2)}{(n+1)(n + \alpha + \beta + 1)(2n + \alpha + \beta)} P_{n-1}^{(\alpha, \beta)}(\mathcal{X}), \end{aligned} \quad (2.35)$$

with $(a)_3 = a(a+1)(a+2)$ and $a = 2n + \alpha + \beta$. In view of Eq. (2.32), the normalizing factor is given by $h_n^{1/2}$ for $P_n^{(\alpha, \beta)}(\mathcal{X})$. In particular, considering the special case $\alpha, \beta = 0$ in Eq. (2.35) (leading to Legendre polynomials), denoting the normalized version of $P_{n+1}^{(0,0)}(\mathcal{X})$ by $\tilde{P}_{n+1}^{(0,0)}(\mathcal{X})$, incorporating the normalized

factor $h_n = 2/(2n + 1)$ and rearranging terms in Eq. (2.35) we obtain:

$$\begin{aligned} \tilde{P}_{n+1}^{(0,0)}(\varkappa) = & \frac{2n+1}{n+1} \left(\frac{2n+3}{2n+1} \right)^{1/2} \varkappa \tilde{P}_n^{(0,0)}(\varkappa) \\ & - \frac{n}{n+1} \left(\frac{2n+3}{2n-1} \right)^{1/2} \tilde{P}_{n-1}^{(0,0)}(\varkappa) \end{aligned} \quad (2.36)$$

In particular, the first two normalized polynomials are

$$\tilde{P}_0^{(0,0)}(\varkappa) = 1/\sqrt{2} \quad \text{and} \quad \tilde{P}_1^{(0,0)}(\varkappa) = \sqrt{3/2}\varkappa. \quad (2.37)$$

2.8.3 Construction of Basis Functions

We utilized the classical Jacobi (Legendre) polynomials as our starting point for construction of the basis functions [46, 50].

Properties of the Set of Polynomials Used in This Analysis

In appendix 2.8.1, we incorporated the weighting function, $g(\varkappa) = (1-\varkappa)^\alpha(1+\varkappa)^\beta$ into the definition of the basis functions. Exhaustive testing with the various permissible values for α and β showed that the choice $\alpha = \beta = 0$ fully suffices for our purposes. Thus with

$$b_n(\varkappa) = b_n^{(0,0)}(\varkappa) = \hat{P}_n^{(0,0)}(\varkappa) \quad (2.38)$$

we have:

$$\int_{-1}^{+1} d\boldsymbol{x} b_n(\boldsymbol{x}) b_{\bar{n}}(\boldsymbol{x}) = \delta_{n,\bar{n}} \quad (2.39)$$

The construction procedure of orthonormal basis functions in two- and three dimensions is immediate: by simply multiplying 1D basis functions we obtain the desired 2D and 3D basis functions. More explicitly, for 2D case we have:

$$B_{l,n}(\xi, \zeta) = b_l(\xi) b_n(\zeta) \quad (2.40)$$

In view of Eqs. (2.39) and (2.40), the orthonormality condition reads:

$$\int_{\square} d\xi d\zeta B_{l,n}(\xi, \zeta) B_{\bar{l},\bar{n}}(\xi, \zeta) = \delta_{l,\bar{l}} \delta_{n,\bar{n}} \quad (2.41)$$

Calculating Derivatives of the Employed Basis Functions

From Eqs. (2.40) and (2.39) it follows that the daunting task involved in solving 2D BVPs can be essentially reduced to much simpler 1D analysis in each of the spatial directions. Thus it suffices to focus on the derivatives of 1D basis functions. Consider a set of $N + 1$ basis functions arranged to build a column vector:

$$\mathbf{b} = \left[b_0(\xi) \quad b_1(\xi) \quad \cdots \quad b_n(\xi) \quad \cdots \quad b_N(\xi) \right]^t \quad (2.42)$$

Since $b_n(\xi)$, $n \in \mathcal{N}_0$ is a polynomial of order n , Eq. (2.42) can be re-written as

$$\mathbf{b} = \begin{bmatrix} k_0^{(0)} & 0 & \cdots & 0 & \cdots & 0 & \cdots & 0 \\ k_0^{(1)} & k_1^{(1)} & \cdots & 0 & \cdots & 0 & \cdots & 0 \\ \vdots & \vdots & \cdots & \ddots & \cdots & \vdots & \cdots & \vdots \\ k_0^{(m)} & k_1^{(m)} & \cdots & k_n^{(m)} & \cdots & k_m^{(m)} & \cdots & 0 \\ \vdots & \vdots & \cdots & \vdots & \cdots & \vdots & \ddots & \vdots \\ k_0^{(N)} & k_1^{(N)} & \cdots & k_n^{(N)} & \cdots & k_m^{(N)} & \cdots & k_N^{(N)} \end{bmatrix} \boldsymbol{\xi}, \quad (2.43)$$

with, $\boldsymbol{\xi} = [\xi^0 \ \xi^1 \ \cdots \ \xi^n \ \cdots \ \xi^N]^t$, and $m, n \in \mathcal{N}_0$. Denoting the derivative of \mathbf{b} with respect to ξ by \mathbf{b}' we have

$$\mathbf{b}' = \begin{bmatrix} 0 & 0 & \cdots & 0 & \cdots & 0 & \cdots & 0 \\ \kappa_0^{(1)} & 0 & \cdots & 0 & \cdots & 0 & \cdots & 0 \\ \vdots & \ddots & \cdots & \vdots & \cdots & \vdots & \cdots & \vdots \\ \kappa_0^{(m)} & \cdots & \kappa_{n-1}^{(m)} & \cdots & \kappa_{m-1}^{(m)} & 0 & \cdots & 0 \\ \vdots & \cdots & \vdots & \cdots & \vdots & \ddots & \cdots & \vdots \\ \kappa_0^{(N)} & \cdots & \kappa_{n-1}^{(N)} & \cdots & \kappa_{m-1}^{(N)} & \cdots & \kappa_{N-1}^{(N)} & 0 \end{bmatrix} \boldsymbol{\xi} \quad (2.44)$$

where, $\kappa_n^{(m)} = (n+1)k_{n+1}^{(m)}$, $m \in \mathcal{N}$ and $n = 0, \dots, m-1$.

Calculating Definite Integrals Involving the Elements of \mathbf{b} and \mathbf{b}'

For efficiently calculating integrals of the products $b_m(\xi)b'_n(\xi)$ we first need to cast products of this form in a symbolically more tractable fashion:

$$b_m(\xi)b'_n(\xi) = \begin{bmatrix} k_0^{(m)} \\ k_1^{(m)} \\ \vdots \\ k_m^{(m)} \end{bmatrix} \otimes \begin{bmatrix} \kappa_0^{(n)} \\ \kappa_1^{(n)} \\ \vdots \\ \kappa_{n-1}^{(n)} \end{bmatrix} : \begin{bmatrix} \xi^0 \\ \xi^1 \\ \vdots \\ \xi^m \end{bmatrix} \otimes \begin{bmatrix} \xi^0 \\ \xi^1 \\ \vdots \\ \xi^{n-1} \end{bmatrix} \quad (2.45)$$

The symbols \otimes and $:$ have to be interpreted as follows: Let \mathbf{p} and \mathbf{q} stand for two column vectors with the components p_0, p_1, \dots, p_m and q_0, q_1, \dots, q_{n-1} , respectively. The exterior product $\mathbf{p} \otimes \mathbf{q}$ is defined as $\mathbf{p} \otimes \mathbf{q} = \mathbf{p}\mathbf{q}^t$. Next, let \mathbf{P} and \mathbf{Q} be two $(I + 1) \times (J + 1)$ matrices with the components $P_{i,j}$ and $Q_{i,j}$. The symbol $\mathbf{P} : \mathbf{Q}$ is defined as $\mathbf{P} : \mathbf{Q} = \sum_{i=0}^I \sum_{j=0}^J P_{i,j} Q_{i,j}$. Based on these conventions the expression $\mathbf{p} \otimes \mathbf{q} : \mathbf{r} \otimes \mathbf{s} = \mathbf{P} : \mathbf{Q}$, (Note that \otimes precedes $:$). Integrating both sides of Eq. (2.45) with respect to ξ from -1 to 1 results in:

$$\int_{-1}^{+1} d\xi b_m(\xi) b'_n(\xi) = \mathbf{k} \otimes \boldsymbol{\kappa} : \int_{-1}^{+1} d\xi \begin{bmatrix} \xi^0 \\ \xi^1 \\ \vdots \\ \xi^i \\ \vdots \\ \xi^m \end{bmatrix} \otimes \begin{bmatrix} \xi^0 \\ \xi^1 \\ \vdots \\ \xi^j \\ \vdots \\ \xi^{n-1} \end{bmatrix} \quad (2.46)$$

Here, \mathbf{k} and $\boldsymbol{\kappa}$, respectively, stand for the first and the second vectors at the RHS of Eq. (2.45). Interpreting \otimes and $:$ as described above and

$$\int_{-1}^{+1} d\xi \xi^{i+j} = \begin{cases} \frac{2}{i+j+1} & \text{for } i+j \text{ even,} \\ 0 & \text{for } i+j \text{ odd,} \end{cases} \quad (2.47)$$

we can determine the results for 1D case. Results for 2D and 3D can be obtained, with virtually no additional computational cost.

Chapter 3

2D Elastodynamic Simulation of Fully-anisotropic Elastic Media Using Self-regularized Dyadic Greens Functions

3.1 Introduction

Micro-acoustic devices involve anisotropic elastic substrates which are typically loaded by a large number of massive metallic electrodes or anisotropic elastic bodies to achieve desirable device characteristics [7, 43]. The presence of the large number of electrodes (several hundreds to a few thousands) in modern devices makes simulation of these devices a herculean task. Additional challenges are due to the extremely high precision of the numerical results required in simulations.

These requirements have prompted the development of customized numerical techniques. The Surface Integral Modeling (SIM) technique for wave propagation problems has been known for quite some time to the micro-acoustic device community. Thereby, particular effort has been devoted to the study of mass-loading effects due to massive electrodes. Approximate numerical solutions to a given system of Partial Differential Equations (PDEs) have traditionally have been obtained by means of Boundary Element Method (BEM), Finite Element Methods (FEM), Finite Difference Methods (FDM), spectral methods in various realizations, or by hybridizing any of these methods [10, 11, 51, 52, 53]. The limitations of BEM, FEM and FDM are widely known. Although, FEM and FDM are straight forward to implement, they are generally not amongst the most accurate techniques. Shortcomings of the methods are well documented in the literature ([54, 55] and references therein). As a general rule, in case of FEM, higher accuracy in the solutions requires denser discretization (finite element meshing). However, with increased mesh refinement, the process of mesh generation, assembly and solving becomes excessively expensive in terms of computational resources. Moreover, the analysts are faced with challenges related to large deformation, low frequency analysis, interpolation errors, and inaccuracy in calculating secondary (derived) variables such as stress and strain, over primary variables, such as displacements. Other major difficulties include instability with respect to changes in material properties, numerical dispersion, and the treatment of boundary conditions. Various alternative methods are opted in order to overcome these

shortcomings. Variations of classical techniques such as spectral methods and comparatively recently developed methods such as meshless methods including, Element-free Galerkin method, Meshless local Petrov-Galerkin method, Point interpolation method, etc. have generated much interest [56, 57, 58, 59, 60]. The finite element approach of substructuring, and domain decomposition methods have also found their prominent places in literature [33, 61, 62]. The main advantage of these techniques over the traditional methods is the reduction of amount of time taken in solving the involved system of equations. The prime reason for this is that substructuring and domain decomposition methods permit taking advantage of parallel computing capabilities.

On the other hand, BEM is generally viewed as the most powerful method amongst the above mentioned analysis techniques, in particular in terms of achievable accuracy [63, 64]. However, BEM is accompanied by a number of drawbacks:

- 1) Problem-specific Green's functions need to be constructed - a task which is not trivial in the case of anisotropic media, due to the lack of closed-form expressions.
- 2) The associated surface integrals become singular when calculating the "interaction" of an element on the boundary with itself (self-action), or with nearby elements.
- 3) The numerical calculation of the involved highly oscillating and/or slowly decaying Fourier-type integrals presents a challenge. This is often the case when mutual interaction of two nearby boundary elements are computed.
- 4) In BEM, the system matrices are *dense matrices* as opposed to *band matrices*

appearing in FEM; thus rapidly exhausting computational resources. For moderately complex structures, the number of unknowns can easily exceed several millions, due to the desired accuracy of the solutions. Any changes made to material parameters or geometric specifications, or varying the operating frequency, necessarily mean re-calculating millions of unknowns. Thus, the traditional numerical methods based on the FEM, BEM, or a combination of both, lack the desired flexibility in producing pre-calculated data and storing them in a LIBRARY for frequent future usage in device design cycles. Ordinarily, the creation of a LIBRARY is regarded as a challenging task because the displacement- and stress distributions are in general strongly frequency dependent. The method of attaching and detaching two or more domains has increasingly gained significance in the last two decades [30, 32, 33, 37]. The methods which have been particularly making their mark are domain decomposition and dynamic substructuring methods. Thereby, various iterative or direct procedures have been proposed in order to ensure the continuity between the subdomains. The general approach in the case of dynamic substructuring is to conserve energy when traversing the interfaces. Where, the iterative techniques such as Penalty-based formulation, Lagrange multipliers, mortar element method, interface element etc., utilized in domain decomposition coupling and substructuring, have particularly gained popularity. Furthermore, in recent works a general approach of hybridization of different methods e.g. FEM/BEM/Spectral Methods FEM/Element-Free Galerkin methods/meshfree methods along with further refined task-sharing strategies have

become necessary in order to utilize each method optimally [26, 65]. Prior to delving into the details, it is perhaps instructive to highlight what is new in this contribution to position it into the context of the existing methods.

<i>Symbols</i>	<i>Description</i>
$\underline{\nabla}$	Auld's 6×3 divergence-type differential operator, [1]
$\underline{\mathbf{N}}_i$	Scaffolding matrices identified in $\underline{\nabla}$ [11]
ρ	Mass density
\mathbf{C}	6×6 Stiffness matrix
ω	Operating frequency
$\tilde{\mathbf{U}}$	Given displacement function evaluated on the boundary
$\tilde{\mathbf{F}}$	Given traction force evaluated on the boundary
\mathbf{u}	Mechanical displacement vector
\mathbf{v}	Test vector
$(\cdot)^t$	Transposition operator
$\boldsymbol{\tau}_i$	$\mathbf{N}_i^t \mathbf{T}$, $i = 1, 2, 3$, stress tensor
Ω	Volume of the 2D medium
Γ	Boundary line of 2D medium
\mathcal{N}_0	The set of numbers $0, 1, \dots, N$
$f \iff F$	F is a discrete representation of the continuum entity f
<i>SAW</i>	Surface Acoustic Wave
<i>BAW</i>	Bulk Acoustic Wave
<i>FEM</i>	Finite Element Method
<i>BEM</i>	Boundary Element Method
<i>DES</i>	Distributed Elementary Source
<i>SR</i>	Self-regularized
<i>DGFs</i>	Dyadic Green's Functions
\mathcal{GF}_s	Distributed-Elementary-Source Self-regularized Dyadic Green's Functions
<i>SIM</i>	Surface Integral Method

Table 3.1: Main symbols and abbreviations used in this manuscript

Novelties presented in this chapter: A novel approach for tearing and interconnecting fully-anisotropic elastic media has been proposed. The method contains distinguished characteristics which can be summarized as follows:

1. The given geometry is first divided into rectangularly formed macro-quadrangles. The resulting quadrangles are then detached by introducing equivalent Distributed-Elementary-Sources.
2. Individual Distributed-Elementary-Sources associated with a given anisotropic quadrangle, and operating at a specific frequency, result in Distributed-Elementary-Source Self-regularized Dyadic Green's Functions (\mathcal{GF} s).
3. The usage of Distributed-Elementary-Sources "naturally" ensures that the singularities associated with the Green's functions are inherently regularized (self-regularized).
4. The proposed method applies equally well to 2D- or 3D boundary value problems (BVPs).
5. The method can easily tackle Dirichlet-, and Neumann boundary conditions, as well as, interface condition in a unified form. In particular, the Dirichlet boundary- and interface conditions are treated in an unconventional manner, enhancing efficiency, conceptually and computationally.
6. The Principles of Exhaustion and Sufficiency have been introduced and implemented to solve different types of boundary- and interface conditions in a unified form.
7. A proposition has been made for physics-based Model-Order-Reduction and implemented in the process of constructing and storing the self-regularized

dyadic Green's functions.

8. A test quadrangle has been analyzed utilizing \mathcal{GF} s from the generated LIBRARY and the numerical results are compared with the reference results, obtained by a standard FEM simulation package.

In addition to the above features, the proposed method also exhibits further favorable properties for simulation of proposed \mathcal{GF} s. The employed basis- and testing functions, constitute a set of smooth functions, ensuring smooth and easily - calculable derivatives. Moreover, the supports of these analyzing and synthesizing functions range over the entire simulation domain, without having any nodal points as it is conventionally the case in FEM or Element-free methods. This property renders the proposed method, purely meshless. Thereby, in constructing \mathcal{GF} s, the integrals are derived in a closed-form over the entire range with virtually no additional computational cost. Furthermore, the distributed nature of the analyzing- and synthesizing functions guarantees that there are no singularities in the involved integrands. The resulting system matrices, constructed with the help of orthonormal basis- and testing functions, consequently become *sparse*, a property which not only reduces the storage space but also accelerates computations significantly. Lastly, since each quadrangle is detached and treated individually the simulation is amenable to the parallel computing.

The chapter is organized as follows: The presentation begins with the geomet-

rical sub-sectioning of the simulation domain and discussing the types of basic quadrangles involved. Next a weak formulation is presented for two dimensional (2D) basic quadrangle. The discussion then focuses on explaining the involved Distributed-Elementary-Source Self-regularized Dyadic Green's Functions (\mathcal{GF} s). The \mathcal{GF} s are then applied to test problems emphasizing different types of boundary conditions. The numerical results obtained show the successful application of the proposed \mathcal{GF} s to a multi-domain test quadrangles, by comparing the numerical results against the data obtained from a commercially available FEM simulation package. Utilizing the \mathcal{GF} s from the generated LIBRARY, the chapter concludes with an analysis of the interface problem involving fully-anisotropic quadrangles.

3.2 Statement of the Problem

The development of a computational method for interfacing and interconnecting fully-anisotropic elastic media by utilizing pre-computed Self-regularized Dyadic Green's Functions in two dimensions.

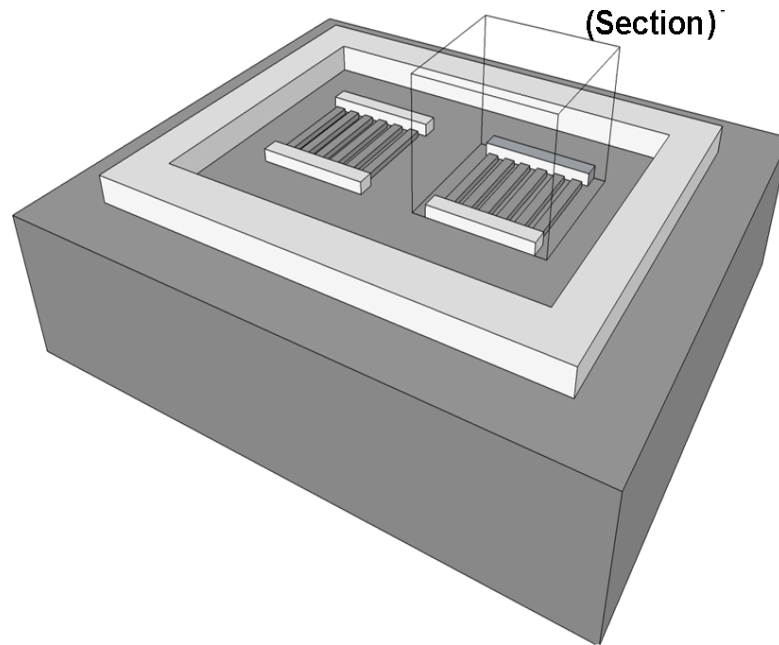


Figure 3.1: A simplified artistic view of typical SAW device geometry

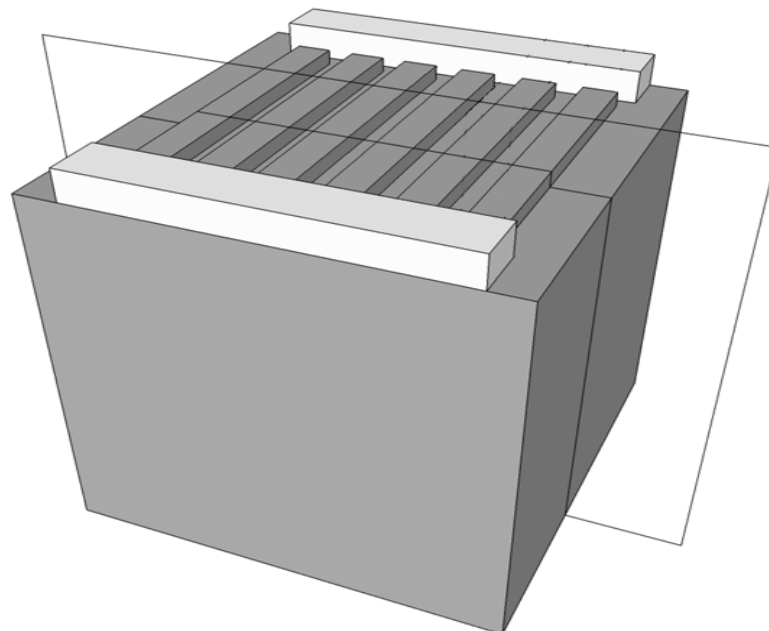


Figure 3.2: Example showing the cross-section of the device geometry

3.3 Construction of the Proposed Distributed-Elementary-Source Self-regularized Dyadic Green's Functions

3.3.1 Partitioning of Simulation Domain

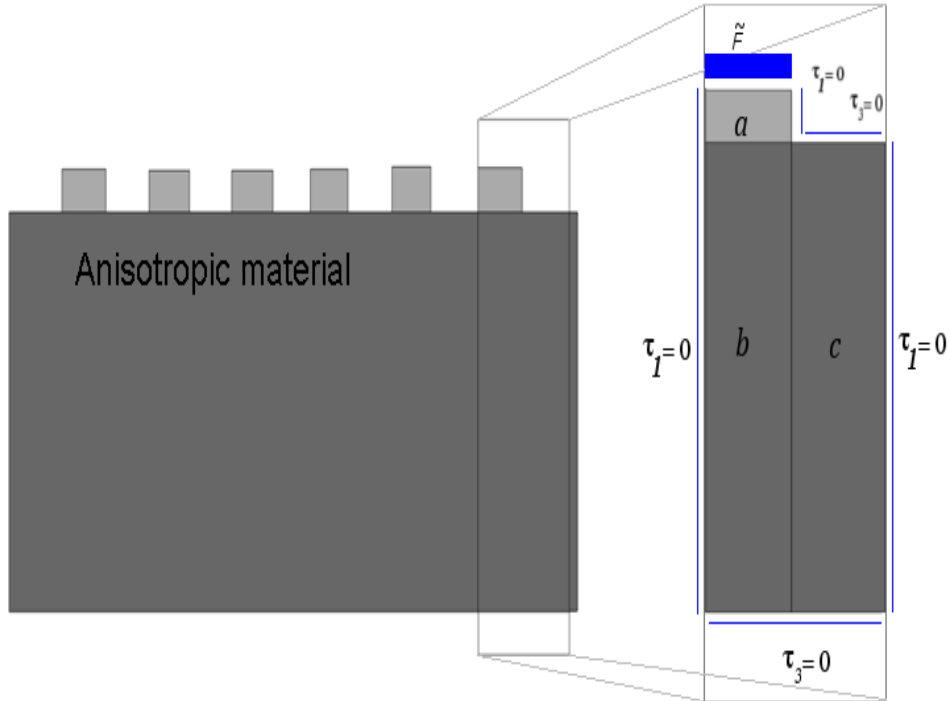


Figure 3.3: Discretization of 2D fully-anisotropic test problem

One of the key features of the proposed SIM technique is the method of the sub-sectioning of the geometry. Consider the geometry of a typical SAW device sketched in Fig. 3.1. The geometry consists of an anisotropic substrate; in majority of cases substrate loaded by a large number of massive metallic (isotropic) electrodes and busbars. In some design realizations the electrodes and the bus-

bars are circumferenced by a protective massive wall structure, as sketched in the figure. Strictly speaking, the structure shown in Fig. 3.1, together with the surrounding media (which may just be free space) defines the simulation domain. Reference to free space is necessary since a more rigorous theory needs also to include effects associated with the piezoelectricity property of the substrate material. However, as it can be readily shown, the inclusion in the analysis of the three dimensionality and the piezoelectric effect does not add anything substantial to the discussion of the proposed method. Consequently, for the purposes in this chapter we ignore the piezoelectric effect and restrict ourselves to 2D test problems. Thus, assume the simplified 2D geometry as shown in Fig. 3.3 (which is a cross-section of the geometry in Fig. 3.2). Then subdivide the geometry into an adequate number of quadrangles. Thereby, one electrode or the entire busbar may be represented by one meshless quadrangles. Each of these quadrangle is appropriately referred to as a messless quadrangles, since there is no meshing of the geometry necessary, as it is the case in FEM or BEM applications. In this way the entire electrode can be considered as an elementary quadrangles in isolation and characterized independently from the rest of the system. These basic quadrangles are then categorized and cataloged for future usage, depending on the number and the nature of the adjacent quadrangles. As an example, a quadrangle is called Basic quadrangle I if only one port, out of four ports of the quadrangle, is allowed to exchange acoustic energy with the adjacent quadrangle or elastic environment. All the electrodes in Fig. 3.3 are one-port problems, pro-

vided they are not additionally excited by any other external sources. However, if the same quadrangle exchanges energy through one side, and with environment through a different side, the quadrangle will more appropriately be referred to as a two-port (Basic Quadrangle II). Consequently, the complete device section is generally a composition of elementary quadrangles of varied types. Each particular type needs to be analyzed individually and systematically. Thereby, since the quadrangles are meshless, the opted basis- and testing functions occupy the entire domain and provide the solution for the entire domain. Consequently, based on the ideas outlined above simulation process involves the following steps:

1. Subdivide the device structure into an adequate number of quadrangles. Thereby, one electrode or the entire busbar may be represented by one meshless quadrangle.
2. Affine transform a given quadrangle to a master square, centered at the origin of the coordinate system, where the basis functions, their derivatives and integrals are readily defined and pre-calculable.
3. Construct a complete set of 2D orthogonal expansion functions, following the proposed recipe in this chapter. These functions possess richly detailed and refined features and are equipped with distinct properties to describe the displacement- and traction variations in quadrangles' interior, surface areas, their edges and corners with prescribed precision.

4. Use Galerkin-type Surface-integral-Modeling technique, for the discretization of the governing integral equations.
5. Derive the \mathcal{GF} s and generate the LIBRARY.

3.3.2 Governing PDEs and their Equivalent Self-regularized Surface-integral Equations

Consider a fully-anisotropic elastic medium as shown in Fig. 3.3. The elastic medium is characterized by the 6×6 stiffness matrix \mathbf{C} , and the constant mass density ρ . The i^{th} quadrangle occupying the volume Ω_i with the boundary surface Γ_i is characterized by $(C)_i$ and ρ_i with $i = a, b, c, \dots$. The following discussion is dedicated to the detailed explanation of proposed Distributed-Elementary-Source Dyadic Green's Functions (\mathcal{GF} s) characterizing the basic quadrangle "a." The analysis of the Green's function associated with the remaining types of quadrangles is immediate.

Remark: In Fig. 3.3 the intermediate bounding surfaces of each quadrangles are, in a fact, fictitious interfaces, induced by the topology and/or inhomogeneity of the structure. Nonetheless, assume that quadrangles are detached from one another such that there is no transfer of energy between the partitioned quadrangles. (The transfer of energy or interconnection between quadrangles is explained as an application of the proposed \mathcal{GF} s.)

It will be assumed that there is no variation in the y -direction, and consequently, the y -derivatives are suppressed. Thus the equation of motion for the basic quadrangle “ a ” reads:

$$\underline{\underline{\nabla}}^t \mathbf{T} = -\rho\omega^2 \mathbf{u}, \quad \text{for } (x, z) \in \Omega_a, \quad (3.1)$$

or, more explicitly,

$$(\mathbf{N}_1^t \partial_x + \mathbf{N}_3^t \partial_z) \mathbf{T} = -\rho\omega^2 \mathbf{u}, \quad \text{for } (x, z) \in \Omega_a. \quad (3.2)$$

The superscript t signifies transposition. A harmonic time-dependence according to $e^{-j\omega t}$ has been assumed. For a detailed discussion of the properties of the differential operator $\underline{\underline{\nabla}}$ and the constituent 6×3 matrices \mathbf{N}_n ($n = 1, 3$) the reader is referred to the discussion in [11]. Here, \mathbf{u} is the mechanical displacement vector and \mathbf{T} stands for the stress tensor. Introducing stresses $\boldsymbol{\tau}_n$ ($n = 1, 3$)

$$\boldsymbol{\tau}_n = \mathbf{N}_n^t \mathbf{T} = \mathbf{N}_n^t \mathbf{C} \underline{\underline{\nabla}} \mathbf{u}, \quad (3.3)$$

we can transform Eq. (3.2) into the convenient form:

$$\partial_x \boldsymbol{\tau}_1 + \partial_z \boldsymbol{\tau}_3 = -\rho\omega^2 \mathbf{u} \quad (3.4)$$

Here, $\boldsymbol{\tau}_n$ comprises the stress components T_{n1}, T_{n3} which act on the surface with the outward unit normal vector \mathbf{n}_n . Multiplying both sides of Eq. (3.4) by the transpose of a 2×1 test vector \mathbf{v} (elementary weighting function representing

any of the vectors $(v_1, 0)^t$, or $(0, v_3)^t$ we obtain:

$$\mathbf{v}^t \partial_x \boldsymbol{\tau}_1 + \mathbf{v}^t \partial_z \boldsymbol{\tau}_3 = -\rho \omega^2 \mathbf{v}^t \mathbf{u} \quad (3.5)$$

Integrate the terms on both sides of this equation over the volume Ω_a , role over the derivatives onto the test vector \mathbf{v} , and apply the Gauss' divergence theorem to obtain boundary integrals, which involve terms with reduced order of the derivatives by one:

$$\begin{aligned} & - \int_{\Omega_a} d\Omega_a (\partial_x \mathbf{v}^t) \boldsymbol{\tau}_1 - \int_{\Omega_a} d\Omega_a (\partial_z \mathbf{v}^t) \boldsymbol{\tau}_3 - \int_{\Gamma_{3,a}^-} dx \mathbf{v}^t \boldsymbol{\tau}_3 \\ & = -\rho \omega^2 \int_{\Omega_a} d\Omega_a \mathbf{v}^t \mathbf{u} \end{aligned} \quad (3.6)$$

The boundary sections $\Gamma_{1,a}^+$, $\Gamma_{1,a}^-$, $\Gamma_{3,a}^+$ and $\Gamma_{3,a}^-$ represent surfaces of the quadrangle “a” facing “east,” “west,” “north,” and “south,” respectively. Substitute the expressions for $\boldsymbol{\tau}_1$ and $\boldsymbol{\tau}_3$ from Eq. (3.3) into the first two terms at the LHS of Eq. (3.6):

$$\begin{aligned} & - \int_{\Omega_a} d\Omega_a (\partial_x \mathbf{v}^t) \mathbf{N}_1^t \mathbf{C} \underline{\underline{\nabla}} \mathbf{u} - \int_{\Omega_a} d\Omega_a (\partial_z \mathbf{v}^t) \mathbf{N}_3^t \mathbf{C} \underline{\underline{\nabla}} \mathbf{u} - \int_{\Gamma_{3,a}^-} dx \mathbf{v}^t \boldsymbol{\tau}_3 \\ & = -\rho \omega^2 \int_{\Omega_a} d\Omega_a \mathbf{v}^t \mathbf{u} \end{aligned} \quad (3.7)$$

Here, $\underline{\underline{\nabla}} = \mathbf{N}_1 \partial_x + \mathbf{N}_3 \partial_z$, as introduced in the transition from Eq. (3.1) to Eq. (3.2).

3.3.3 Distributed-Elementary-Sources and the Associated Self-regularized Dyadic Green's Functions

Rearranging the terms in Eq. (3.7):

$$\begin{aligned} & \int_{\Omega_a} d\Omega_a (\partial_x \mathbf{v}^t) \mathbf{N}_1^t \mathbf{C} \underline{\underline{\nabla}} \mathbf{u} + \int_{\Omega_a} d\Omega_a (\partial_z \mathbf{v}^t) \mathbf{N}_3^t \mathbf{C} \underline{\underline{\nabla}} \mathbf{u} - \rho \omega^2 \int_{\Omega_a} d\Omega_a \mathbf{v}^t \mathbf{u} \\ &= - \int_{\Gamma_{3,a}^-} dx \mathbf{v}^t \boldsymbol{\tau}_3 \end{aligned} \quad (3.8)$$

In order to solve the problem the primary field variables, here the displacement vector, needs to be discretized. Let \mathbf{u} stand for the displacement vector with the components $u_1(x, z)$ and $u_3(x, z)$:

$$\mathbf{u} = \begin{bmatrix} u_1(x, z) \\ u_3(x, z) \end{bmatrix} \quad (3.9)$$

The independent scalar functions $u_i(x, z)$ ($i = 1, 3$) have to be individually expressed in terms of a suitably chosen complete set of infinitely countable orthonormal basis functions, denoted by $B_{l,n}(x, z)$. Thus truncating the double series, by keeping only a finite number of expansion terms, displacement components, say $u_1(x, z)$, can be synthesized in terms of $B_{l,n}(x, z)$ by introducing $(L+1) \times (N+1)$ *a priori* unknown expansion coefficients $u_{l,n}^{(1)}$:

$$u_1(x, z) \approx \sum_{l=0}^L \sum_{n=0}^N u_{l,n}^{(1)} B_{l,n}(x, z) \quad (3.10)$$

For brevity the variables x and z in $B_{l,n}(x, z)$ will be suppressed in the remaining discussion. A similar series expansion can be written for $u_3(x, z)$. Employing

matrix notation the displacement vector \mathbf{u} can then be cast in the following computationally convenient matrix form:

$$\mathbf{u} \approx \begin{bmatrix} [\cdots B_{l \odot n} \cdots] [\cdots 0_{l \odot n} \cdots] \\ [\cdots 0_{l \odot n} \cdots] [\cdots B_{l \odot n} \cdots] \end{bmatrix} \begin{bmatrix} \vdots \\ u_{l \odot n}^{(1)} \\ \vdots \\ \vdots \\ u_{l \odot n}^{(3)} \\ \vdots \end{bmatrix} \quad (3.11a)$$

$$= \mathbf{B}\mathbf{U} \quad (3.11b)$$

Introduction of the matrix \mathbf{B} and the vector \mathbf{U} , in the transition from Eq. (3.11a) to Eq. (3.11b) should be self-explanatory. The matrix \mathbf{B} accommodates the basis functions, and the vector U comprises the unknown expansion coefficients. Here, the symbol $l \odot n$ refers to the arrangement of the indices l and n in the following form: Fix a value for l in the the interval $[0, L]$, say l_0 , and run over all the possible $n_0 \in [0, N]$; obtaining, $[l_0, 0], \cdots, [l_0, n_0], \cdots, [l_0, N]$. Subsequently vary the value of l_0 from 0 to L to obtain an $(L + 1) \times (N + 1)$ index matrix. Concatenating the rows of the above matrix results in a string of $(L + 1) \times (N + 1)$ index pairs (l, n) . More explicitly, we obtain:

$$[(0, 0), \cdots, (0, n_0), \cdots, (0, N), \cdots, (l_0, 0), \cdots, (l_0, N), \cdots, (L, N)].$$

On elaborating the integrals in Eq. (3.8), the first and second terms result in the “stiffness” matrix \mathbf{K} , whereas the third term at the LHS leads to the “mass” matrix \mathbf{M} . Using Eq. (3.11b) and letting \mathbf{B} , represent (\iff) the known weighting

function \mathbf{v} (with components v_1 and v_3), we obtain

$$-\rho\omega^2 \iint dx dz \mathbf{v}^t \mathbf{u} \iff -\rho\omega^2 \iint dx dz \mathbf{B}^t \mathbf{B} \mathbf{U} = -\omega^2 \mathbf{M} \mathbf{U} \quad (3.12)$$

for the diagonal mass matrix \mathbf{M} . In performing the second transition in Eq. (3.12), we used $\iint dx dz \mathbf{B}^t \mathbf{B} = \mathbf{I}$, a fact which is the manifestation of orthonormality property of the basis functions. Here, ‘ \mathbf{I} ’ stands for identity matrix.

Remark: In the above, the integral of a matrix is understood as a matrix, the entries of which are integrals of the underlying corresponding matrix elements, a convention which is symbolized as $\iint dx dz [a_{ij}] = [\iint dx dz a_{ij}]$. A further comment concerns the derivatives and integrals of the basis functions. The basis functions considered here are normalized Legendere polynomials, orthogonal over the domain $[-1, 1]$. Finding derivatives and integrals of these polynomials over domain $[-1, 1]$ is an easy task and they can be pre-calculated and tabulated for frequent use. This task was carried out in the current work for obtaining the often-mentioned LIBRARY. The pre-calculated derivatives and integrals can then be transformed to any desired domain by multiplying them with respective transformation coefficients, as it is done in various other methods [45, 46].

The $\boldsymbol{\tau}_3$ in the integral on RHS of Eq. (3.8) comprises the stress components T_{31} and T_{33} , which act on the surface $\Gamma_{3,a}^-$. Making use of the introduced representation

\Leftrightarrow , we obtain the following symbolic form:

$$\int_{\Gamma_{3,a}^-} dx \mathbf{v}^t \boldsymbol{\tau}_3 = \int_{\Gamma_{3,a}^-} dx \mathbf{v}^t T_{31} \Leftrightarrow \begin{bmatrix} F_{31} \\ 0 \end{bmatrix}_{\Gamma_{3,a}^-} \quad (3.13)$$

Summarizing our results, Eq. (3.8) reads:

$$[\mathbf{K} - \omega^2 \mathbf{M}]_a \mathbf{U}_a^{(31)} = - \begin{bmatrix} F_{31} \\ 0 \end{bmatrix}_{\Gamma_{3,a}^-} \quad (3.14)$$

A similar set of equations can be set up for the stress component T_{33} :

$$[\mathbf{K} - \omega^2 \mathbf{M}]_a \mathbf{U}_a^{(33)} = - \begin{bmatrix} 0 \\ F_{33} \end{bmatrix}_{\Gamma_{3,a}^-} \quad (3.15)$$

The 0-augmented vectors $F_{31}|_{\Gamma_{3,a}^-}$ and $F_{33}|_{\Gamma_{3,a}^-}$ appearing at the RHS of Eqs. (3.14) and (3.15), have been introduced in the obvious form.

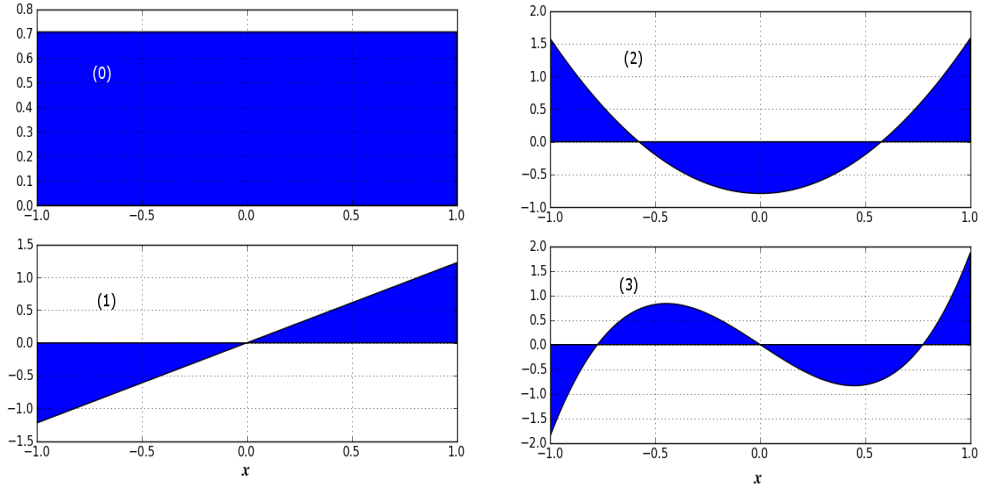


Figure 3.4: Distributive Elementary Sources: $b_0(x)$ (upper left), $b_1(x)$ (lower left), $b_2(x)$ (upper, right) and $b_3(x)$ (lower right)

Distributed Elementary Sources

The elementary excitation sources (the components of the traction forces) can be any of the basis functions $b_n(x)$ $n \in \mathcal{N}_0$, with $b_n(x)$ being a polynomial of order n (in the present case they are chosen to be normalized Legendre polynomials). The first four lowest order polynomials (sources) are shown in Fig. 3.4. We remind ourselves that traction component T_{31} , acting on the test boundary $\Gamma_{3,a}^-$, is a one-dimensional function of the variable x . Consequently, T_{31} can be approximated in an \mathcal{N}_0 -dimensional subspace by the superposition of \mathcal{N}_0 basis functions $b_n(x)$. The n^{th} component of T_{31} can then be represented by $\langle b_n, T_{31} \rangle b_n$, where the angled brackets stand for inner product. Thus if the test boundary is excited by a force component $b_n(x)$ the response of the medium is corrected by the projection $\langle b_n, T_{31} \rangle$, which returns the response of the medium due to the traction force T_{31} . Hence, the surface integral term in Eq. (3.13) is:

$$\int_{\Gamma_{3,a}^-} dx \mathbf{v}^t \boldsymbol{\tau}_3 = \int_{\Gamma_{3,a}^-} dx \mathbf{v}^t \begin{bmatrix} T_{31}^{(n)} \\ 0 \end{bmatrix}_{\Gamma_{3,a}^-} = \int_{\Gamma_{3,a}^-} dx \mathbf{v}^t \begin{bmatrix} b_n(x) \\ 0 \end{bmatrix}_{\Gamma_{3,a}^-} \quad (3.16)$$

Here, $n \in \mathcal{N}_0$. Proceeding similarly with the remaining basis functions $b_n(x)$ we realize that \mathcal{N}_0 independent experiments exhaust all possible excitations of the boundary surface of interest with forces parallel to the surface (tangential forces). A similar consideration leads to the further set of \mathcal{N}_0 independent excitations $b_n(x)$ acting in the direction normal to the surface. Additionally, for composite 2D basis-functions, e.g., $B_{l,n}(x, z) = b_l(x)b_n(z)$ evaluated at the boundary, we write,

$B_{l,n}(\text{const}, z) = \alpha_l b_n(z)$ and $B_{l,n}(x, \text{const}) = \gamma_n b_l(x)$, with α_l and γ_n , respectively, being the function values of $b_l(x = \text{const})$ and $b_n(z = \text{const})$.

Self-regularized Dyadic Green's Functions (\mathcal{GF}_s)

Traditionally Green's functions are defined as responses of the medium under consideration to localized elementary excitations. Thereby, ordinarily Dirac's delta function excitations are considered - a fact which has rendered Green's functions the name tag "impulse responses." Isolated localized excitation forces result in Green's functions which are in general singular. The Green's function singularities can be strong or hyper strong. The singularities may severely hamper the accuracy of the numerical results achievable and thus, considerable effort is required for their regularization [51]. Utilizing the proposed DES, the complications associated with the singularities can be simply and elegantly bypassed. Solving Eqs. (3.14) and (3.15) for, $b_0(x)$, the first and the lowest order DES function, results in the \mathcal{GF}_s ,

$$\mathfrak{G}_{[T_{31}]_{\Gamma_{3,a}^-}^{(0)}}(x, z) = \begin{bmatrix} \mathfrak{G}_{[T_{31}]_{\Gamma_{3,a}^-}^{(0)}}^{(1)}(x, z) \\ \mathfrak{G}_{[T_{31}]_{\Gamma_{3,a}^-}^{(0)}}^{(3)}(x, z) \end{bmatrix} \quad (3.17)$$

and

$$\mathfrak{G}_{[T_{33}]_{\Gamma_{3,a}^-}^{(0)}}(x, z) = \begin{bmatrix} \mathfrak{G}_{[T_{33}]_{\Gamma_{3,a}^-}^{(0)}}^{(1)}(x, z) \\ \mathfrak{G}_{[T_{33}]_{\Gamma_{3,a}^-}^{(0)}}^{(3)}(x, z) \end{bmatrix}. \quad (3.18)$$

In these equations, Green's functions with the superscripts 1 and 3, respectively, stand for the displacement components $u_1(x, z)$ and $u_3(x, z)$, which are displacement field responses to the chosen DES. Consequently, collecting the \mathcal{N}_0 resultant (2×1) column vectors of a \mathcal{GF} s, forms following $2 \times \mathcal{N}_0$ matrix of DGFs:

$$\begin{aligned} & \left[\mathcal{G}_{[T_{31}]_{\Gamma_{3,a}^-}^{(0)}}(x, z) \quad \mathcal{G}_{[T_{31}]_{\Gamma_{3,a}^-}^{(1)}}(x, z) \quad \cdots \quad \mathcal{G}_{[T_{31}]_{\Gamma_{3,a}^-}^{(N)}}(x, z) \right] \\ &= \begin{bmatrix} \mathcal{G}_{[T_{31}]_{\Gamma_{3,a}^-}^{(0)}}^{(1)}(x, z) & \mathcal{G}_{[T_{31}]_{\Gamma_{3,a}^-}^{(1)}}^{(1)}(x, z) & \cdots & \mathcal{G}_{[T_{31}]_{\Gamma_{3,a}^-}^{(N)}}^{(1)}(x, z) \\ \mathcal{G}_{[T_{31}]_{\Gamma_{3,a}^-}^{(0)}}^{(3)}(x, z) & \mathcal{G}_{[T_{31}]_{\Gamma_{3,a}^-}^{(1)}}^{(3)}(x, z) & \cdots & \mathcal{G}_{[T_{31}]_{\Gamma_{3,a}^-}^{(N)}}^{(3)}(x, z) \end{bmatrix} \end{aligned} \quad (3.19)$$

Similarly the series of elementary traction forces (DES) $T_{33}^{(n)}$ results in

$$\begin{aligned} & \left[\mathcal{G}_{[T_{33}]_{\Gamma_{3,a}^-}^{(0)}}(x, z) \quad \mathcal{G}_{[T_{33}]_{\Gamma_{3,a}^-}^{(1)}}(x, z) \quad \cdots \quad \mathcal{G}_{[T_{33}]_{\Gamma_{3,a}^-}^{(N)}}(x, z) \right] \\ &= \begin{bmatrix} \mathcal{G}_{[T_{33}]_{\Gamma_{3,a}^-}^{(0)}}^{(1)}(x, z) & \mathcal{G}_{[T_{33}]_{\Gamma_{3,a}^-}^{(1)}}^{(1)}(x, z) & \cdots & \mathcal{G}_{[T_{33}]_{\Gamma_{3,a}^-}^{(N)}}^{(1)}(x, z) \\ \mathcal{G}_{[T_{33}]_{\Gamma_{3,a}^-}^{(0)}}^{(3)}(x, z) & \mathcal{G}_{[T_{33}]_{\Gamma_{3,a}^-}^{(1)}}^{(3)}(x, z) & \cdots & \mathcal{G}_{[T_{33}]_{\Gamma_{3,a}^-}^{(N)}}^{(3)}(x, z) \end{bmatrix}. \end{aligned} \quad (3.20)$$

Remark: Each of the above $2 \times \mathcal{N}_0 \times 2$ \mathcal{GF} s in Eqs. (3.19) and (3.20) corresponds to a specific \mathcal{GF} in the generated LIBRARY. For example, $\mathcal{G}_{[T_{33}]_{\Gamma_{3,a}^-}^{(0)}}^{(1)}(x, z)$ stands for a \mathcal{GF} , which is the “1st” component of the displacement vector, i.e. $u_1(x, z)$, in response to the applied stress component “ T_{33} ” acting on the boundary section “ $\Gamma_{3,a}^-$.” Moreover, each of these \mathcal{GF} s is the response to a specific DES. In the present case the superscript ‘(0)’ reveals the fact that the selected basis function has been $b_0(x)$.

The \mathcal{GF} s thus constructed provide complete information necessary to characterize all types of excitation over the test boundary subject to any boundary conditions. To further illuminate the construction of the \mathcal{GF} s, we here constructed a set of Green's functions by exciting the boundary section $\Gamma_{3,a}^-$, and assuming the remaining sections of the boundary to be stress free. Furthermore, it should be pointed out that each of the \mathcal{GF} s also depends on the operating frequency (ω), once the size of quadrangle and the constitutive properties have been specified. We have generated a LIBRARY of such \mathcal{GF} s for each test boundary and commonly-used material properties, such that they can be employed for future usage. We thus proceed to the next section which is dedicated to solving various types of boundary conditions with the help of aforementioned, Sufficiency- and Exhaustion principles.

3.4 Interpretation and Solution Strategy for Various Boundary Conditions

Given the governing equations for the quadrangle Ω with the boundary surface Γ , we proceed as follows. The surface of the quadrangle is subject to boundary condition which can be Dirichlet, Neumann or interface condition. Both displacement- and stress functions evaluated on the boundary can be individually synthesized in terms of \mathcal{N}_0 basis functions weighted by \mathcal{N}_0 *a priori* unknown expansion coefficients. The task is the determination of these expansion coefficients such that the

governing equation are satisfied in Ω and the boundary condition matches given function on the boundary, in weak sense. This objective can be achieved by employing various methods. The aim here is to utilize the constructed LIBRARY of pre-calculated Green's functions to solve the given BVPs.

Comment: The treatment of the eigenvalue problems, even though quite straight forward and convenient, is not the subject of the current chapter.

3.4.1 Algorithm for Solving Inhomogeneous Neumann Boundary Conditions

Consider the test quadrangle “ a ” shown in first row of Table 3.2. The imposition of the inhomogeneous Neumann boundary condition on the test boundary ($\Gamma_{3,a}^-$) of this quadrangle implies that the traction force applied over the boundary is prescribed and non-zero and stress free over remaining boundary sections, identical to Eq. (3.8). It is important to mention that Eq. (3.8) is essentially an inhomogeneous Neumann problem. The sources in previous case where DES, whereas here the applied source is an arbitrary force function. Thus, for easy reference it is instructive to reproduce Eq. (3.8):

$$\begin{aligned} & \int_{\Omega_a} d\Omega_a (\partial_x \mathbf{v}^t) \mathbf{N}_1^t \mathbf{C} \underline{\underline{\nabla}} \mathbf{u} + \int_{\Omega_a} d\Omega_a (\partial_z \mathbf{v}^t) \mathbf{N}_3^t \mathbf{C} \underline{\underline{\nabla}} \mathbf{u} - \rho \omega^2 \int_{\Omega_a} d\Omega_a \mathbf{v}^t \mathbf{u} \\ & = - \int_{\Gamma_{3,a}^-} dx \mathbf{v}^t \boldsymbol{\tau}_3 \end{aligned} \quad (3.21)$$

Consider a force vector $\tilde{\mathbf{F}}$ in (x, z) co-ordinate plane, with two-components \tilde{F}_1 and \tilde{F}_3 operating at the frequency ω , and being applied on $\Gamma_{3,a}^-$. The traction force term on the RHS of Eq. (3.21) is then:

$$\boldsymbol{\tau}_3 = \tilde{\mathbf{F}} = \begin{bmatrix} \tilde{F}_1 \\ \tilde{F}_3 \end{bmatrix} \quad (3.22)$$

The components of force \tilde{F}_1 and \tilde{F}_3 , can each be written as linear combinations of an adequate number of basis functions with support $\Gamma_{3,a}^-$. Thus, $\tilde{F}_1 \approx \sum_{n \in \mathcal{N}_0} p_n^{(1)} b_n|_{\Gamma_{3,a}^-}$ and $\tilde{F}_3 \approx \sum_{n \in \mathcal{N}_0} p_n^{(3)} b_n|_{\Gamma_{3,a}^-}$, where coefficients $p_n^{(1)}$ and $p_n^{(3)}$ are already known. Additionally, at this point it is imperative to remind ourselves that the displacement responses to the involved basis functions in \tilde{F}_1 and \tilde{F}_3 are already pre-calculated and available to us in the LIBRARY in the form of Green's functions \mathcal{GF} s. (Strictly speaking only expansion coefficients of the Green's functions in terms of basis function have encoded and recoded compactly in the LIBRARY). Thus, the expression, providing the desired solution for the given inhomogeneous Neumann boundary condition over the edge $\Gamma_{3,a}^-$, while the remaining boundary sections being characterized by homogeneous Neumann condition, is given by:

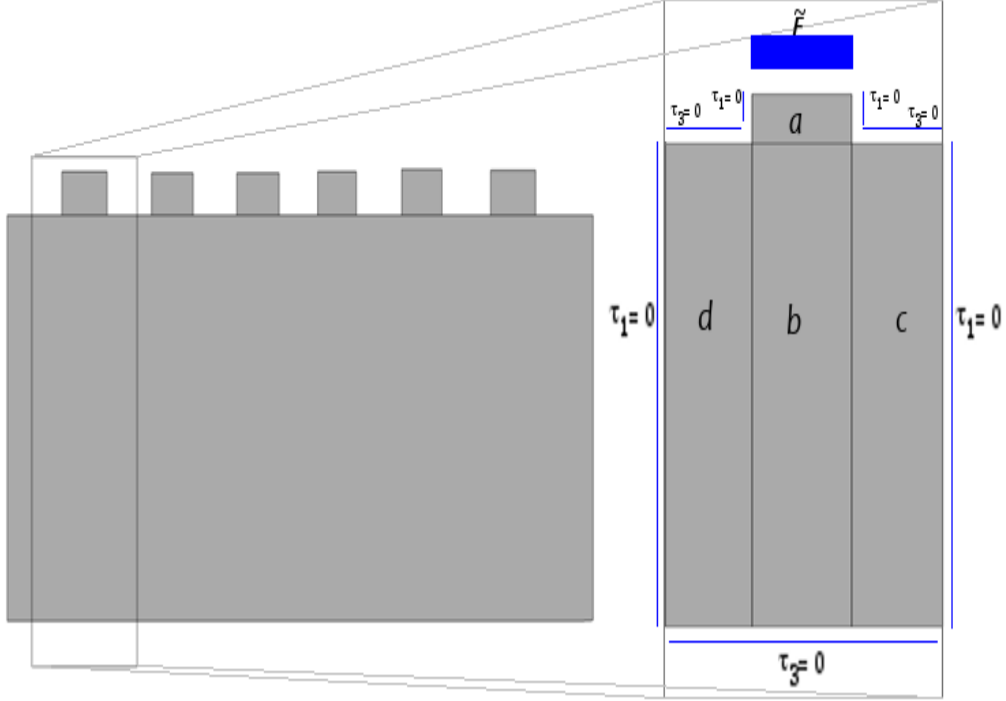


Figure 3.5: Discretization of 2D multi-quadrangle test problem with all the quadrangles exhibiting same material properties

$$\begin{aligned}
 \mathbf{u}(x, z) = & \begin{bmatrix} \mathcal{G}_{[\tilde{F}_1]_{\Gamma_{3,a}^-}^-}^{(1)}(x, z) & \dots & \mathcal{G}_{[\tilde{F}_1]_{\Gamma_{3,a}^-}^-}^{(N)}(x, z) \\ \mathcal{G}_{[\tilde{F}_1]_{\Gamma_{3,a}^-}^-}^{(3)}(x, z) & \dots & \mathcal{G}_{[\tilde{F}_1]_{\Gamma_{3,a}^-}^-}^{(N)}(x, z) \end{bmatrix} \begin{bmatrix} p_0^{(1)} \\ \vdots \\ p_N^{(1)} \end{bmatrix} \\
 & + \begin{bmatrix} \mathcal{G}_{[\tilde{F}_3]_{\Gamma_{3,a}^-}^-}^{(1)}(x, z) & \dots & \mathcal{G}_{[\tilde{F}_3]_{\Gamma_{3,a}^-}^-}^{(N)}(x, z) \\ \mathcal{G}_{[\tilde{F}_3]_{\Gamma_{3,a}^-}^-}^{(3)}(x, z) & \dots & \mathcal{G}_{[\tilde{F}_3]_{\Gamma_{3,a}^-}^-}^{(N)}(x, z) \end{bmatrix} \begin{bmatrix} p_0^{(3)} \\ \vdots \\ p_N^{(3)} \end{bmatrix} \quad (3.23)
 \end{aligned}$$

3.4.2 Algorithm for Solving Inhomogeneous Dirichlet Boundary Conditions

Inhomogeneous Dirichlet boundary condition by definition means that the displacement is fixed on the test-boundary, refer to the middle figure in Table 3.2, i.e.

$$\mathbf{u} = \tilde{\mathbf{U}}, \quad \text{on } \Gamma_{3,a}^- \quad (3.24)$$

The objective here is to solve the inhomogeneous Dirichlet boundary condition by utilizing pre-computed \mathcal{GF} s. The task is comparatively more involved in this case since here, the displacement on $\Gamma_{3,a}^-$ is given, while the stress on the $\Gamma_{3,a}^-$ is *a priori* unknown. Assume that the stress distribution over the boundary can be synthesized using \mathcal{N}_0 basis functions weighted by coefficients $p_n^{(31)}$ with $n \in \mathcal{N}_0$ for T_{31} :

$$T_{31}|_{\Gamma_{3,a}^-} = \sum_{n \in \mathcal{N}_0} p_n^{(31)} b_n|_{\Gamma_{3,a}^-} \quad (3.25)$$

and similarly, for T_{33} . Consequently, the system matrix in this case can be written as:

$$\begin{aligned} & [\mathbf{K} - \omega^2 \mathbf{M}]_a \begin{bmatrix} \tilde{\mathbf{U}}_a^{(31)} \\ \tilde{\mathbf{U}}_a^{(33)} \end{bmatrix} \\ &= - \int_{\Gamma_{3,a}^-} d\mathbf{A} \mathbf{B}^t \begin{bmatrix} p_0^{(31)} b_0 + p_1^{(31)} b_1 + \cdots + p_N^{(31)} b_N & 0 \\ 0 & p_0^{(33)} b_0 + p_1^{(33)} b_1 + \cdots + p_N^{(33)} b_N \end{bmatrix} \end{aligned} \quad (3.26)$$

For the determination of $p_n^{(31)}$ and $p_n^{(33)}$, $n \in \mathcal{N}_0$, the displacement boundary conditions in Eq. (3.25) needs to be satisfied in weak form. Upon assumption, determining $p_n^{(31)}$ and $p_n^{(33)}$ in Eq. (3.26) means, finding such a force distribution that the resultant displacement function inhabits the required boundary condition $\tilde{\mathbf{U}}$ on the $\Gamma_{3,a}^-$ boundary and stress-free elsewhere. The Eq. (3.26) also brings the pre-calculated \mathcal{GF} s into the picture, since solution to these DES are already stored in LIBRARY utilizing physics-based MOR as explained in preceding section. More precisely, any component of \mathcal{GF} can be written in terms of a linear combination of the Green's function coefficients and a set of basis function:

$$\mathcal{G}_{[T_{31}]_{\Gamma_{3,a}^-}^{(m)}}^{(1)}(x, z) = \sum_{n \in \mathcal{N}_0} \sum_{l \in \mathcal{N}_0} g_{[T_{31}]_{\Gamma_{3,a}^-}^{(m)(n,l)}}^{(1)} b_n(x) b_l(z) \quad (3.27)$$

Rewriting the expression for the Green's function coefficients over the test boundary, we have:

$$\mathcal{G}_{[T_{31}]_{\Gamma_{3,a}^-}^{(m)}}^{(1)}(x, z)|_{\Gamma_{3,a}^-} = \sum_{n \in \mathcal{N}_0} b_n(x) \sum_{l \in \mathcal{N}_0} g_{[T_{31}]_{\Gamma_{3,a}^-}^{(m)(n,l)}}^{(1)} b_l(z)|_{\Gamma_{3,a}^-} \quad (3.28)$$

or equivalently

$$\mathcal{G}_{[T_{31}]_{\Gamma_{3,a}^-}^{(m)}}^{(1)}(x, z)|_{\Gamma_{3,a}^-} = \sum_{n \in \mathcal{N}_0} G_{[T_{31}]_{\Gamma_{3,a}^-}^{(m)(n)}}^{(1)}|_{\Gamma_{3,a}^-} b_n(x) \quad (3.29)$$

Extracting coefficients $G_{[T_{31}]_{\Gamma_{3,a}^-}^-}^{(1)(m)(n)}$, along with the $G_{[T_{31}]_{\Gamma_{3,a}^-}^-}^{(3)(m)(n)}$ coefficients, form a set of coefficient for T_{31} excitation,

$$\begin{bmatrix} G_{[T_{31}]_{\Gamma_{3,a}^-}^-}^{(1)(m)(n)} \\ G_{[T_{31}]_{\Gamma_{3,a}^-}^-}^{(3)(m)(n)} \end{bmatrix}_{\Gamma_{3,a}^-} \quad (3.30)$$

for $m, n \in \mathcal{N}_0$, with observation boundary being $\Gamma_{3,a}^-$. Similarly, we retrieve the Green's function coefficients corresponding to T_{33} excitation. We form a set of coefficients as narrated in the Exhaustion principle to solve the imposed boundary condition. Obviously, the determination of the spectral components (expansion coefficients) specifying the components of $\tilde{\mathbf{U}} = [\tilde{\mathbf{U}}_1 \tilde{\mathbf{U}}_3]^t$, in terms of basis functions is immediate

$$\tilde{U}_n^{(l)} = \int_{\Gamma_{3,a}^-} dx b_n(x) \tilde{U}_l, \quad l = 1, 3. \quad (3.31)$$

Consequently:

$$\begin{bmatrix} G_{[T_{31}]_{\Gamma_{3,a}^-}^-}^{(1)(0)(0)} & \cdots & G_{[T_{31}]_{\Gamma_{3,a}^-}^-}^{(1)(M)(0)} & G_{[T_{33}]_{\Gamma_{3,a}^-}^-}^{(1)(0)(0)} & \cdots & G_{[T_{33}]_{\Gamma_{3,a}^-}^-}^{(1)(M)(0)} \\ \vdots & \ddots & \vdots & \vdots & \ddots & \vdots \\ G_{[T_{31}]_{\Gamma_{3,a}^-}^-}^{(1)(0)(N)} & \cdots & G_{[T_{31}]_{\Gamma_{3,a}^-}^-}^{(1)(M)(N)} & G_{[T_{33}]_{\Gamma_{3,a}^-}^-}^{(1)(0)(N)} & \cdots & G_{[T_{33}]_{\Gamma_{3,a}^-}^-}^{(1)(M)(N)} \\ G_{[T_{31}]_{\Gamma_{3,a}^-}^-}^{(3)(0)(0)} & \cdots & G_{[T_{31}]_{\Gamma_{3,a}^-}^-}^{(3)(M)(0)} & G_{[T_{33}]_{\Gamma_{3,a}^-}^-}^{(3)(0)(0)} & \cdots & G_{[T_{33}]_{\Gamma_{3,a}^-}^-}^{(3)(M)(0)} \\ \vdots & \ddots & \vdots & \vdots & \ddots & \vdots \\ G_{[T_{31}]_{\Gamma_{3,a}^-}^-}^{(3)(0)(N)} & \cdots & G_{[T_{31}]_{\Gamma_{3,a}^-}^-}^{(3)(M)(N)} & G_{[T_{33}]_{\Gamma_{3,a}^-}^-}^{(3)(0)(N)} & \cdots & G_{[T_{33}]_{\Gamma_{3,a}^-}^-}^{(3)(M)(N)} \end{bmatrix}_{\Gamma_{3,a}^-} \begin{bmatrix} p_0^{(31)} \\ \vdots \\ p_M^{(31)} \\ p_0^{(33)} \\ \vdots \\ p_M^{(33)} \end{bmatrix} = \begin{bmatrix} \tilde{U}_0^{(1)} \\ \vdots \\ \tilde{U}_M^{(1)} \\ \tilde{U}_0^{(3)} \\ \vdots \\ \tilde{U}_M^{(3)} \end{bmatrix}_{\Gamma_{3,a}^-} \quad (3.32)$$

will provide the required unknowns. These unknowns $p_n^{(i)}$, are then multiplied by their respective \mathcal{GF} s and synthesized, to obtain the required displacement obeying all the prescribed boundary conditions. The algorithm presented in this section can be viewed as a preparatory step for tackling the important tearing and interconnecting problem, which is explained in detail next.

3.5 Tearing and connecting subsystems: problem description

Consider the problem as shown in the third figure of Table 3.2. The problem can be characterized using the BVPs of two individual quadrangles awaiting to be interconnected. Each quadrangles “ a ” and “ b ” can be characterized by their respective integral equations, for Ω_a

$$\begin{aligned}
-\int_{\Omega_a} d\Omega_a(\partial_x \mathbf{v}^t) \mathbf{N}_1^t \mathbf{C} \underline{\underline{\nabla}} \mathbf{u} &- \int_{\Omega_a} d\Omega_a(\partial_z \mathbf{v}^t) \mathbf{N}_3^t \mathbf{C} \underline{\underline{\nabla}} \mathbf{u} - \int_{\Gamma_{3,a}^-} dx \mathbf{v}^t \boldsymbol{\tau}_3 \\
&+ \int_{\Gamma_{3,a}^+} dx \mathbf{v}^t \boldsymbol{\tau}_3 = -\rho\omega^2 \int_{\Omega_a} d\Omega_a \mathbf{v}^t \mathbf{u}, \quad (3.33)
\end{aligned}$$

and consecutively, for Ω_b

$$\begin{aligned}
-\int_{\Omega_b} d\Omega_b(\partial_x \mathbf{v}^t) \mathbf{N}_1^t \mathbf{C} \underline{\underline{\nabla}} \mathbf{u} &- \int_{\Omega_b} d\Omega_b(\partial_z \mathbf{v}^t) \mathbf{N}_3^t \mathbf{C} \underline{\underline{\nabla}} \mathbf{u} + \int_{\Gamma_{3,b}^+} dx \mathbf{v}^t \boldsymbol{\tau}_3 \\
&= -\rho\omega^2 \int_{\Omega_b} d\Omega_b \mathbf{v}^t \mathbf{u}. \quad (3.34)
\end{aligned}$$

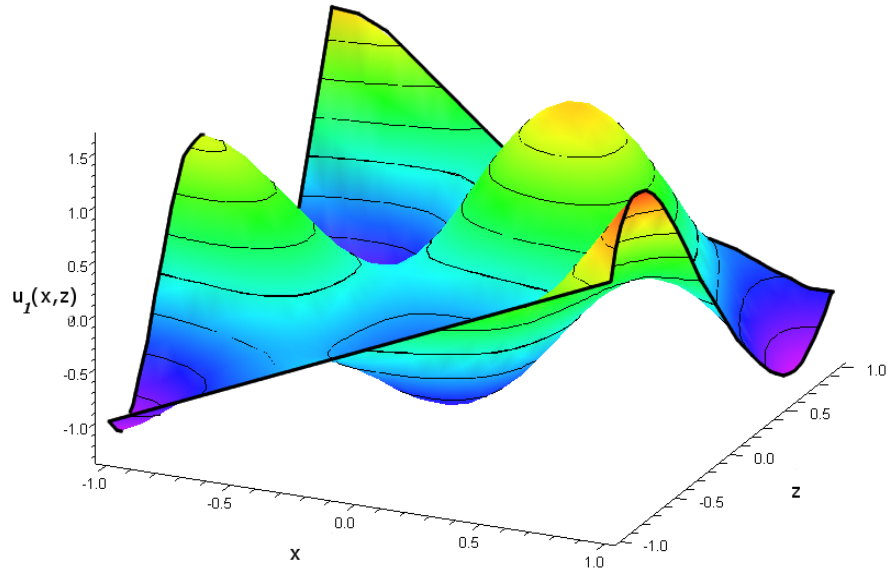
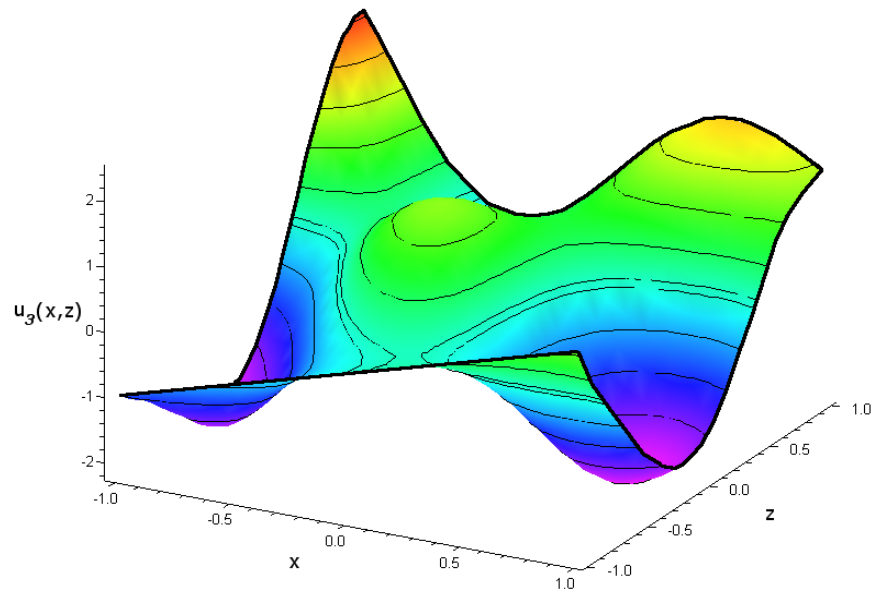
(a) Displacement component $u_1(x, z)$ (b) Displacement component $u_3(x, z)$

Figure 3.6: Dirichlet boundary condition solved with the help of principle of Exhaustion and Sufficiency principle utilizing pre-computed \mathcal{GF} s

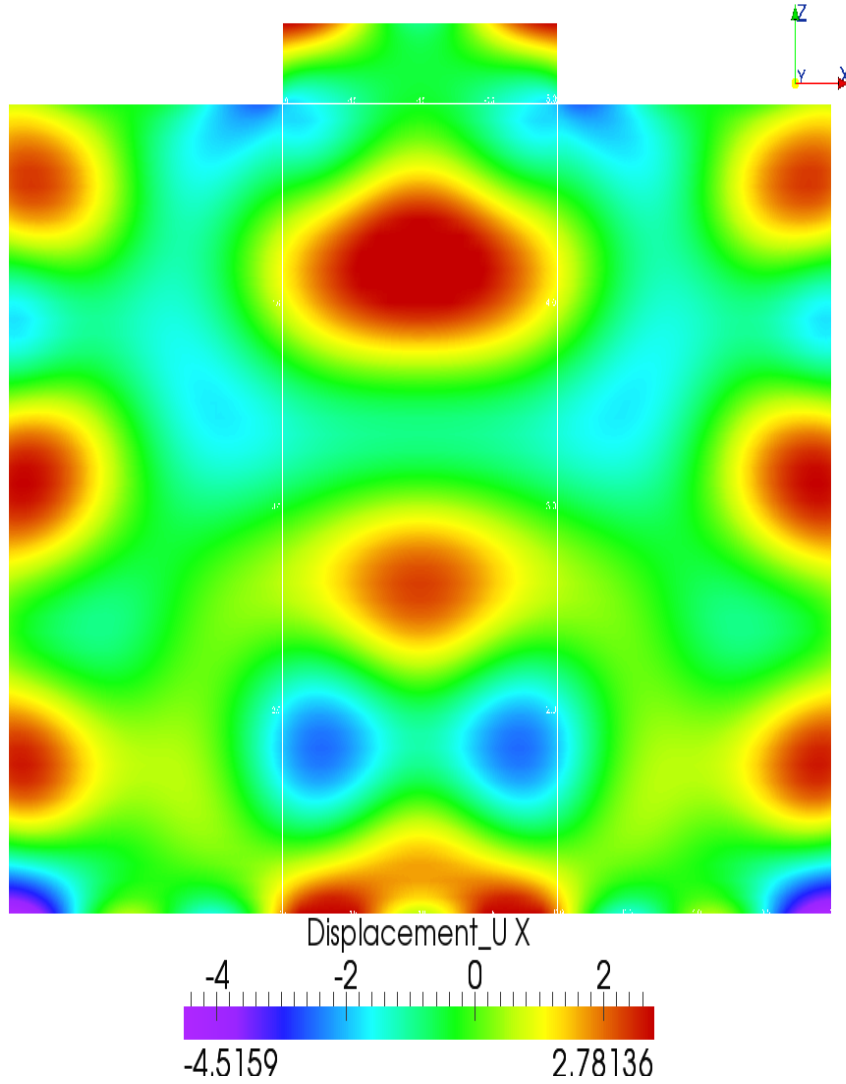


Figure 3.7: Displacement component $u_1(x, z)$ showing interconnection between multi-quadrangle modelled utilizing \mathcal{GF} s

The two quadrangle are, here, separated by introducing the unknown traction force $\boldsymbol{\tau}_3$ at the interfaces $\Gamma_{3,a}^-$ and $\Gamma_{3,b}^+$ of respective quadrangle. Consequently, for $\Omega_a \cup \Omega_b = \Omega$ and $\Omega_a \cap \Omega_b = \phi$, the resulting system of equation for Ω can be

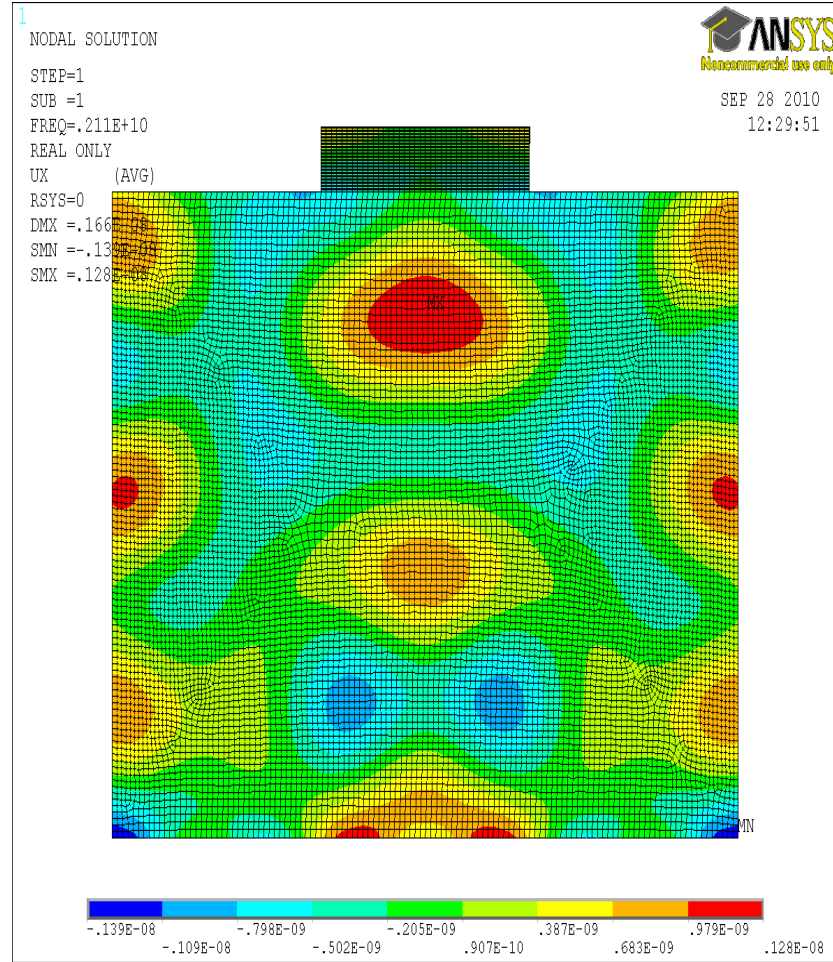


Figure 3.8: Displacement component u_1 for the model problem solved using ANSYS (a FEM based Software package)

written as:

$$\begin{aligned}
 & - \int_{\Omega} d\Omega (\partial_x \mathbf{v}^t) \mathbf{N}_1^t \mathbf{C} \underline{\underline{\nabla}} \mathbf{u} - \int_{\Omega} d\Omega (\partial_z \mathbf{v}^t) \mathbf{N}_3^t \mathbf{C} \underline{\underline{\nabla}} \mathbf{u} + \int_{\Gamma_3^+} dx \mathbf{v}^t \boldsymbol{\tau}_3 \\
 & = -\rho \omega^2 \int_{\Omega} d\Omega \mathbf{v}^t \mathbf{u}
 \end{aligned} \tag{3.35}$$

In Eqs. (3.33) and (3.35), we assume that the traction force is given and applied over the northern boundary $\Gamma_{3,a}^+$ operating at the specified frequency ω , such that

$$\int_{\Gamma_{3,a}^+} dx \mathbf{v}^t \boldsymbol{\tau}_3 = \int_{\Gamma_3^+} dx \mathbf{v}^t \boldsymbol{\tau}_3 = \int_{\Gamma_3^+} dx \mathbf{v}^t \tilde{\mathbf{F}}. \quad (3.36)$$

Thus in order to fuse the quadrangles it is necessary that both stress and displacement are continuous across the interface:

$$[\boldsymbol{\tau}_a^-]_{Interface} = [\boldsymbol{\tau}_b^+]_{Interface} \quad \text{and} \quad [\mathbf{u}_a^-]_{Interface} = [\mathbf{u}_b^+]_{Interface}. \quad (3.37)$$

Thus the surface integral Eqs. (3.33) and (3.34) along with the inhomogeneous Neumann boundary- and interface condition, Eqs. (3.36) and (3.37), respectively define the BVP for the interconnection problem. The stress free boundary conditions as shown in third figure of Table 3.2 are also accounted in problem definition.

3.5.1 Solution Algorithm for Interface Problem

We utilize precalculated \mathcal{GF} as exemplified in the Sufficiency- and Exhaustion principles in order to solve the frequency-dependent interconnection (composite) problem. The quadrangles Ω_a and Ω_b can be represented by the frequency-dependent systems of Eqs. (3.33) and (3.34), respectively. The applied boundary conditions are specified as shown in the figure in the third row of Table 3.2. However, solving the respective systems of equations is not possible unless the traction

force $\boldsymbol{\tau}_3$ at the interfaces $\Gamma_{3,a}^-$ and $\Gamma_{3,b}^+$ is known. Each component of the unknown traction force (T_{31} and T_{33}) can be represented as a linear combination of basis functions weighted by *a priori* unknown coefficients for traction component T_{31} :

$$T_{31}|_{\Gamma_{3,a}^-} = T_{31}|_{\Gamma_{3,b}^+} = \sum_{n \in \mathcal{N}_0} p_n^{(31)} b_n|_{\Gamma_{3,a}^-} \quad (3.38)$$

Similarly, for the traction component T_{33} :

$$T_{33}|_{\Gamma_{3,a}^-} = T_{33}|_{\Gamma_{3,b}^+} = \sum_{n \in \mathcal{N}_0} p_n^{(33)} b_n|_{\Gamma_{3,a}^-}. \quad (3.39)$$

It should be noted that individual solutions for a given quadrangle (Ω_a or Ω_b) subject to elementary basis functions are already been calculated and stored in the LIBRARY. Furthermore, in order to satisfy interface condition, Eq. (3.37) with the help of Green's functional technique we need the Green's function coefficients over the interface. Thus we retrieve the coefficients of the \mathcal{GF} s, with the $\Gamma_{3,a}^-$ as observation boundary

$$\left[\begin{array}{cccccc} G_{[T_{31}]_{\Gamma_{3,a}^-}}^{(1)(0)(0)} & \cdots & G_{[T_{31}]_{\Gamma_{3,a}^-}}^{(1)(M)(0)} & G_{[T_{33}]_{\Gamma_{3,a}^-}}^{(1)(0)(0)} & \cdots & G_{[T_{33}]_{\Gamma_{3,a}^-}}^{(1)(M)(0)} \\ \vdots & \ddots & \vdots & \vdots & \ddots & \vdots \\ G_{[T_{31}]_{\Gamma_{3,a}^-}}^{(1)(0)(N)} & \cdots & G_{[T_{31}]_{\Gamma_{3,a}^-}}^{(1)(M)(N)} & G_{[T_{33}]_{\Gamma_{3,a}^-}}^{(1)(0)(N)} & \cdots & G_{[T_{33}]_{\Gamma_{3,a}^-}}^{(1)(M)(N)} \\ G_{[T_{31}]_{\Gamma_{3,a}^-}}^{(3)(0)(0)} & \cdots & G_{[T_{31}]_{\Gamma_{3,a}^-}}^{(3)(M)(0)} & G_{[T_{33}]_{\Gamma_{3,a}^-}}^{(3)(0)(0)} & \cdots & G_{[T_{33}]_{\Gamma_{3,a}^-}}^{(3)(M)(0)} \\ \vdots & \ddots & \vdots & \vdots & \ddots & \vdots \\ G_{[T_{31}]_{\Gamma_{3,a}^-}}^{(3)(0)(N)} & \cdots & G_{[T_{31}]_{\Gamma_{3,a}^-}}^{(3)(M)(N)} & G_{[T_{33}]_{\Gamma_{3,a}^-}}^{(3)(0)(N)} & \cdots & G_{[T_{33}]_{\Gamma_{3,a}^-}}^{(3)(M)(N)} \end{array} \right]_{\Gamma_{3,a}^-} \quad (3.40)$$

from the LIBRARY for Ω_a and consecutively for the quadrangle, Ω_b ,

$$\left[\begin{array}{cccccc} G_{[T_{31}]_{\Gamma_{3,b}^+}^{(0)(0)}}^{(1)} & \cdots & G_{[T_{31}]_{\Gamma_{3,b}^+}^{(M)(0)}}^{(1)} & G_{[T_{33}]_{\Gamma_{3,b}^+}^{(0)(0)}}^{(1)} & \cdots & G_{[T_{33}]_{\Gamma_{3,b}^+}^{(M)(0)}}^{(1)} \\ \vdots & \ddots & \vdots & \vdots & \ddots & \vdots \\ G_{[T_{31}]_{\Gamma_{3,b}^+}^{(0)(N)}}^{(1)} & \cdots & G_{[T_{31}]_{\Gamma_{3,b}^+}^{(M)(N)}}^{(1)} & G_{[T_{33}]_{\Gamma_{3,b}^+}^{(0)(N)}}^{(1)} & \cdots & G_{[T_{33}]_{\Gamma_{3,b}^+}^{(M)(N)}}^{(1)} \\ G_{[T_{31}]_{\Gamma_{3,b}^+}^{(0)(0)}}^{(3)} & \cdots & G_{[T_{31}]_{\Gamma_{3,b}^+}^{(M)(0)}}^{(3)} & G_{[T_{33}]_{\Gamma_{3,b}^+}^{(0)(0)}}^{(3)} & \cdots & G_{[T_{33}]_{\Gamma_{3,b}^+}^{(M)(0)}}^{(3)} \\ \vdots & \ddots & \vdots & \vdots & \ddots & \vdots \\ G_{[T_{31}]_{\Gamma_{3,b}^+}^{(0)(N)}}^{(3)} & \cdots & G_{[T_{31}]_{\Gamma_{3,b}^+}^{(M)(N)}}^{(3)} & G_{[T_{33}]_{\Gamma_{3,b}^+}^{(0)(N)}}^{(3)} & \cdots & G_{[T_{33}]_{\Gamma_{3,b}^+}^{(M)(N)}}^{(3)} \end{array} \right]_{\Gamma_{3,b}^+} \quad (3.41)$$

The Eqs. (3.40) and (3.41) are collection of all the \mathcal{GF} s as a result of the excitations in both parallel (31) and normal (33) directions. Additionally, the quadrangle Ω_a is excited by the external traction force $\tilde{\mathbf{F}}$ and the influence of this force on the quadrangle Ω_b needs to be determined. Thus a particular solution for

$$\begin{aligned} - \int_{\Omega_a} d\Omega_a (\partial_x \mathbf{v}^t) \mathbf{N}_1^t \mathbf{C} \underline{\underline{\nabla}} \mathbf{u} & - \int_{\Omega_a} d\Omega_a (\partial_z \mathbf{v}^t) \mathbf{N}_3^t \mathbf{C} \underline{\underline{\nabla}} \mathbf{u} + \int_{\Gamma_{3,a}^+} dx \mathbf{v}^t \tilde{\mathbf{F}} \\ & = -\rho\omega^2 \int_{\Omega_a} d\Omega_a \mathbf{v}^t \mathbf{u} \end{aligned} \quad (3.42)$$

is also needed. The solution to this specified is also projected over the interface, written in discretized form:

$$\left[\begin{array}{cccccc} U_{[\tilde{F}_1]_{\Gamma_{3,a}^+}^{(0)}}^{(1)} & \cdots & U_{[\tilde{F}_1]_{\Gamma_{3,a}^+}^{(M)}}^{(1)} & U_{[\tilde{F}_1]_{\Gamma_{3,a}^+}^{(0)}}^{(3)} & \cdots & U_{[\tilde{F}_1]_{\Gamma_{3,a}^+}^{(M)}}^{(3)} \end{array} \right]_{\Gamma_{3,a}^-}^t \quad (3.43)$$

Equating the difference of the \mathcal{GF} s of each quadrangle to the specified displacement coefficients, hence

$$\begin{aligned}
& \begin{bmatrix} G_{[T_{31}]_{\Gamma_{3,a}^-}^{(0)(0)}}^{(1)} & \cdots & G_{[T_{31}]_{\Gamma_{3,a}^-}^{(M)(0)}}^{(1)} & G_{[T_{33}]_{\Gamma_{3,a}^-}^{(0)(0)}}^{(1)} & \cdots & G_{[T_{33}]_{\Gamma_{3,a}^-}^{(M)(0)}}^{(1)} \\ \vdots & \ddots & \vdots & \vdots & \ddots & \vdots \\ G_{[T_{31}]_{\Gamma_{3,a}^-}^{(0)(N)}}^{(1)} & \cdots & G_{[T_{31}]_{\Gamma_{3,a}^-}^{(M)(N)}}^{(1)} & G_{[T_{33}]_{\Gamma_{3,a}^-}^{(0)(N)}}^{(1)} & \cdots & G_{[T_{33}]_{\Gamma_{3,a}^-}^{(M)(N)}}^{(1)} \\ G_{[T_{31}]_{\Gamma_{3,a}^-}^{(0)(0)}}^{(3)} & \cdots & G_{[T_{31}]_{\Gamma_{3,a}^-}^{(M)(0)}}^{(3)} & G_{[T_{33}]_{\Gamma_{3,a}^-}^{(0)(0)}}^{(3)} & \cdots & G_{[T_{33}]_{\Gamma_{3,a}^-}^{(M)(0)}}^{(3)} \\ \vdots & \ddots & \vdots & \vdots & \ddots & \vdots \\ G_{[T_{31}]_{\Gamma_{3,a}^-}^{(0)(N)}}^{(3)} & \cdots & G_{[T_{31}]_{\Gamma_{3,a}^-}^{(M)(N)}}^{(3)} & G_{[T_{33}]_{\Gamma_{3,a}^-}^{(0)(N)}}^{(3)} & \cdots & G_{[T_{33}]_{\Gamma_{3,a}^-}^{(M)(N)}}^{(3)} \end{bmatrix}_{\Gamma_{3,a}^-} \begin{bmatrix} p_0^{(31)} \\ \vdots \\ p_M^{(31)} \\ p_0^{(33)} \\ \vdots \\ p_M^{(33)} \end{bmatrix} \\
& + \begin{bmatrix} U_{[\tilde{F}_1]_{\Gamma_{3,a}^+}^{(0)}}^{(1)} & \cdots & U_{[\tilde{F}_1]_{\Gamma_{3,a}^+}^{(M)}}^{(1)} & U_{[\tilde{F}_1]_{\Gamma_{3,a}^+}^{(0)}}^{(3)} & \cdots & U_{[\tilde{F}_1]_{\Gamma_{3,a}^+}^{(M)}}^{(3)} \end{bmatrix}_{\Gamma_{3,a}^-}^t \\
& = \begin{bmatrix} G_{[T_{31}]_{\Gamma_{3,b}^+}^{(0)(0)}}^{(1)} & \cdots & G_{[T_{31}]_{\Gamma_{3,b}^+}^{(M)(0)}}^{(1)} & G_{[T_{33}]_{\Gamma_{3,b}^+}^{(0)(0)}}^{(1)} & \cdots & G_{[T_{33}]_{\Gamma_{3,b}^+}^{(M)(0)}}^{(1)} \\ \vdots & \ddots & \vdots & \vdots & \ddots & \vdots \\ G_{[T_{31}]_{\Gamma_{3,b}^+}^{(0)(N)}}^{(1)} & \cdots & G_{[T_{31}]_{\Gamma_{3,b}^+}^{(M)(N)}}^{(1)} & G_{[T_{33}]_{\Gamma_{3,b}^+}^{(0)(N)}}^{(1)} & \cdots & G_{[T_{33}]_{\Gamma_{3,b}^+}^{(M)(N)}}^{(1)} \\ G_{[T_{31}]_{\Gamma_{3,b}^+}^{(0)(0)}}^{(3)} & \cdots & G_{[T_{31}]_{\Gamma_{3,b}^+}^{(M)(0)}}^{(3)} & G_{[T_{33}]_{\Gamma_{3,b}^+}^{(0)(0)}}^{(3)} & \cdots & G_{[T_{33}]_{\Gamma_{3,b}^+}^{(M)(0)}}^{(3)} \\ \vdots & \ddots & \vdots & \vdots & \ddots & \vdots \\ G_{[T_{31}]_{\Gamma_{3,b}^+}^{(0)(N)}}^{(3)} & \cdots & G_{[T_{31}]_{\Gamma_{3,b}^+}^{(M)(N)}}^{(3)} & G_{[T_{33}]_{\Gamma_{3,b}^+}^{(0)(N)}}^{(3)} & \cdots & G_{[T_{33}]_{\Gamma_{3,b}^+}^{(M)(N)}}^{(3)} \end{bmatrix}_{\Gamma_{3,b}^+} \begin{bmatrix} p_0^{(31)} \\ \vdots \\ p_M^{(31)} \\ p_0^{(33)} \\ \vdots \\ p_M^{(33)} \end{bmatrix} \quad (3.44)
\end{aligned}$$

The solution to the matrix Eq. (3.44) will be the required matched coefficients. These coefficients are then multiplied with the respective \mathcal{GF} s and added to the known displacement in Ω_a to provide the total solution for fused or interconnected problem.

3.6 Numerical Results and Discussion

In this section a glimpse of the numerical results are presented to illustrate the application of the proposed Distributed Elementary Source Self-regularized Dyadic Green's Functions (\mathcal{GF} s) in conjunction with the introduced Sufficiency principle and Exhaustion principle. Thereby, a pre-computed data set representing \mathcal{GF} s is utilized to tackle boundary conditions which typically arise in elastodynamic analysis of micro-acoustic devices.

Three examples have been designed to illustrate the flexibility and rigor of the technique. 1) The solution to the BVP with the Dirichlet boundary condition problem sketched in the figure in the second row of Table 3.2. 2) The solution of the multi-quadrangle problem (Fig. 3.5), involving interface- and Neumann boundary conditions. 3) The solution of a composite structure involving different types of materials (Fig. 3.3). The latter example manifestly demonstrates the strength of the proposed Green's function technique in solving fully-anisotropic elastodynamic problems. Invariably in all the examples the problem domains have been analyzed at the operating frequency of 2.1 GHz.

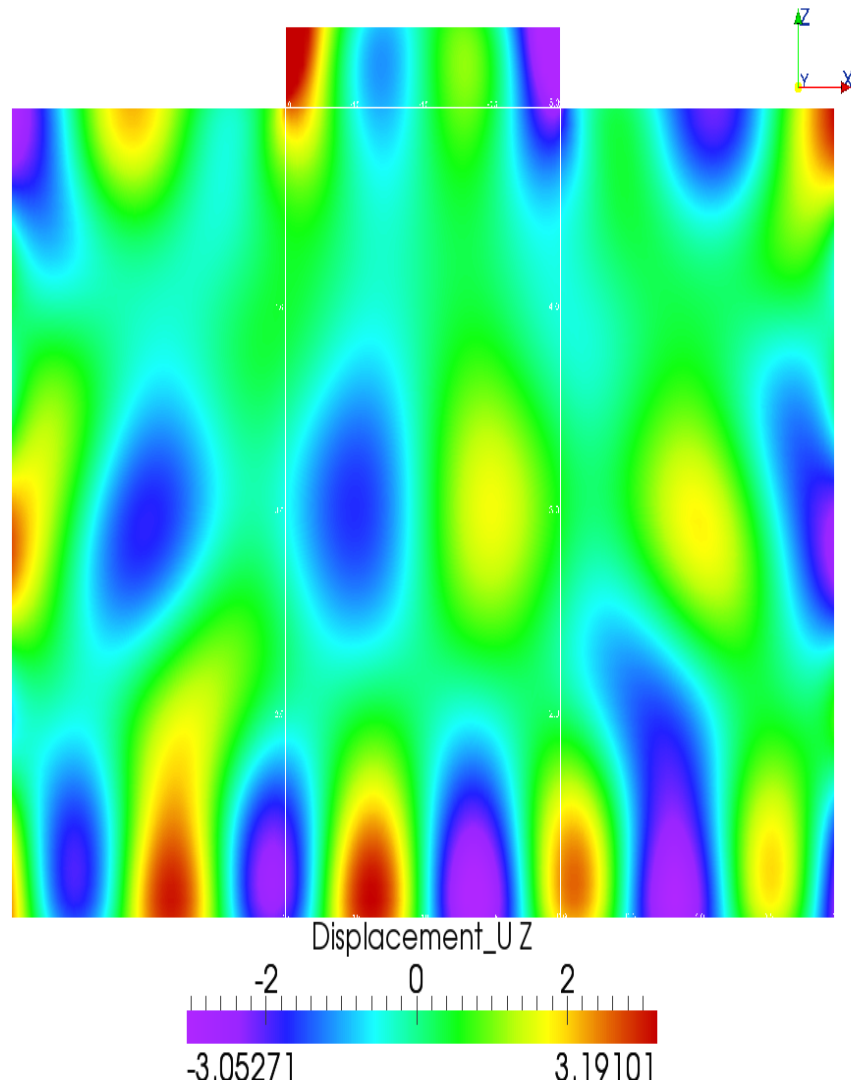


Figure 3.9: Displacement component $u_3(x, z)$ showing interconnection between multi-quadrangles modelled utilizing \mathcal{GF} s

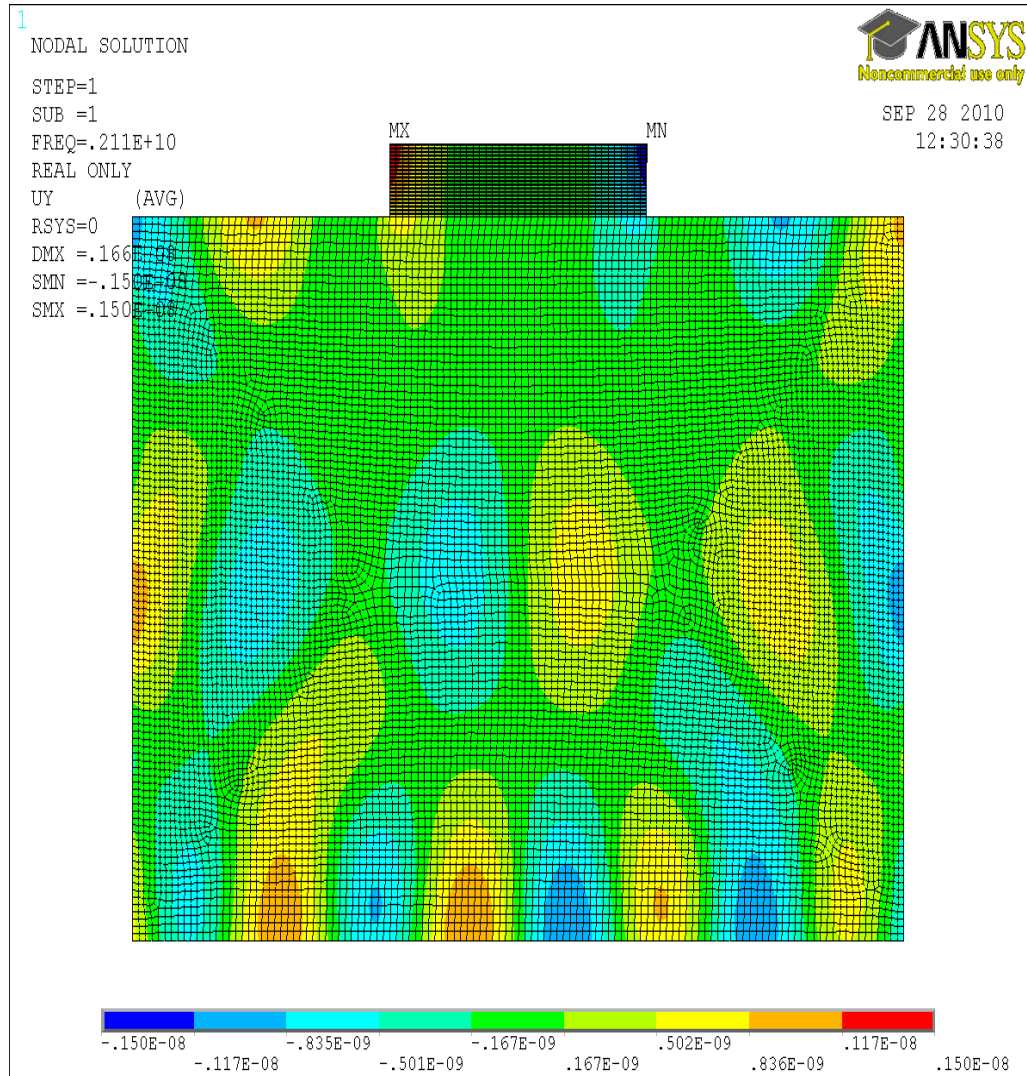


Figure 3.10: Displacement component u_3 for the model problem solved using ANSYS (a FEM based Software package)

3.6.1 Verification of Dirichlet Boundary Condition on Test Boundary

Consider an independent quadrangle exhibiting the material properties of Aluminium (refer to Table 3.3), and geometrically extending from -1 to 1 microns

in both x - and z - directions. The applied boundary conditions for the quadrangles are as shown in the second figure of Table 3.2. The edge $z = -1$ refers to the southern edge and is subject to the fixed displacement boundary condition $\tilde{U}(x) = x$ and stress-free boundary condition on the remaining edges. The numerical results of the displacement components obtained by the aforementioned Green's Functional method are shown in Fig. 3.6. The results manifestly prove the self-consistency of the method. The computed displacement components shown in Fig. 3.6 invariably obey the imposed Dirichlet boundary condition over the southern boundary. It should also be mentioned that the homogeneous Neumann boundary conditions on the remaining boundary sections are complied in weak sense.

3.6.2 Verification of Solution for Multi-quadrangles

Consider a multi-quadrangle problem (Fig. 3.5). Thereby, all the quadrangles, denoted by $\Omega_i, i = a, b, c, d$ are embodying the same material. The boundary conditions for the entire unit are as shown in Fig. 3.5. External force $F_1(x) = 0.707 \text{ N/m}^2$ and $F_3(x) = 0$ operating at $\omega = 2.1 \text{ GHz}$, are applied on the northern edge of quadrangle Ω_a , with remaining sections of boundary, stress-free. Between any two adjacent quadrangles there are fictitious interfaces, introduced due to the partitioning. The interconnection method ensure the satisfaction of the interface condition such that the energy is transferred from one quadrangle to another in

a smooth form. In particular, we considered the quadrangle to be constituted by Aluminium with material properties as shown in Table 3.3. Figs. 3.7 and 3.8 show the comparison between the displacement component $u_1(x, z)$ obtained utilizing the proposed \mathcal{GF} s method and the results obtained by the standard FEM simulation package (ANSYS), respectively. The comparison confirms the applicability of the proposed method in case of constrains on the displacement component $u_3(x, z)$ as well. Thereby, the self-consistency analysis for the Dirichlet boundary condition and the comparison of the solved interface condition with the results obtained by commercially available package confirms the applicability of the proposed method, to practice relevant problems. This comparison should suffice the primary aim of this chapter.

3.6.3 Solution of Multi-quadrangle Composite Problems With Varying Material Constitutions

Finally we return to the original model problem (Fig. 3.3), whereby quadrangles with different material properties are interconnected. To be more specific, quadrangle Ω_a is Aluminium, whereas Ω_b and Ω_c are Lithium Niobate. In regard to the boundary conditions, all the boundary sections are, as shown in Fig. 3.3, stress-free condition, except the top edge of Ω_a , where the external force vector $\mathbf{F} = (F_1, F_3)$ with $F_1(x) = 0.707 \text{ N/m}^2$ and $F_3(x) = 0$ is time harmonically ($e^{-j\omega t}$) operating at $\omega = 2.1 \text{ GHz}$. It is worth mentioning that the electrode occupying

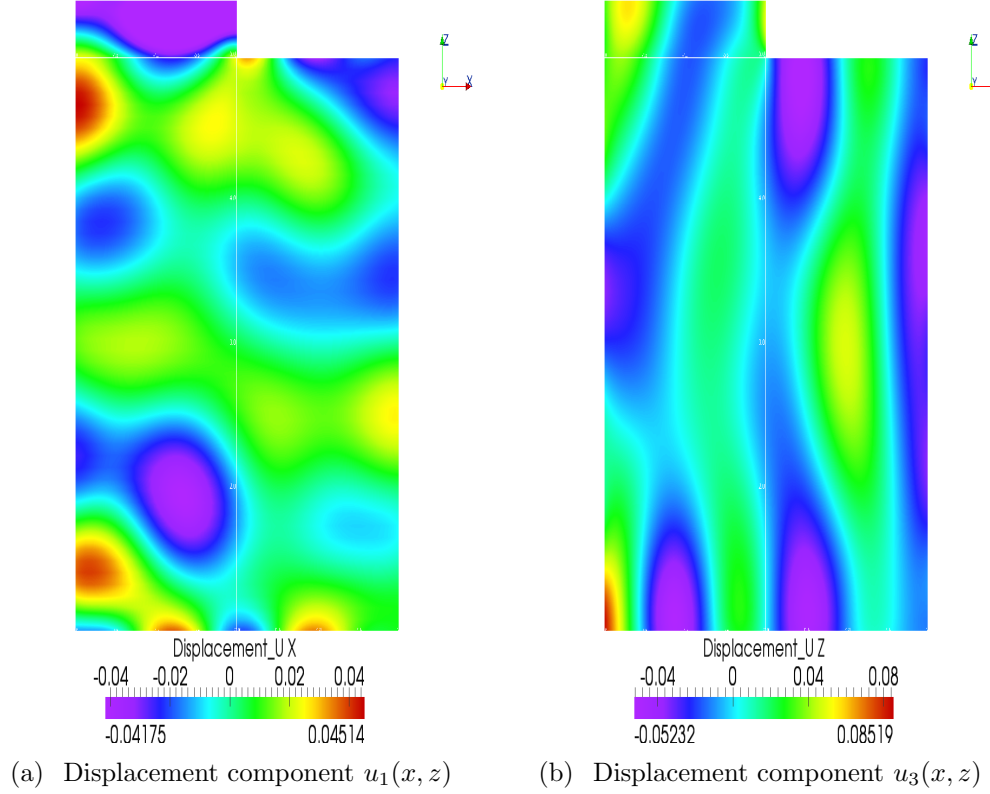


Figure 3.11: Fully-anisotropic elastodynamic problem showing interconnection between quadrangles with different types of material properties modelled utilizing proposed \mathcal{GF} s method

region Ω_a is the same in the model problems depicted in both Figs. 3.5 and 3.3. However, the substrate quadrangles in Fig. 3.5 are replaced by totally different elastic media, i.e., Lithium Niobate, which has very complex material properties expressed in terms of stiffness constants (Table 3.3). Figure 3.11 shows the corresponding solution of the composite structure comprising Aluminium and Lithium Niobate quadrangles, and utilizing the proposed Green's functional technique.

Remark: We shall disclose the superiority of the proposed Greens's function

technique manifests itself in just important feature: The pre-calculated \mathcal{GF} s, associated with a given material, size and shape, remains unaltered regardless of the relative position of the considered quadrangles. Essentially meaning, all the quadrangles in a given device geometry of same size, shape and material constants needs to be calculated only once, rest are treated as copy of original quadrangle. This property has significant implication in numerical calculations. Hence computing all possible \mathcal{GF} s for only one electrode subsection, suffices to characterize all electrode subsections appearing in both model problems Figs. 3.3 and 3.5. The realization of this property enables us to save computational resources (both time and storage space) by orders of magnitudes. In view of the fact that practical micro-acoustic devices can be assembled of only a dozen of “macro-quadrangles,” the implication of the above-mentioned saving of resources can fundamentally change the way how simulations are carried out. In particular, and somehow paradoxical, the savings are more prominent, the larger the devices are. The reason for this most favorable property is again due to the fact the larger devices can typically be assembled from a comparatively small number of macro-quadrangles, we only need the relative data from the LIBRARY into the “WORKING MEMORY” more often. This feature of the proposed algorithm, once fully exploited, can thus not only accelerate computations but also allow the computational scientists to create the required LIBRARIES independent of the concrete geometries at hand.

3.7 Concluding Remarks

The concept of Distributed Elementary Source Self-regularized Dyadic Green's Functions (\mathcal{GF}) was introduced for the elastodynamic analysis of the massloading effect in 2D micro-acoustic devices with fully-anisotropic elastic substrate materials. The proposed Green's functions were derived utilizing Galerkin procedure for the discretization of the involved surface integrals. A physics-based Model-Order-Reduction method was also introduced for compactly storing the Green's functions in a LIBRARY for future usage. This strategy enabled an unprecedented data compression without compromising the accuracy of the solutions. For the construction of Green's functions, the Exhaustion principle was presented. Introducing yet another concept, the Sufficiency principle, it was shown that the data stored in the LIBRARY fully suffice to address typical (Dirichlet and Neumann) boundary- and interface conditions. Each type of the boundary condition could be addressed by merely loading an insignificant amount of data into WORKING MEMORY and carrying out elementary postprocessing to build the system matrix for determination of unknowns (only existing at interfaces) in the problem. It was demonstrated how composite structures can be analyzed by concatenating the individual matrices and building the assembly matrix for the interconnection problem.

The Distributed Elementary Source Self-regularized Dyadic Green's Functional method possesses distinct advantages over the traditional methods such as FEM

and BEM. The geometry of the device is partitioned into a number of quadrangles, such that, the given Boundary Value Problem is schematically divided into a system of individual surface integral equations, each defining quadrangles. In contrast to the traditional BEM the proposed \mathcal{GF} s technique leads to a simplified form of integral equations with no singularities involved. Thus, a main limitation of the conventional BEM when applied to fully-anisotropic elastodynamic problems has been removed. In solving the interconnection problem for assemblage of two or more quadrangles, the method also manages to bypass the exhaustive iterative computations or expansive convolution calculations or back-and-forth Fourier or Laplace transformations, as it is the case traditionally. The interconnection problem was solved rather non-trivially with the help of \mathcal{GF} s which were pre-computed and stored in the LIBRARY.

The demonstrated numerical examples attest simplified applicability of the proposed Green's functional method even in the case of fully-anisotropic problems. The method presented in this chapter is applicable *mutatis mutandis* to various other fields in engineering such as applied mechanics, geophysics and general acoustics. Full potential of the proposed Green's function method can be realized once it is applied to fully three dimensional problems [47]. Future research work will be dedicated to solve fully-anisotropic micro-acoustic elastodynamic problems in 3D.

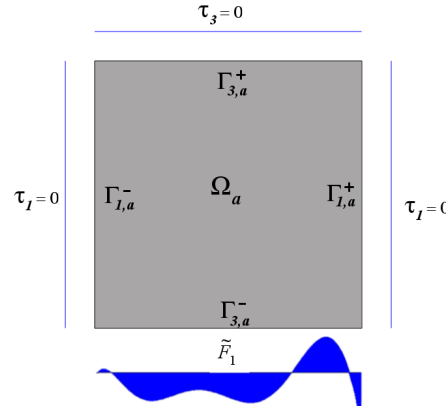
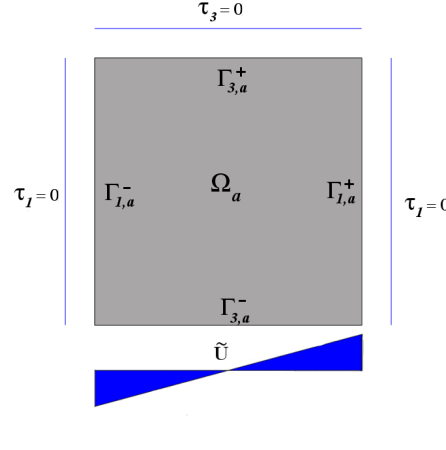
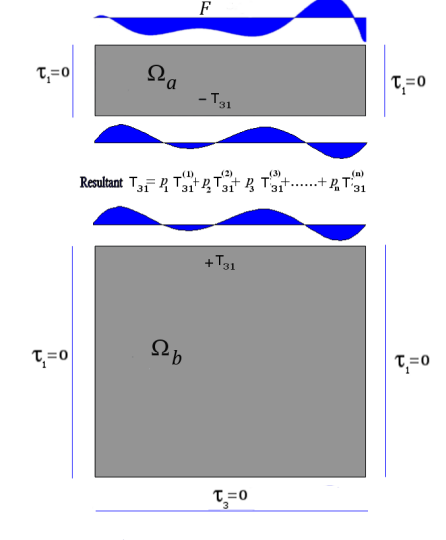
No.	Configuration	Boundary and interface conditions
1		<p><i>Inhomogeneous Neumann condition on a given edge of the quadrangle:</i> We synthesis τ_i in terms of appropriately chosen basis functions, by introducing an adequate number of expansion coefficients.</p>
2		<p><i>Inhomogeneous Dirichlet condition (fixed non-zero displacements on the given edge of the boundary):</i> We shall process this type of boundary conditions by taking rather an unconventional route. One of the important results in this chapter is that the inhomogeneous Dirichlet boundary condition can be satisfied with the help of pre-computed Green's Functions.</p>
3		<p><i>Interface condition:</i> The solution strategy for this type of interface conditions will be illustrated in this chapter. The Sufficiency- and Exhaustion principle applied utilizing the precalculated \mathcal{GF}s available in the LIBRARY to solve this type of boundary condition.</p>

Table 3.2: On the boundary conditions: interpretation and solution strategy

<i>Material type</i>	<i>Material property</i>	<i>Units</i>
Aluminium	$\rho = 2.77$	$\times 10^3 \text{kg/m}^3$
	$C_{11} = C_{22} = C_{33} = 10.80,$ $C_{44} = C_{55} = C_{66} = 2.85,$ $C_{12} = C_{21} = C_{31} = C_{13} = C_{32} = C_{23} = 5.10$	$\times 10^{10} \text{N/m}^2$
Lithium Niobate	$\rho = 4.7$	$\times 10^3 \text{kg/m}^3$
	$C_{11} = C_{22} = 20.3, C_{33} = 24.5, C_{44} = C_{55} = 6.0,$ $C_{12} = C_{21} = 5.3, C_{23} = C_{32} = C_{13} = C_{31} = 7.5,$ $C_{14} = C_{41} = C_{56} = C_{65} = 0.9, C_{24} = C_{42} = -0.9,$ $C_{66} = 0.5(C_{11} - C_{12})$	$\times 10^{10} \text{N/m}^2$

Table 3.3: Materials and its properties utilized in numerical examples

Chapter 4

3D Elastodynamic Simulation of Anisotropic/Isotropic Interface Problems in Elastic Media

4.1 Introduction

Considerable research effort has been dedicated to the simulation of harmonically time varying 3D isotropic elastodynamic problems in the last two decades. However, when it comes to anisotropic elastic problems publications are rare, due to the involvement of a large number of independent material constants for specifically various materials. Furthermore, the computation of fundamental solutions for a 3D anisotropic, inhomogeneous media has generated interest in various engineering fields including acoustics, solid mechanics, electromagnetics, geophysics and seismology [66, 67, 68]. The fundamental solutions, generally referred to as

‘Green’s functions,’ depending on conditions under which they are constructed, contain considerable information about the associated Boundary Value Problems (BVPs). Thus a question arises whether and how efficiently the Green’s functions can be constructed and stored. The latter property is advantageous since once the data have been calculated, they can be recycled for frequent future usage. However, the Green’s functions associated with anisotropic media for static, transient or time-harmonic problems, cannot be generally expressed in closed-form. The traditional methods for constructing Green’s functions, which are mostly based on integral transforms, are in such cases not only complicated (to implement) but are also computationally cumbersome. In this chapter we focus on the derivation and application of fundamental solutions for fully-anisotropic media, while avoiding the mentioned shortcomings and obstacles.

A variety of alternative methods are also proposed to solve BVPs associated with 3D anisotropic media in recent times. In applied mechanics a class of problems related to time-domain is effectively analyzed with the time-domain Boundary Element Method (BEM). The 3D time-domain BEM establishes an integral representation for the solution of wave equations to be in integral form. The integral presentation expresses the displacement vector field in terms of boundary values of displacement and traction by means of certain problem-specific dyadic Green’s functions. The convolution of the Green’s functions with specified force vectors gives the solution to the required problem (Yakhno and Cerdik Yaslan

[69] and references therein). The derivation of Green's functions becomes important not only for time-domain but also for static and frequency-domain analysis. A brief study of different methods in case of eigenvalue analysis using BEM was shown by Ali et. al. [70]. Tewary [71] derived the 3D Green's functions for anisotropic solids by efficiently solving Christoffel equation in response to Dirac delta functions excitations. The method was applied to calculate the time-domain and static displacement field due to point source excitation in infinite and semi-infinite anisotropic cubic solids. Applications of BEM to elastostatic problems with anisotropic media was attempted by Pan and Tonon, Wang and Denda, Sharma, Niu and Dravinski [68, 72, 73, 74] and the authors referred to in their works. Pan and Tonon [68] applied Radon transformation to obtain integral expressions for the (displacement) Green's functions, additionally providing an efficient procedure of calculating their derivatives. Aspects of the numerical calculation of the involved line integrals over the unit semi-circle were detailed by Wang and Denda [72]. The correlation-type reciprocity theorem was utilized by Wapenaar [67] to retrieve the Green's functions from the cross-correlation of observed wave fields. A similar approach of utilizing dual reciprocity method was utilized by Kogl and Gaul [75] in order to circumvent the problems related to the anisotropic dynamic fundamental solutions. Implementing Finite Element Method (FEM) and Finite Difference Method (FDM) for solving 3D anisotropic elastodynamic problems, occurring in acoustics, is generally perceived to be a difficult task. A detailed survey of articles was compiled by Thompson, Harari

[76, 77] for various classes of acoustical problems, where different FEM approaches with key features such as absorbing boundary conditions, infinite elements and absorbing layers are solved. Numerical model for the coupled analysis of arbitrary shaped cross-sections made of heterogeneous anisotropic materials under 3D combined loading was formulated by Garcia and Bernat [78]. A 3D fracture analysis of anisotropic elastic media was carried out by Rungamornrat and Mear [79], where a coupling of weakly singular symmetric Galerkin BEM and standard FEM was achieved. Lovane and Nasedkin [80], utilized FEM along with extend Rayleigh models to solve 3D dynamic problems with anisotropic porous materials.

Simulation of the mass-loading effect in Surface Acoustic Wave (SAW) and Bulk Acoustic Wave (BAW) devices has been of paramount interest and significance in the micro-acoustic device community [51, 53, 66, 81]. Where, the authors have shown application of FEM, BEM and their hybridization mixture of both to study mass-loading related effects.

Solving any given BVPs subject to stringent time- and other resources constraints, without compromising accuracy of the numerical results, has always been the prime consideration in developing or selecting a method. In the past two decades the reduction of the computational time through parallel computing has gained popularity amongst the engineers. In order to take advantage of the multiprocessing CUPs the methods such as FEM, BEM and Spectral techniques utilized various substructuring techniques. The methods such as Domain Decomposition,

Discontinuous Galerkin, Penalty-based interface technique, Multidomain spectral method have been implemented to solve various static ([33, 37, 82]) and dynamic ([83, 84]) problems.

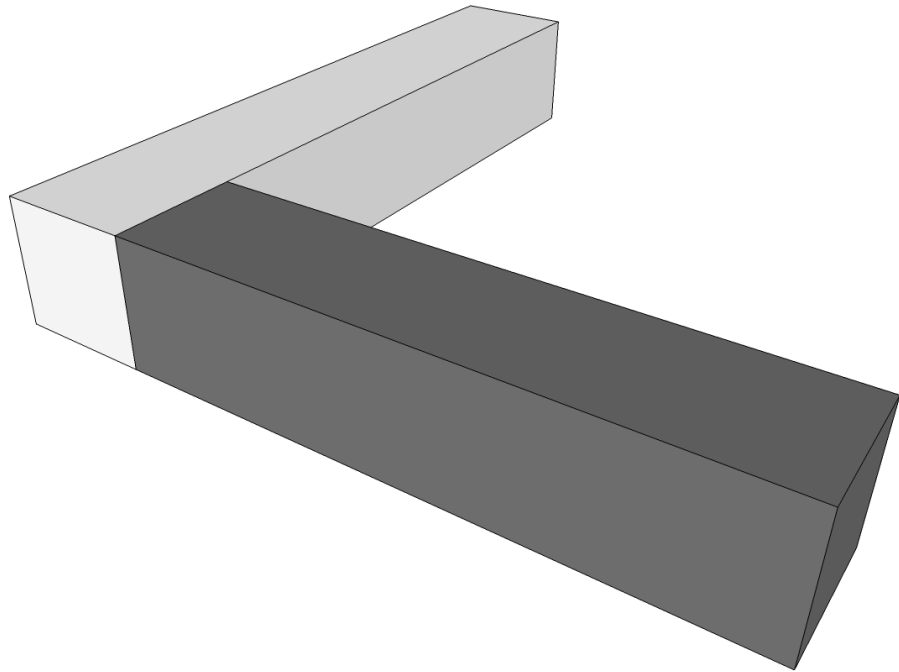


Figure 4.1: A L-shaped joint with interface between anisotropic and isotropic medium

The problems related to large deformation, low frequency analysis, interpolation errors, inaccuracy of secondary variables, e.g. stress and strain derived from the primary variables such as displacements. Traditional calculations based on the FEM, BEM or a combination of both lack the desired flexibility in producing pre-calculated data and storing them in libraries for frequent future use in device design cycles. Ordinarily, this is regarded as a challenging task because stress distributions for elastodynamic simulation are in general strongly

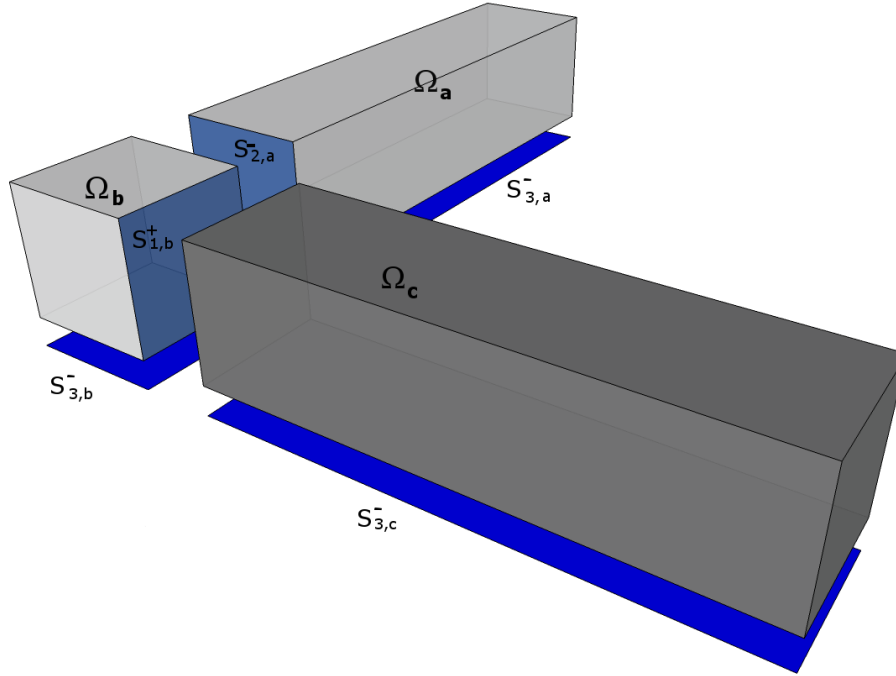


Figure 4.2: Example showing the partitioning of the L-shaped joint

frequency-dependent. The above-mentioned issues call for a numerical method with the distinct properties including: (a) The method should be conservative in the sense that continuum property of the involved differential operators remain unaltered after partitioning the problem. (b) The method should be computationally efficient. (c) The method should be comparatively easily implementable, (d) The accuracy should not be compromised. In the proposed method several ideas are chosen and adapted from various realms of computational engineering, e.g. spectral analysis, the weak formulation of Galerkin procedure, and Green's functional theory. Furthermore, the method utilizes orthonormal basis functions adapted from spectral element method. The integrals and derivatives required to solve the system of Partial Differential Equations (PDEs) are cal-

culated for the entire domain rather than over the nodes, as it is the case for FEM, BEM or FDM, allowing the method to fall in the category of mesh-free or element-free methods exhibiting certain advantages over FEM. Aspects of these tools are refined and combined in a sophisticated manner to achieve our objective of mass-loading analysis by generating and pre-calculating a LIBRARY of problem-related Self-regularized Dyadic Green's functions. Thereby, the proposed Self-regularized Dyadic Green's functions are not calculated as it is usually the case (with energy functional technique); rather they are computed by minimizing a functional in weak form (Galerkin method). Additionally, in order to emphasize the distinct way of constructing inherently regularized dyadic Green's function we graphically and computationally illustrate the necessary steps involved. We shall underline this utmost important feature in our problem by referring to the constructed Green's functions, Distributed-Elementary-Source Self-regularized Dyadic Green's functions and refer to them collectively as \mathcal{GF} . With the help of the precalculated \mathcal{GF} s we also propose that each major device section can be isolated from the rest of the problem (detached) and replaced by equivalent forces and displacements at the surfaces where the device section has been detached. Distant analogy to this prescription could be found in well known methods such as domain decomposition, tearing and interconnecting methods, penalty-based finite element interface technology, etc. However, the scope of this analogy is rather limited; The construction and processing of the dyadic Green's functional technique utilized for solving the interface problem is unique and novel

as applied to time-harmonic analysis of massive cuboids.

The proposed method for solving the mass-loading effect in three spatial dimensions comprises the following steps:

- i) Subdivide 3D geometry into an adequate number of massive cuboids. Thereby, a given cuboid can be represented by one mesh-less hexahedron with no further meshing necessary.
- ii) Define the BVP for the construction of the associated \mathcal{GF} s for each individual cuboid.
- iii) Following the recipe proposed in this chapter, construct a complete set of 3D orthonormal expansion functions. These functions possess richly detailed and refined features and are equipped with distinct properties to describe the displacement- and traction spatial distributions in the target cuboids' interior, surface areas, their edges and corners, with prescribed precision.
- iv) Use a weak formulation, to account for the effect of the massive cuboids, in terms of the induced traction forces defined in their support-regions on the substrate surface.
- v) Compute the Self-regularized Dyadic Green's functions derived as a result of applied DES for each independent cuboids.
- vi) Encode compactly and store the information characterizing \mathcal{GF} s and their spatial derivatives, in a LIBRARY.
- vii) Retrieve the Dyadic Green's functions to solve the required boundary or

interface condition to form the device assembly, hence solving the problem.

4.2 Theory and Principles Utilized for Tearing and Interconnecting Isotropic and Anisotropic Cuboids

Before delving into the mathematical details it is imperative to clearly point out what is new in this chapter. This seems necessary not only to position the paper relative to preceding publications but also to help the reader to have a better understanding of the ideas put forward here. We restrict ourselves to the 3D elastodynamic analysis of fully-anisotropic test problems. Since the trust of the chapter is the utilization of the pre-computed 3D Green's functions, the geometrical complexity will not add anything other than the need for higher level

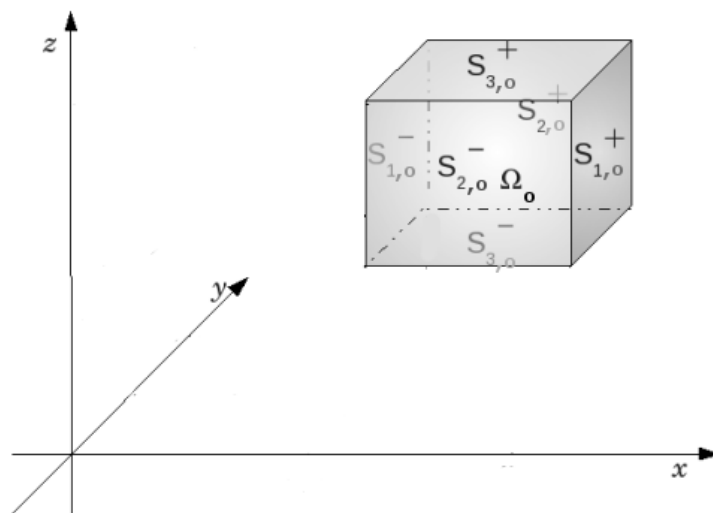


Figure 4.3: An arbitrarily located cuboid

of assembly procedure. For simplicity purpose, consider the structure sketched in Fig. 4.1 as the test problem. The figure shows a bonded, anisotropic (Lithium Niobate) and isotropic (Aluminium), 3D “L-shaped” elastic media.

4.2.1 Distributed-Elementary-Source Self-regularized Dyadic Green’s functions (\mathcal{GF}) versus Dirac delta-function excitation of the media

Given a boundary value problem Green’s functions are traditionally defined as responses of the media to elementary excitations. Ordinarily Dirac delta-function are considered as the elementary excitations- a fact which has rendered Green’s function the name tag ‘impulse response’ or ‘fundamental solutions.’ Isolated excitation forces generally result in Green’s functions which are singular. The Green’s function singularities can be strong or hyper-strong and require special treatment for their regularization. In contrast to conventional schemes here we employ Distributed-Elementary-Sources (DES) which result in Self-regularized Dyadic Green’s functions (\mathcal{GF} s). As elementary sources, we choose normalized Legendre polynomials which alludes to the Distributed-Elementary-Sources. The responses to the elastic medium due to the DES are regularized (nonsingular) displacement components; hence Self-regularized. Furthermore, since the involved forces and associated displacement responses are vector functions, we speak of dyadic Green’s functions.

The idea of domain decomposition and equivalent forces in FEM and other numerical techniques is common place. To convey the essence of the idea, it suffices to consider scalar-valued sources and responses and thus talk about scalar Green's functions only for this section. In the text the ideas will be extended to vector-valued quantities and thus notion of dyadic Green's functions will enter our discussion. The idea introduced here utilizes the ability which is innate to the concepts of Green's functions, and previously introduced Sufficiency principle and principle of Exhaustion. In the discussion which will follow we consider excitations of fully-anisotropic 3D media by forces positioned on the bounding surfaces of the media. Furthermore, we talk about a medium occupying the volume Ω with its bounding surface S . Forces applied to the surfaces will be operating at the frequency ω .

In this chapter we demonstrate effective implementation of above tools. Next section describes the partitioning of the device geometry into a number of cuboids and the problem description. Considerable effort has been undertaken to clarify the way partitioning is carried out and subsequently prepared to take advantage of the available data in the LIBRARY. The following section describes the details of the weak formulation of Galerkin type applied to each independent cuboids. Each cuboid is excited with DES, resulting into Self-regularized Dyadic Green's functions. These Green's functions are then utilized to solve the interface conditions over the interface area with the help of the Sufficiency- and Exhaustion

principles, leading to the results and the conclusion section.

4.3 Statement of the Problem

Interfacing and interconnecting fully-anisotropic and isotropic 3D elastic media by utilizing pre-computed Self-regularized Dyadic Green's Functions.

4.3.1 Partitioning a Given Structure into an Adequate Number of Hexahedrons and Problem Description

Consider the L-shape structure shown in Fig. 4.1. The structure is subject to the constant (spatially uniform) force vector $\tilde{\mathbf{F}}$, applied at the 'southern' surface S_3^- , time-harmonically ($e^{-j\omega t}$) operating at the frequency ω . More precisely, we have the governing equation:

$$\underline{\underline{\nabla}}^t \mathbf{T} = -\rho\omega^2 \mathbf{u}, \quad \text{in } \Omega, \quad (4.1)$$

and the boundary conditions

$$\boldsymbol{\tau}_3|_{S_3^-} = \tilde{\mathbf{F}}, \quad \text{on } S_3^- \quad (4.2)$$

with other surfaces being stress-free. In order to solve the BVP, we propose the method of Distributed-Elementary-Source Dyadic Green's functions. Thereby, the given BVP is partitioned into independent BVPs, separated in terms of

equivalent DES at the interfaces. Thus the task will be reduced to imposition of interface condition for each adjacent cuboids.

4.3.2 Partitioning into Hexahedrons

We partition the volume Ω into Ω_a , Ω_b and Ω_c as shown in Fig. 4.2. The subsystems a , b and c touch each other at the common fictitious interfaces $S_{2,a}^- (= S_{2,b}^+)$ and $S_{1,b}^- (= S_{1,c}^+)$. We note the stress-free boundary conditions on all the remaining surfaces. In view of Eqs. (4.1) and (4.2), we obtain the following equations for the subsystems a , b and c , respectively:

$$\underline{\underline{\nabla}}^t \mathbf{T}_i = -\rho\omega^2 \mathbf{u}_i, \quad \text{in } \Omega_i, \quad (4.3)$$

and

$$\boldsymbol{\tau}_{3,i}|_{S_{3,i}^-} = \tilde{\mathbf{F}}_i, \quad \text{on } S_{3,i}^-, \quad (4.4)$$

with $i = a, b, c$ and assuming that $\tilde{\mathbf{F}}_a \cup \tilde{\mathbf{F}}_b \cup \tilde{\mathbf{F}}_c = \tilde{\mathbf{F}}$. Additionally, the conditions

$$\boldsymbol{\tau}_{2,a}|_{S_{2,a}^-} = \boldsymbol{\tau}_{2,b}|_{S_{2,b}^+} \quad \text{and} \quad \mathbf{u}|_{S_{2,a}^-} = \mathbf{u}|_{S_{2,b}^+}, \quad (4.5)$$

need to be satisfied at the interface $S_{2,a}^- = S_{2,b}^+$ and

$$\boldsymbol{\tau}_{1,b}|_{S_{1,b}^-} = \boldsymbol{\tau}_{1,c}|_{S_{1,c}^+} \quad \text{and} \quad \mathbf{u}|_{S_{1,b}^+} = \mathbf{u}|_{S_{1,c}^-}, \quad (4.6)$$

at the interface, $S_{1,b}^+ = S_{1,c}^-$, ensuring the continuity of both stress- and displacement functions. With Eqs. (4.3)-(4.6) we employ the concept of divide and rule. *A priori* unknown dynamic equivalent forces are introduced on the interfaces. Each cuboid is considered to be an individual problem and is treated in isolation. The proposed Dyadic Green's functions are derived for each cuboid with the help of Galerkin method. However, these Dyadic Green's functions are due to distributed elementary sources rather than traditional point like sources. The procedure for the derivation of these Green's functions is described next. These sets up the stage to introduce to the type of dyadic Green's functions we utilize.

4.4 Distributed-Elementary-Source Self-regularized Dyadic Green's Functions

4.4.1 Description of Weak-Galerkin Formulation

Consider a fully-anisotropic homogeneous elastic cuboid as shown in Fig. 4.3. The given elastic medium characterized by the 6×6 stiffness matrix \mathbf{C} and the constant mass density ρ , occupies the volume Ω_o with the boundary surface S_o . The equation of motion for this medium reads:

$$\underline{\underline{\nabla}}^t \mathbf{T} = -\rho\omega^2 \mathbf{u}, \quad \text{in } \Omega_o, \quad (4.7)$$

or, equivalently,

$$[\mathbf{N}_1^t \partial_x + \mathbf{N}_2^t \partial_y + \mathbf{N}_3^t \partial_z] \mathbf{T} = -\rho \omega^2 \mathbf{u}, \quad \text{in } \Omega_o. \quad (4.8)$$

The superscript t signifies transposition. A harmonic time-dependence according to $e^{-j\omega t}$ has been assumed. Here, \mathbf{u} is the mechanical displacement vector and \mathbf{T} stands for the stress tensor, which appears in our calculations as a column vector with six components T_i ($i = 1, \dots, 6$). $\underline{\underline{\nabla}}$ is Auld's 6×3 divergence-type differential operator [1]. Introduce stresses $\boldsymbol{\tau}_i$, ($i = 1, 2, 3$)

$$\boldsymbol{\tau}_i = \mathbf{N}_i^t \mathbf{T} = \mathbf{N}_i^t \mathbf{C} \underline{\underline{\nabla}} \mathbf{u} \quad (4.9)$$

where,

$$\mathbf{N}_1 = \begin{bmatrix} 1 & 0 & 0 \\ 0 & 0 & 0 \\ 0 & 0 & 0 \\ 0 & 0 & 0 \\ 0 & 0 & 1 \\ 0 & 1 & 0 \end{bmatrix}, \quad \mathbf{N}_2 = \begin{bmatrix} 0 & 0 & 0 \\ 0 & 1 & 0 \\ 0 & 0 & 0 \\ 0 & 0 & 1 \\ 0 & 0 & 0 \\ 1 & 0 & 0 \end{bmatrix}, \quad \mathbf{N}_3 = \begin{bmatrix} 0 & 0 & 0 \\ 0 & 0 & 0 \\ 0 & 0 & 1 \\ 0 & 1 & 0 \\ 1 & 0 & 0 \\ 0 & 0 & 0 \end{bmatrix}. \quad (4.10)$$

For a detailed discussion of the properties of the operator $\underline{\underline{\nabla}}$ and the constituent 6×3 matrices \mathbf{N}_i ($i = 1, 2, 3$) we refer to the discussion in [11]. With these definitions Eq. (4.8) can be transformed into the following convenient form:

$$\partial_x \boldsymbol{\tau}_1 + \partial_y \boldsymbol{\tau}_2 + \partial_z \boldsymbol{\tau}_3 = -\rho \omega^2 \mathbf{u} \quad (4.11)$$

Here, $\boldsymbol{\tau}_i$ comprises the stress components T_{1i}, T_{2i}, T_{3i} which act on the surface with the outward unit normal vector \mathbf{n}_i . Multiplying both sides of Eq. (4.11) by the transpose of a 3×1 test-vector \mathbf{v} (elementary weighting function representing any of the vectors $(v_1 \ 0 \ 0)^t$, $(0 \ v_2 \ 0)^t$, or $(0 \ 0 \ v_3)^t$) we obtain:

$$\mathbf{v}^t \partial_x \boldsymbol{\tau}_1 + \mathbf{v}^t \partial_y \boldsymbol{\tau}_2 + \mathbf{v}^t \partial_z \boldsymbol{\tau}_3 = -\rho \omega^2 \mathbf{v}^t \mathbf{u} \quad (4.12)$$

Obviously, by rolling over the derivatives onto the test-vector \mathbf{v} , Eq. (4.12) is equivalent with:

$$\begin{aligned} & \partial_x(\mathbf{v}^t \boldsymbol{\tau}_1) - (\partial_x \mathbf{v}^t) \boldsymbol{\tau}_1 + \partial_y(\mathbf{v}^t \boldsymbol{\tau}_2) - (\partial_y \mathbf{v}^t) \boldsymbol{\tau}_2 \\ & + \partial_z(\mathbf{v}^t \boldsymbol{\tau}_3) - (\partial_z \mathbf{v}^t) \boldsymbol{\tau}_3 = -\rho \omega^2 \mathbf{v}^t \mathbf{u} \end{aligned} \quad (4.13)$$

Integrate the terms on both sides of this equation over the volume Ω_o , and apply the Gauss' divergence theorem to obtain boundary integrals, which involve terms with reduced order of derivatives by one:

$$\begin{aligned} & - \int_{\Omega_o} d\Omega_o (\partial_x \mathbf{v}^t) \boldsymbol{\tau}_1 - \int_{\Omega_o} d\Omega_o (\partial_y \mathbf{v}^t) \boldsymbol{\tau}_2 - \int_{\Omega_o} d\Omega_o (\partial_z \mathbf{v}^t) \boldsymbol{\tau}_3 \\ & + \iint_{S_{1,o}^+} dy dz \mathbf{v}^t \boldsymbol{\tau}_1 + \iint_{S_{2,o}^+} dx dz \mathbf{v}^t \boldsymbol{\tau}_2 + \iint_{S_{3,o}^+} dx dy \mathbf{v}^t \boldsymbol{\tau}_3 \\ & - \iint_{S_{1,o}^-} dy dz \mathbf{v}^t \boldsymbol{\tau}_1 - \iint_{S_{2,o}^-} dx dz \mathbf{v}^t \boldsymbol{\tau}_2 - \iint_{S_{3,o}^-} dx dy \mathbf{v}^t \boldsymbol{\tau}_3 \\ & = -\rho \omega^2 \int_{\Omega_o} d\Omega_o \mathbf{v}^t \mathbf{u} \end{aligned} \quad (4.14)$$

The interest is in deriving Green's functions characterizing the cuboid Ω_o having the surfaces $S_{1,o}^+, S_{1,o}^-, S_{2,o}^+, S_{2,o}^-, S_{3,o}^+$ and $S_{3,o}^-$. Assume all surfaces of the volume

Ω_o are stress-free ($\boldsymbol{\tau}_i = 0$), except $S_{1,o}^+$. Thus Eq. (4.14) and Eq. (4.9) followed by a routine manipulation leads to:

$$\begin{aligned}
& - \int_{\Omega_o} d\Omega_o (\partial_x \mathbf{v}^t) \mathbf{N}_1^t \mathbf{C} \underline{\underline{\nabla}} \mathbf{u} - \int_{\Omega_o} d\Omega_o (\partial_y \mathbf{v}^t) \mathbf{N}_2^t \mathbf{C} \underline{\underline{\nabla}} \mathbf{u} \\
& - \int_{\Omega_o} d\Omega_o (\partial_z \mathbf{v}^t) \mathbf{N}_3^t \mathbf{C} \underline{\underline{\nabla}} \mathbf{u} + \iint_{S_{1,o}^+} dy dz \mathbf{v}^t \boldsymbol{\tau}_1 \\
& = -\rho\omega^2 \int_{\Omega_o} d\Omega_o \mathbf{v}^t \mathbf{u}
\end{aligned} \tag{4.15}$$

Considering, $\underline{\underline{\nabla}} = \mathbf{N}_1 \partial_x + \mathbf{N}_2 \partial_y + \mathbf{N}_3 \partial_z$ the Eq. (4.15) becomes:

$$\begin{aligned}
& - \int_{\Omega_o} d\Omega_o (\partial_x \mathbf{v}^t) \mathbf{N}_1^t \mathbf{C} [\mathbf{N}_1 \partial_x + \mathbf{N}_2 \partial_y + \mathbf{N}_3 \partial_z] \mathbf{u} \\
& - \int_{\Omega_o} d\Omega_o (\partial_y \mathbf{v}^t) \mathbf{N}_2^t \mathbf{C} [\mathbf{N}_1 \partial_x + \mathbf{N}_2 \partial_y + \mathbf{N}_3 \partial_z] \mathbf{u} \\
& - \int_{\Omega_o} d\Omega_o (\partial_z \mathbf{v}^t) \mathbf{N}_3^t \mathbf{C} [\mathbf{N}_1 \partial_x + \mathbf{N}_2 \partial_y + \mathbf{N}_3 \partial_z] \mathbf{u} \\
& + \iint_{S_{1,o}^+} dy dz \mathbf{v}^t \boldsymbol{\tau}_1 = -\rho\omega^2 \int_{\Omega_o} d\Omega_o \mathbf{v}^t \mathbf{u}
\end{aligned} \tag{4.16}$$

With the explicit definitions of \mathbf{N}_1 , \mathbf{N}_2 and \mathbf{N}_3 , and considering a general 6×6 positive definitive stiffness matrix \mathbf{C} , Eq. (4.16) reads:

$$\begin{aligned}
& - \int_{\Omega_o} d\Omega_o [\partial_x \mathbf{v}^t \mathbf{P}_{11} \partial_x + \partial_x \mathbf{v}^t \mathbf{P}_{12} \partial_y + \partial_x \mathbf{v}^t \mathbf{P}_{13} \partial_z] \mathbf{u} \\
& - \int_{\Omega_o} d\Omega_o [\partial_y \mathbf{v}^t \mathbf{P}_{21} \partial_x + \partial_y \mathbf{v}^t \mathbf{P}_{22} \partial_y + \partial_y \mathbf{v}^t \mathbf{P}_{23} \partial_z] \mathbf{u} \\
& - \int_{\Omega_o} d\Omega_o [\partial_z \mathbf{v}^t \mathbf{P}_{31} \partial_x + \partial_z \mathbf{v}^t \mathbf{P}_{32} \partial_y + \partial_z \mathbf{v}^t \mathbf{P}_{33} \partial_z] \mathbf{u} \\
& + \iint_{S_{1,o}^+} dy dz \mathbf{v}^t \boldsymbol{\tau}_1 = -\rho\omega^2 \int_{\Omega_o} d\Omega_o \mathbf{v}^t \mathbf{u}
\end{aligned} \tag{4.17}$$

Here, $\mathbf{P}_{ij} = \mathbf{N}_i^t \mathbf{C} \mathbf{N}_j$ with $i, j = 1, 2, 3$. As an example, we have

$$\begin{aligned} \mathbf{P}_{11} &= \begin{bmatrix} 1 & 0 & 0 \\ 0 & 0 & 0 \\ 0 & 0 & 0 \\ 0 & 0 & 0 \\ 0 & 0 & 1 \\ 0 & 1 & 0 \end{bmatrix}^t \begin{bmatrix} C_{11} & \cdots & C_{16} \\ \vdots & \ddots & \vdots \\ C_{61} & \cdots & C_{66} \end{bmatrix} \begin{bmatrix} 1 & 0 & 0 \\ 0 & 0 & 0 \\ 0 & 0 & 0 \\ 0 & 0 & 0 \\ 0 & 0 & 1 \\ 0 & 1 & 0 \end{bmatrix} \\ &= \begin{bmatrix} C_{11} & C_{16} & C_{15} \\ C_{61} & C_{66} & C_{65} \\ C_{51} & C_{56} & C_{55} \end{bmatrix}. \end{aligned} \quad (4.18)$$

Similarly, the remaining $\mathbf{P}_{i,j}$ can be obtained.

4.4.2 Discretization of Eq. (4.17)

In Eq. (4.17) \mathbf{u} stands for the displacement vector with the components u_1, u_2 and u_3 .

More explicitly we can write:

$$\mathbf{u} = \begin{bmatrix} u_1(x, y, z) \\ u_2(x, y, z) \\ u_3(x, y, z) \end{bmatrix} \quad (4.19)$$

Thus far the scalar function $u_i(x, y, z)$ are considered as entire domain functions without any discretization. The displacement functions can be approximated in terms of the complete set of basis functions $B_{l,m,n}(x, y, z)$.

$$u_1(x, y, z) \approx \sum_{l=0}^L \sum_{m=0}^M \sum_{n=0}^N u_{l,m,n}^{(1)} B_{l,m,n}(x, y, z). \quad (4.20)$$

This set of 3D basis functions are entire domain basis functions since each basis function is just product of three 1D basis functions in each direction, i.e. $B_i(x, y, z) = B_{l \odot m \odot n}(x, y, z) = b_l(x) \cdot b_m(y) \cdot b_n(z)$ with $l = 0, \dots, L$, $m = 0, \dots, M$, $n = 0, \dots, N$ and $i = 0, \dots, L \times M \times N$. Due to this index-dependent feature, yet factorized form of basis functions, calculating the derivatives of the 3D polynomials can be reduced to 1D calculations. A similar conclusion can be drawn for the calculation of the involved integrals that are necessary in order to solve the system of coupled equations characterizing our BVP. A further comment concerns the derivatives and integrals of the basis functions. The basis functions considered in this chapter are normalized Legendre polynomials, over the domain $[-1, 1]$. Finding derivatives and integrals of these polynomials over domain $[-1, 1]$ is an easy task and they can be pre-calculated and tabulated for frequent use. The pre-calculated derivatives and integrals can then be transformed to any desired domain (by multiplying them with respective transformation coefficients, as it is done in various other methods). For brevity of the notation in the following, we suppress the variable x, y and z in $B_{l,m,n}$. Obviously, series expansions similar to Eq. (4.20) can be obtained for the functions $u_2(x, y, z)$ and $u_3(x, y, z)$ by introducing expansion coefficients $u_{l,m,n}^{(2)}$ and $u_{l,m,n}^{(3)}$. Employing matrix notation the approximate displacement components $u_1(x, y, z)$, $u_2(x, y, z)$ and $u_3(x, y, z)$ can

be cast in the following convenient form:

$$\mathbf{u} \approx \begin{bmatrix} [\cdots B_{l\ominus m\ominus n} \cdots] [\cdots 0_{l\ominus m\ominus n} \cdots] [\cdots 0_{l\ominus m\ominus n} \cdots] \\ [\cdots 0_{l\ominus m\ominus n} \cdots] [\cdots B_{l\ominus m\ominus n} \cdots] [\cdots 0_{l\ominus m\ominus n} \cdots] \\ [\cdots 0_{l\ominus m\ominus n} \cdots] [\cdots 0_{l\ominus m\ominus n} \cdots] [\cdots B_{l\ominus m\ominus n} \cdots] \end{bmatrix} \begin{bmatrix} \vdots \\ u_{l\ominus m\ominus n}^{(1)} \\ \vdots \\ \vdots \\ u_{l\ominus m\ominus n}^{(2)} \\ \vdots \\ \vdots \\ u_{l\ominus m\ominus n}^{(3)} \\ \vdots \end{bmatrix} \quad (4.21a)$$

$$= \mathbf{B}\mathbf{U} \quad (4.21b)$$

In transition from Eq. (4.21a) to (4.21b), the structure of \mathbf{B} and \mathbf{U} should be immediate. In Eq. (4.17) the vector \mathbf{v}^t plays a pivotal role. As pointed out earlier the components v_1, v_2 and v_3 of \mathbf{v} can assume the basis functions $B_{l\ominus m\ominus n}$. Therefore, the discretization of Eq. (4.17), leading to a matrix equation can be simplified significantly by introducing repressing \mathbf{v} by the matrix \mathbf{B} :

$$\mathbf{v} \Leftrightarrow \mathbf{B} = \begin{bmatrix} [\cdots B_{l\ominus m\ominus n} \cdots] [\cdots 0_{l\ominus m\ominus n} \cdots] [\cdots 0_{l\ominus m\ominus n} \cdots] \\ [\cdots 0_{l\ominus m\ominus n} \cdots] [\cdots B_{l\ominus m\ominus n} \cdots] [\cdots 0_{l\ominus m\ominus n} \cdots] \\ [\cdots 0_{l\ominus m\ominus n} \cdots] [\cdots 0_{l\ominus m\ominus n} \cdots] [\cdots B_{l\ominus m\ominus n} \cdots] \end{bmatrix} \quad (4.22)$$

Thus replacing $\mathbf{u} = \mathbf{B}\mathbf{U}$ and representing (\Leftrightarrow) \mathbf{v}^t by \mathbf{B}^t and integrating terms, Eq. (4.17) results in the following system of equations for the determination of

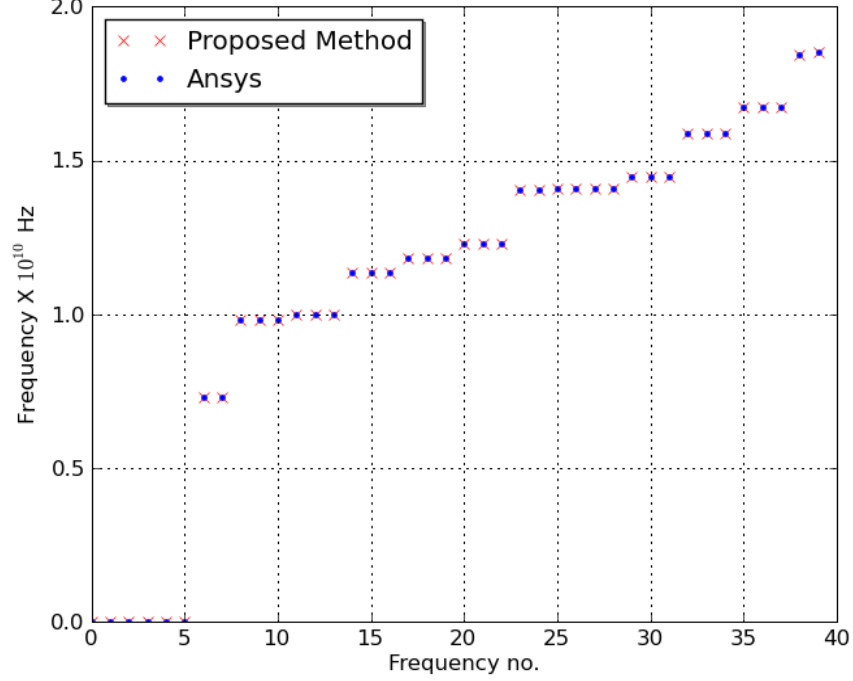


Figure 4.4: A comparison between eigenfrequencies obtained by the proposed method and the numerical results obtained by FEM package ANSYS

\mathbf{U} . Where, \mathbf{U} contains the expansion coefficients of $u_i(x, y, z)$, $i = 1, 2, 3$:

$$[\mathbf{K} - \omega^2 \mathbf{M}]_{\Omega_o} \mathbf{U} = [\mathbf{F}]_{S_{3,o}^+}. \quad (4.23)$$

On elaborating the terms in Eq. (4.17), the volume integral terms at the LHS result in the ‘stiffness’ matrix \mathbf{K} , whereas, the term at the RHS leads to the ‘mass’ matrix \mathbf{M} . In particular, with the help of Eqs. (4.21) and (4.22) the mass matrix can be written as,

$$-\rho\omega^2 \iiint_{\Omega_o} dx dy dz \mathbf{v}^t \mathbf{u} = -\rho\omega^2 \iiint_{\Omega_o} dx dy dz \mathbf{B}^t \mathbf{B} \mathbf{U} = -\omega^2 \mathbf{M} \mathbf{U}. \quad (4.24)$$

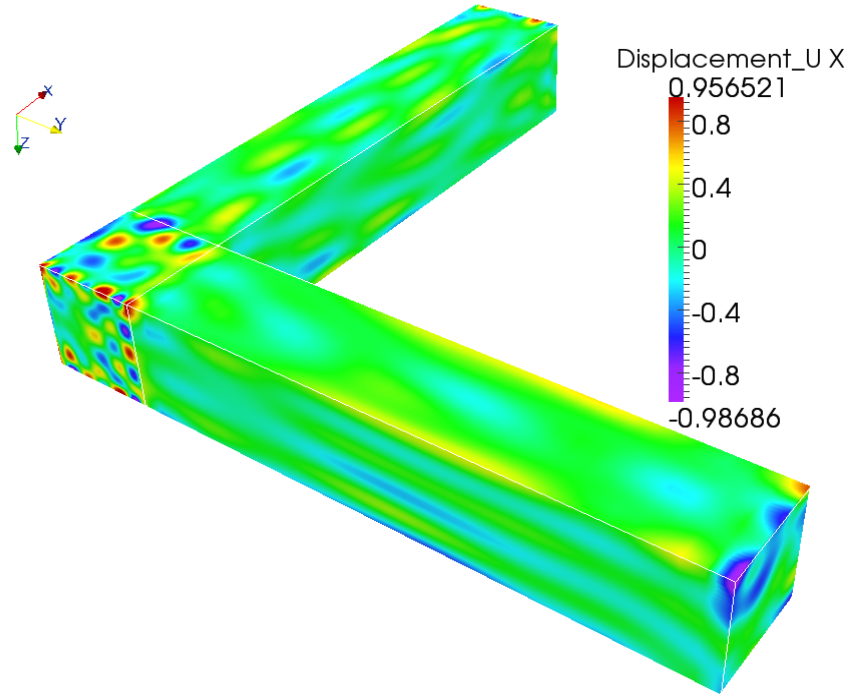


Figure 4.5: Displacement component $u_1(x, y, z)$ for a 3D elastodynamic problem after solving the interface conditions between anisotropic and isotropic cuboids

Here, $\iiint_{\Omega_o} dx dy dz \mathbf{B}^t \mathbf{B}$ turns out to be an identity matrix \mathbf{I} .

4.4.3 Distributed Elementary Sources and Associated Green's Functions

The last term on the LHS of Eq. (4.17) generates the 'source' vector \mathbf{F} , which is due to the traction force $\boldsymbol{\tau}_1$ applied on the surface $S_{1,o}^+$. The traction force $\boldsymbol{\tau}_1$, by

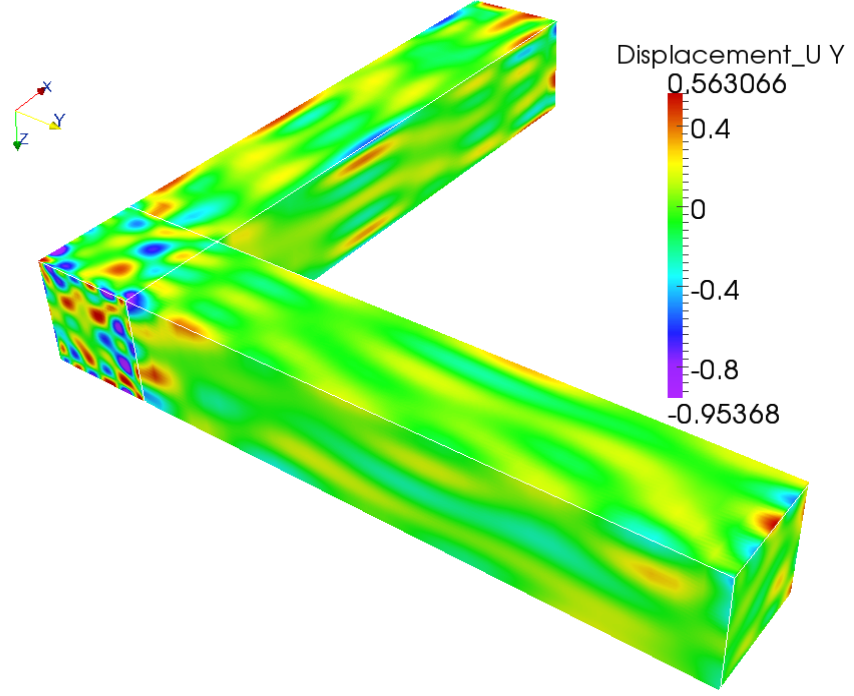


Figure 4.6: Displacement component $u_2(x, y, z)$ for a 3D elastodynamic problem after solving the interface conditions between anisotropic and isotropic cuboids

definition, consist of three components T_{11}, T_{12} and T_{13} :

$$\boldsymbol{\tau}_1(\mathbf{y}, z)|_{S_{1,o}^+} = \begin{bmatrix} T_{11}(\mathbf{y}, z) \\ T_{12}(\mathbf{y}, z) \\ T_{13}(\mathbf{y}, z) \end{bmatrix}_{S_{1,o}^+} \quad (4.25)$$

Next, in order to generate a series of elementary sources we need to reduce the source vector, such that

$$\boldsymbol{\tau}_1(\mathbf{y}, z)|_{S_{1,o}^+} = \begin{bmatrix} T_{11}(\mathbf{y}, z) \\ 0 \\ 0 \end{bmatrix}_{S_{1,o}^+} . \quad (4.26)$$

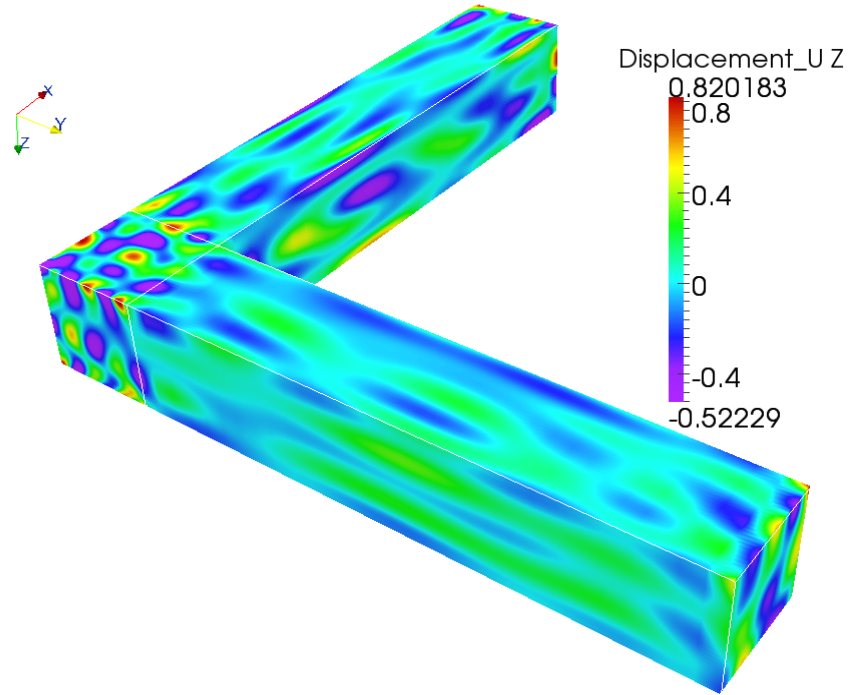


Figure 4.7: Displacement component $u_3(x, y, z)$ derived for three cuboids and placed side by side after determining the equivalent forces at the interfaces

This simplified source function can be interpreted in following way: the applied traction force Eq. 4.26, has a component normal to the surface $S_{1,o}^+$ while the remaining two transversal traction forces are suppressed ($T_{12}, T_{13} = 0$). Obviously each traction force component is a scalar function. Moreover, upon assumption and necessity (for determination of Green's functions) the traction force component must be a known elementary source function. For this class of problems we choose a set of 2D basis functions as the independent source functions, with their support being the entire surface (distributed sources). Each 2D basis function is derived from the product of two 1D orthonormal basis functions. For example

we select $\tilde{B}_i(y, z) = \tilde{B}_{m \odot n}(y, z) = b_m(y) \cdot b_n(z)$, where indices are arranged as follows: Fix a value for m in the interval $[0, M]$, say m_0 , and run over all the possible $n_0 \in [0, N]$; obtaining, $[m_0, 0], \dots, [m_0, n_0], \dots, [m_0, N]$. Subsequently vary the value of m_0 from 0 to M to obtain an $(M + 1) \times (N + 1)$ index matrix. Concatenating the rows of the above matrix results in a string of $(M + 1) \times (N + 1)$ index pairs (m, n) . More explicitly, we obtain:

$[(0, 0), \dots, (0, n_0), \dots, (0, N), \dots, (m_0, 0), \dots, (m_0, N), \dots, (M, N)]$. In terms of the symbol $m \odot n$ we include all the $(M + 1) \times (N + 1)$ index terms.

Thus we have excess to $(M + 1) \times (N + 1)$ independent source functions, or more precisely, Distributed Elementary Sources. Making use of this convention, the surface term in Eq. (4.17) reads:

$$\iint_{S_{1,o}^+} dydz \mathbf{v}^t \boldsymbol{\tau}_1 \Leftrightarrow \iint_{S_{1,o}^+} dydz \mathbf{B}^t \begin{bmatrix} T_{11}^{(i)}(y, z) \\ 0 \\ 0 \end{bmatrix} = \iint_{S_{1,o}^+} dydz \mathbf{B}^t \begin{bmatrix} \tilde{B}_i(y, z) \\ 0 \\ 0 \end{bmatrix} \quad (4.27)$$

The last term in Eq. (4.27) leads to the discrete version of the force vector $\mathbf{F}_{11}^{(i)}$ (i being any of the index terms $m \odot n$) appearing as \mathbf{F} in Eq. (4.23). Thus we conduct $(M + 1) \times (N + 1)$ numerical experiments. The displacement functions as a response to each of these DESs is a “fundamental solution,” alternatively termed as “Green’s functions.” As mentioned several times in the course of our discussion, since the sources are distributed the resultant Green’s functions are automatically regularized (\mathcal{GF} s). Consider one such dyadic Green’s function de-

rived as a response due to first DES:

$$\mathfrak{G}_{[T_{11}]_{S_{1,o}^+}^{(0)}}(x, y, z) = \begin{bmatrix} \mathfrak{G}_{[T_{11}]_{S_{1,o}^+}^{(0)}}^1(x, y, z) \\ \mathfrak{G}_{[T_{11}]_{S_{1,o}^+}^{(0)}}^2(x, y, z) \\ \mathfrak{G}_{[T_{11}]_{S_{1,o}^+}^{(0)}}^3(x, y, z) \end{bmatrix} \quad (4.28)$$

For example, $\mathfrak{G}_{[T_{11}]_{S_{1,o}^+}^{(0)}}^1(x, y, z)$ stands for a \mathfrak{GF} , which is the ‘1st’ component of the displacement vector, i.e. $u_1(x, y, z)$, in response to the applied stress component ‘ T_{11} ’ acting on the boundary section ‘ $S_{1,o}^+$.’ Furthermore, the superscript ‘(0)’ to source T_{11} indicates that the selected basis function has been $\tilde{B}_0(y, z)$. Subsequently, the sources are replaced by all the available traction force functions, not just for T_{11} , but similarly by $\boldsymbol{\tau}_1(y, z)|_{S_{1,o}^+} = \begin{bmatrix} 0 & T_{12}(y, z) & 0 \end{bmatrix}_{S_{1,o}^+}^t$ and $\boldsymbol{\tau}_1(y, z)|_{S_{1,o}^+} = \begin{bmatrix} 0 & 0 & T_{13}(y, z) \end{bmatrix}_{S_{1,o}^+}^t$. Alternatively the solution to

$$[\mathbf{K} - \omega^2 \mathbf{M}]_{\Omega_o} [\mathbf{g}_{m \odot n}^{11} \mathbf{g}_{m \odot n}^{12} \mathbf{g}_{m \odot n}^{13}] = [\mathbf{F}_{11}^{(m \odot n)} \mathbf{F}_{12}^{(m \odot n)} \mathbf{F}_{13}^{(m \odot n)}]_{S_{1,o}^+}, \quad (4.29)$$

leads to a derivation of a set of all the plausible \mathfrak{GF} s associated with excitation sources on the surface $S_{1,o}^+$. The set of \mathfrak{GF} s evaluated at the surface $S_{1,o}^+$ are sufficient to describe, any boundary condition; Dirichlet, Neumann, or interface conditions, over the surface $S_{1,o}^+$. The latter statement is *alter ego* to previously explained Sufficiency principle. Next, repeat the numerical experiments similarly for the remaining surfaces $S_{1,o}^-$, $S_{2,o}^+$, $S_{2,o}^-$, $S_{3,o}^+$ and $S_{3,o}^-$. The generated set of \mathfrak{GF} s in response to their respective DESs (their respective traction components on all the surfaces) ‘exhaust’ all the relevant boundary- or interface conditions applied

on the volume Ω_o .

4.4.4 Algorithm for Solving Inhomogeneous Neumann Boundary Conditions: Implementation of Sufficiency- and Exhaustion Principles

Before delving into the problem of interconnection, consider a BVP with inhomogeneous Neumann boundary condition. The solution procedure is meant to shed light on how the Green's functions are applied, to tackle more realistic problems. Consider the test hexahedron “ o ” shown in Fig. 4.3. The imposition of the inhomogeneous Neumann boundary condition on the test boundary $S_{1,o}^+$, of the cuboid, implies that the prescribed traction force is non-zero over the surface (Eq. 4.17), while the remaining boundary sections are stress-free. It should be reminded that the source functions considered in the previous case were DES, whereas here, the applied source is an arbitrary force function. For easy reference Eq. (4.17) has been reproduced here:

$$\begin{aligned}
& - \int_{\Omega_o} d\Omega_o [\partial_x \mathbf{v}^t \mathbf{P}_{11} \partial_x + \partial_x \mathbf{v}^t \mathbf{P}_{12} \partial_y + \partial_x \mathbf{v}^t \mathbf{P}_{13} \partial_z] \mathbf{u} \\
& - \int_{\Omega_o} d\Omega_o [\partial_y \mathbf{v}^t \mathbf{P}_{21} \partial_x + \partial_y \mathbf{v}^t \mathbf{P}_{22} \partial_y + \partial_y \mathbf{v}^t \mathbf{P}_{23} \partial_z] \mathbf{u} \\
& - \int_{\Omega_o} d\Omega_o [\partial_z \mathbf{v}^t \mathbf{P}_{31} \partial_x + \partial_z \mathbf{v}^t \mathbf{P}_{32} \partial_y + \partial_z \mathbf{v}^t \mathbf{P}_{33} \partial_z] \mathbf{u} \\
& + \iint_{S_{1,o}^+} dy dz \mathbf{v}^t \tilde{\mathbf{F}} = -\rho\omega^2 \int_{\Omega_o} d\Omega_o \mathbf{v}^t \mathbf{u}
\end{aligned} \tag{4.30}$$

Consider an arbitrary force vector function $\tilde{\mathbf{F}}$ defined on the (y, z) co-ordinate plane. The components \tilde{F}_1 , \tilde{F}_2 and \tilde{F}_3 of $\tilde{\mathbf{F}}$, operate time-harmonically at the frequency ω , and is applied on the surface $S_{1,o}^+$. The surface term at the RHS of Eq. (4.30) is then:

$$\tilde{\mathbf{F}} = \begin{bmatrix} \tilde{F}_1 \\ \tilde{F}_2 \\ \tilde{F}_3 \end{bmatrix} \quad (4.31)$$

The force components F_1 , F_2 and F_3 , can each be written as a linear combination of an adequate number of basis functions, with their support being the surface $S_{1,o}^+$. Thus, we can write $\tilde{F}_1(x, y) \approx \sum_{i \in \mathcal{N}_0 \times \mathcal{N}_0} p_i^{(1)} B_i(x, y)|_{S_{1,o}^+}$, and in a similar manner, the same can be written for \tilde{F}_2 and \tilde{F}_3 . The expansion coefficients $p_i^{(j)}$, $j = 1, 2, 3$ are readily calculable. At this point, it should be reminded that the displacement responses to the basis functions appearing in the expansions for \tilde{F}_1 , \tilde{F}_2 and \tilde{F}_3 are already calculated, and is available in terms of \mathcal{GF} s. Therefore, considering the given inhomogeneous Neumann boundary condition on $S_{1,o}^+$, with the remaining boundary sections being described by the homogeneous Neumann

condition. The expression for the resulting displacement vector is given by:

$$\begin{aligned}
\mathbf{u}_o(x, y, z) &= \begin{bmatrix} \mathcal{G}_{[\tilde{F}_1]_{S_{3,o}^-}}^{(1)}(x, y, z) & \mathcal{G}_{[\tilde{F}_1]_{S_{1,o}^+}}^{(1)}(x, y, z) \\ \mathcal{G}_{[\tilde{F}_1]_{S_{1,o}^+}}^{(2)}(x, y, z) & \dots & \mathcal{G}_{[\tilde{F}_1]_{S_{1,o}^+}}^{(2)}(x, y, z) \\ \mathcal{G}_{[\tilde{F}_1]_{S_{1,o}^+}}^{(3)}(x, y, z) & \mathcal{G}_{[\tilde{F}_1]_{S_{1,o}^+}}^{(3)}(x, y, z) \end{bmatrix} \begin{bmatrix} p_0^{(1)} \\ \vdots \\ p_I^{(1)} \end{bmatrix} \\
&+ \begin{bmatrix} \mathcal{G}_{[\tilde{F}_2]_{S_{1,o}^+}}^{(1)}(x, y, z) & \mathcal{G}_{[\tilde{F}_2]_{S_{1,o}^+}}^{(1)}(x, y, z) \\ \mathcal{G}_{[\tilde{F}_2]_{S_{1,o}^+}}^{(2)}(x, y, z) & \dots & \mathcal{G}_{[\tilde{F}_2]_{S_{1,o}^+}}^{(2)}(x, y, z) \\ \mathcal{G}_{[\tilde{F}_2]_{S_{1,o}^+}}^{(3)}(x, y, z) & \mathcal{G}_{[\tilde{F}_2]_{S_{1,o}^+}}^{(3)}(x, y, z) \end{bmatrix} \begin{bmatrix} p_0^{(2)} \\ \vdots \\ p_I^{(2)} \end{bmatrix} \\
&+ \begin{bmatrix} \mathcal{G}_{[\tilde{F}_3]_{S_{1,o}^+}}^{(1)}(x, y, z) & \mathcal{G}_{[\tilde{F}_3]_{S_{1,o}^+}}^{(1)}(x, y, z) \\ \mathcal{G}_{[\tilde{F}_3]_{S_{1,o}^+}}^{(2)}(x, y, z) & \dots & \mathcal{G}_{[\tilde{F}_3]_{S_{1,o}^+}}^{(2)}(x, y, z) \\ \mathcal{G}_{[\tilde{F}_3]_{S_{1,o}^+}}^{(3)}(x, y, z) & \mathcal{G}_{[\tilde{F}_3]_{S_{1,o}^+}}^{(3)}(x, y, z) \end{bmatrix} \begin{bmatrix} p_0^{(3)} \\ \vdots \\ p_I^{(3)} \end{bmatrix} \quad (4.32a) \\
&= \mathbf{G}_o(x, y, z)\mathbf{p} \quad (4.32b)
\end{aligned}$$

In the transition from Eq. (4.32a) to (4.32b), the vector \mathbf{p} is introduced as a vertical concatenation of the vectors $[p_0^{(j)} \dots p_I^{(j)}]^t, j = 1, 2, 3$. Similarly, the matrix $\mathbf{G}_o(x, y, z)$ is a horizontal concatenation of the matrices $[\dots \mathcal{G}_{[\tilde{F}_j]_{S_{3,o}^-}}^{(i)}(x, y, z) \dots]$ for $i = 0, \dots, N_0 \times N_0$ and $\tilde{F}_j, j = 1, 2, 3$.

4.4.5 Construction and Optimization of Library

A proposal is made here that computation and generation of the \mathcal{GF} s for the cuboids of a given device structure is done only once. Having generated the required \mathcal{GF} s, they are stored in a LIBRARY. The LIBRARY is enriched by \mathcal{GF} s

for different types of typical materials and relevant range of frequencies. This scheme allows the real-time analysis of an entire section of a device, whenever it is necessary in future. The computational overhead in retrieving the required \mathcal{GF} s is greatly reduced, since the \mathcal{GF} s are already computed and stored in `LIBRARY`. Whenever the relevant \mathcal{GF} s are needed for post-processing, it is only a matter of copying these functions into the `WORKING MEMORY`.

Material type	Material property
Aluminium	$\rho = 2.77$
	$C_{11} = C_{22} = C_{33} = 10.80,$ $C_{44} = C_{55} = C_{66} = 2.85,$ $C_{12} = C_{21} = C_{31} = C_{13} = C_{32} = C_{23} = 5.10$
Lithium Niobate	$\rho = 4.7$
	$C_{11} = C_{22} = 20.3, C_{33} = 24.5, C_{44} = C_{55} = 6.0,$ $C_{12} = C_{21} = 5.3, C_{23} = C_{32} = C_{13} = C_{31} = 7.5,$ $C_{14} = C_{41} = C_{56} = C_{65} = 0.9, C_{24} = C_{42} = -0.9,$ $C_{66} = 0.5(C_{11} - C_{12})$

Table 4.1: Materials and its properties utilized in numerical examples. The units of ρ and C are 10^3kg/m^3 and 10^{10}N/m^2 respectively

Here, an example is used to illustrate the optimization procedure. Consider $L, M, N = 10$ basis functions in each direction, this leads to $L \times M \times N = 1000$ three dimensional basis functions. However, since we are dealing with vector fields which consist of 3 components, we have a total number of $3 \times 1000 = 3000$ basis functions. As per the definitions in Eqs. (4.19) and (4.20), each displacement vector or \mathcal{GF} consists of 3000 of these basis functions and associated expansion coefficients. However, each \mathcal{GF} is the response to $6 \times 3 \times (M+1) \times (N+1)$ independent DES in three directions (one normal and two parallel), on six surfaces. As a

result, there are 1800 \mathcal{GF} s, sufficient to characterize the acoustodynamical behavior of the given volume with prescribed material properties at a given frequency. However, this form of storing the \mathcal{GF} s would be crude and bulky. The storing technique of \mathcal{GF} s can be optimized with their exhaustive knowledge. Consider one component of such a \mathcal{GF} :

$$\mathcal{G}_{[T_{31}]_{S_{3,o}^-}^{(4)}}^{(1)}(x, y, z) = \sum_{l \in \mathcal{N}_0} \sum_{m \in \mathcal{N}_0} \sum_{n \in \mathcal{N}_0} g_{[T_{31}]_{S_{3,o}^-}^{(4)(l,m,n)}}^{(1)} b_l(x) b_m(y) b_n(z) \quad (4.33)$$

In Eq. (4.33), under the assumption that $\mathcal{N}_0 = [0, \dots, 9]$, the super-index ‘4’ denotes the ‘fourth’ DES. This expression can also be written in algebraic form, with a row vector of coefficients and a column vector of 1000 basis functions. Note that the considered component of the \mathcal{GF} is defined in the entire volume. However, for application, only the \mathcal{GF} s over the surfaces are needed, since there are no body forces considered in the simulation. Therefore, upon evaluating the expression for the Green’s function over one of the ‘observation’ surfaces, for example $S_{2,o}^+$, we have:

$$\mathcal{G}_{[T_{31}]_{S_{3,o}^-}^{(4)}}^{(1)}(x, y, z)|_{S_{2,o}^+} = \sum_{l \in \mathcal{N}_0} \sum_{n \in \mathcal{N}_0} b_l(x) b_n(z) \sum_{m \in \mathcal{N}_0} g_{[T_{31}]_{S_{3,o}^-}^{(4)(l,m,n)}}^{(1)} b_m(y)|_{S_{2,o}^+} \quad (4.34)$$

or equivalently,

$$\mathcal{G}_{[T_{31}]_{S_{3,o}^-}^{(4)}}^{(1)}(x, y, z)|_{S_{2,o}^+} = \sum_{l \in \mathcal{N}_0} \sum_{n \in \mathcal{N}_0} G_{[T_{31}]_{S_{3,o}^-}^{(4)(l,n)}}^{(1)} b_l(x) b_n(z)|_{S_{2,o}^+} \quad (4.35)$$

Extracting the coefficients $G_{[T_{31}]_{S_{3,o}^-}^{(4)(l,n)}}^{(1)}$, along with $G_{[T_{31}]_{S_{3,o}^-}^{(4)(l,n)}}^{(2)}$ and $G_{[T_{31}]_{S_{3,o}^-}^{(4)(l,n)}}^{(3)}$ coefficients, a new compact set of coefficient is formed for the T_{31} -excitation, as

observed on $S_{2,o}^+$, resulting in a total of 300 coefficients. In the same manner, a set of coefficients for the remaining five surfaces can be extracted. Thus, a compact set of coefficients (6×300) are drawn out of original 3000 coefficients. Thus the scheme reduces the storage space required, by 40 percent. This example illuminates the notion of a physics-based Model-Order-Reduction: a scheme for reducing and compressing data inspired by the considerations which have their origin in the physical model of the problem at hand. Let us introduce a new nomenclature for this set of Green's function coefficients $\mathbf{G}(S_{3,o}^-, S_{3,o}^-)$, where the first term inside the bracket indicates the observing surface and second term refers to the source surface. More explicitly, $\mathbf{G}(S_{1,o}^-, S_{3,o}^-)$ for example, symbolizes the following: consider a cuboid “ o ,” subject to all the possible DESs acting on surface $S_{3,o}^-$. The evaluated displacement responses to these excitations are only observed on the surface $S_{1,o}^-$. Thus, in compressing the data, as explained above, the set $\mathbf{G}(S_{1,o}^-, S_{3,o}^-)$ comprises of all the required \mathcal{GF} s on that boundary.

4.5 Result and Discussion

4.5.1 Numerical Comparison with ANSYS: Eigenvalue Problem

An massive cuboid with $x, y, z \in [-1, 1]$ consisting of an isotropic material (Aluminium) was considered as simulation domain in order to compute the eigenfre-

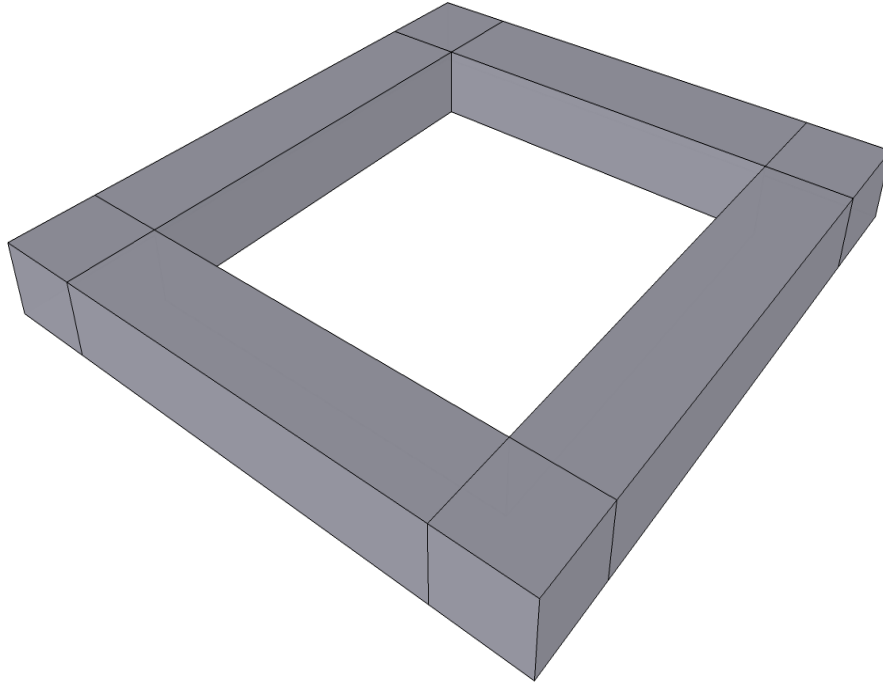


Figure 4.8: A complex wall-shaped enclosure structure

quencies summarized in Fig. 4.4 (Refer to Table 4.1 for the material properties of Aluminium used in the simulation). The comparison is a testimony for the accuracy and efficiency of the proposed method in terms of computational resources required. The results shown in Fig. 4.4 are encouraging. The ‘system’ matrix is highly sparse, due to the orthogonality property of the basis functions leading to moderate storage space requirements. The given cuboid is characterized with the help of 3D basis functions with their support being the entire simulation domain, with no meshing necessary. However, the eigenfrequencies achieved matches the solution obtained utilizing FEM. The commercially available FEM package ANSYS utilized linear elements with highly dense meshing, as a result

the computational time and resources required for solving the problem increased dramatically. Moreover, using the \mathcal{GF} s technique proposed here we can achieve an acceleration of computation by nearly one order of magnitude. Despite the advantages concerning the reduced storage space, and faster computation times, the main feature of our method is the utility of the tabulated \mathcal{GF} s. The results in the next sections shed light on this important property.

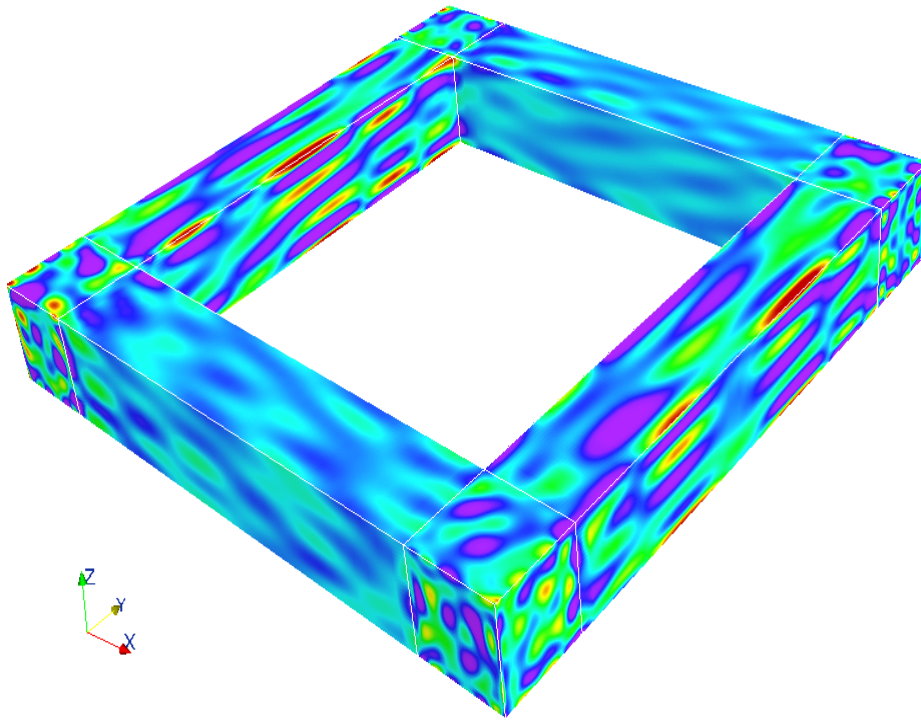


Figure 4.9: Displacement component $u_1(x, y, z)$ for the wall-shaped enclosure computed with the help of proposed \mathcal{GF} s method

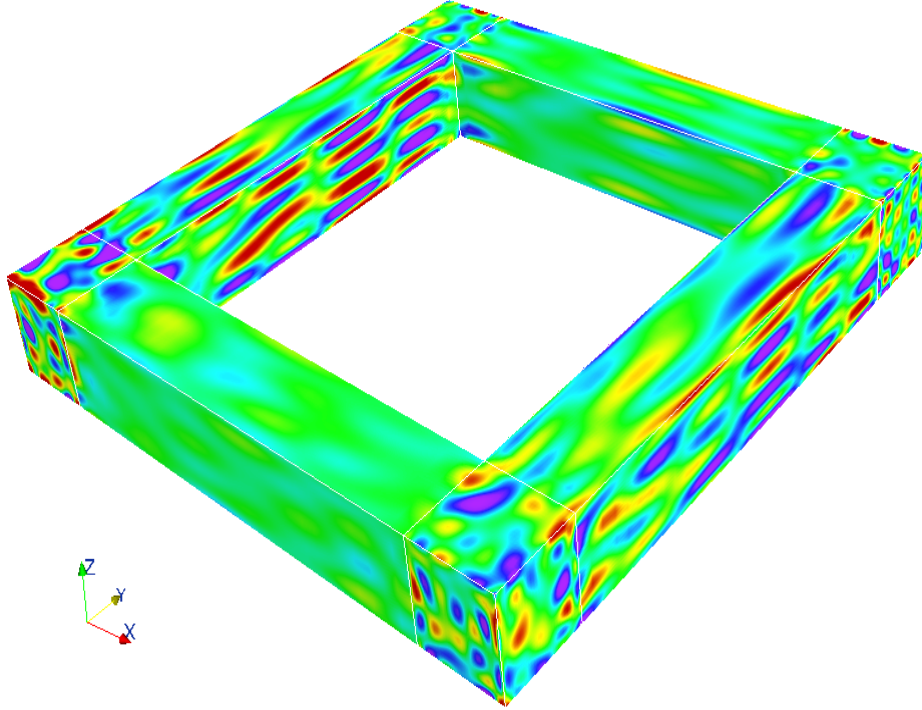


Figure 4.10: Displacement component $u_2(x, y, z)$ for the wall-shaped enclosure computed with the help of proposed \mathcal{GF} s method

4.5.2 Application of Superposition and Exhaustion Principle by Utilizing \mathcal{GF} s: Enforced Problems

At this stage we are prepared to communicate the ‘punch’ of our technique and explain clearly how it allows to carrying out computations with enhanced accuracy while simultaneously reducing the order of the complexity (physics-based MOR). Referring, to the composite structure in Fig. 4.1, the external force function $\tilde{\mathbf{F}}$ excites the structure at the southern surface S_3^- operating at the given frequency $\omega = 2.01$ GHz. The goal here is to determine the displacement func-

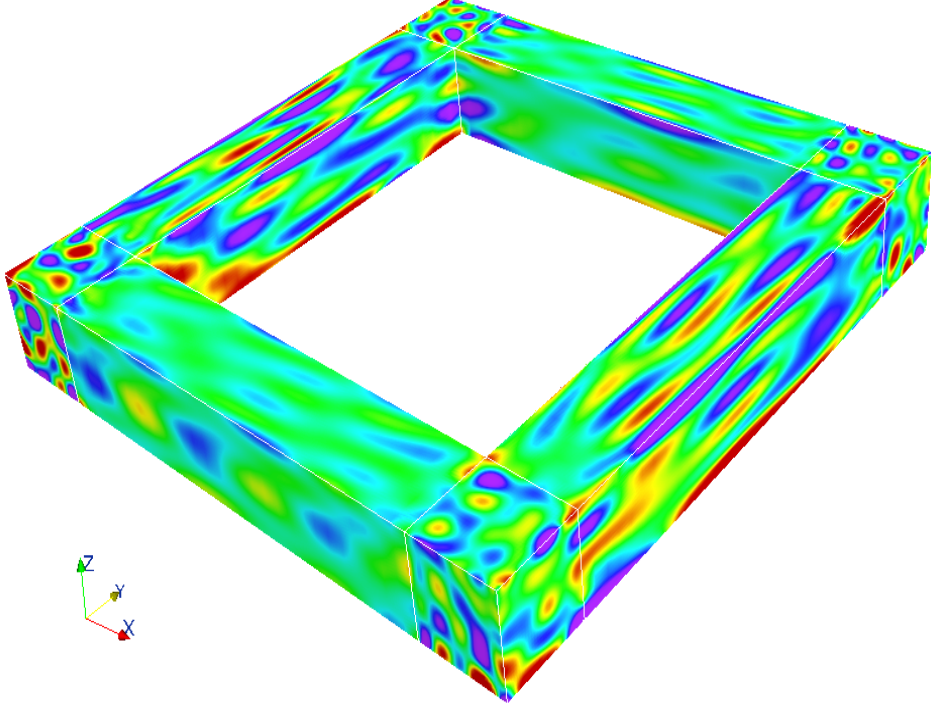


Figure 4.11: Displacement component $u_3(x, y, z)$ for the wall-shaped enclosure computed with the help of proposed \mathcal{GF} s method

tions $u_1(x, y, z)$, $u_2(x, y, z)$ and $u_3(x, z)$ for the entire structure, comprising of the cuboids “a,” “b” and “c,” subject to the Neumann boundary condition. Figure 4.2 shows the composite structure being segmented into three hexahedrons by introducing stress distributions over the interfaces. Note that while $\tilde{\mathbf{F}} = [0.7, 0, 0]^t$ (units in N/m^2) is known, the traction at the interfaces are *a priori* unknown. The problem “a” is recognized as a two-port problem, since it only exchanges acoustic energy with environment over the $S_{3,a}^-$ (southern) and $S_{2,a}^-$ (front) ports. This consideration is also true for the problem “c,” where $S_{1,c}^-$ (left) and $S_{3,c}^-$ (southern) ports exchange energy. Whereas, problem “b” is referred to as a three-port

problem due to obvious reasons.

Focus on the cuboid “ a .” The results are summarized as follows: $\tilde{\mathbf{F}}_a$ being a given function can be expressed in terms of the basis functions $B_i(x, y)$ $i = 0, \dots, (L+1) \times (M+1)$, resulting in $(L+1) \times (M+1)$ known expansion coefficients $\alpha_{a,k1}^{(i)}$, associated with the resulting total of $3 \times (L+1) \times (M+1)$ \mathcal{GF} s, including each components ($\alpha_{a,k2}^{(i)}, \alpha_{a,k3}^{(i)} = 0$). The forces at the interfaces, i.e., $T_{21}^a(x, z), T_{22}^a(x, z)$ and $T_{23}^a(x, z)$ are not given. Nonetheless, $T_{21}^a(x, z), T_{22}^a(x, z)$ and $T_{23}^a(x, z)$ can each be expressed in terms of $(L+1) \times (N+1)$ basis functions, resulting in the unknown expansion coefficients $\alpha_{a,u1}^{(i)}, \alpha_{a,u2}^{(i)}$ and $\alpha_{a,u3}^{(i)}$, $i = 0, \dots, (L+1) \times (N+1)$. The responses to the DES (i.e. \mathcal{GF} s) at the southern and front ports of “ a ” are already available and expressed in terms of the aforementioned $3 \times 18 \times (M+1) \times (N+1)$ numbers, which includes all the components, $\mathbf{G}_a^{(1)}(S_{2,a}^-, S_{2,a}^-)$, are retrieved from the LIBRARY and copied to WORKING MEMORY. We can describe the vibrational behavior of cuboid “ a ” $u_1^a(x, y, z)$, $u_2^a(x, y, z)$ and $u_3^a(x, y, z)$ evaluated at the front port ($S_{2,a}^-$) by means of $(L+1) \times (M+1)$ known expansion coefficients $\alpha_{a,k}^{(i)}$ and $3 \times (L+1) \times (N+1)$ unknown expansion coefficients $\alpha_{a,u1}^{(i)}, \alpha_{a,u2}^{(i)}$ and $\alpha_{a,u3}^{(i)}$. Which can be written as:

$$\mathbf{u}_a|_{S_{2,a}^-} = \mathbf{G}_a^{(1)}(S_{2,a}^-, S_{2,a}^-)\mathbf{q}_1 + \mathbf{G}_a^{(2)}(S_{2,a}^-, S_{3,a}^-)\mathbf{p}_a \quad (4.36)$$

Here, $\mathbf{p}_a = [\alpha_{a,k1}^{(i)}, 0, 0]^t$ is the known coefficient vector as observed on the interface $S_{2,a}^-$, and $\mathbf{q}_1 = [\alpha_{a,u1}^{(i)}, \alpha_{a,u2}^{(i)}, \alpha_{a,u3}^{(i)}]^t$ is the unknown expansion coefficient

vector at the interface. For the determination of the $3 \times (L+1) \times (N+1)$ unknown expansion coefficients $\alpha_{a,u1}^{(i)}$, $\alpha_{a,u2}^{(i)}$ and $\alpha_{a,u3}^{(i)}$, the acoustic energy exchange between the hexahedrons “a,” “b” and “c” needs to be accounted for, by imposing the interface conditions (in the weak sense). This brings cuboids “b” and “c” into the picture. Next, the \mathcal{GF} s characterizing “c” are transferred into the WORKING MEMORY. The cuboid “c,” as per the earlier understanding, is also a two-port problem and follows a procedure similar to “a” hence:

$$\mathbf{u}_c|_{S_{1,c}^-} = \mathbf{G}_c^{(1)}(S_{1,c}^-, S_{1,c}^-)\mathbf{q}_2 + \mathbf{G}_c^{(2)}(S_{1,c}^-, S_{3,c}^-)\mathbf{p}_c \quad (4.37)$$

Thus, the vibrational behavior $u_1^c(x, y, z)$, $u_2^c(x, y, z)$ and $u_3^c(x, y, z)$ evaluated at the left port can be described by the $3 \times (L+1) \times (M+1)$ known expansion coefficients $\alpha_{c,k1}^{(i)}$ and $\alpha_{c,k2}^{(i)}$, $\alpha_{c,k3}^{(i)} = 0$, and $3 \times (M+1) \times (N+1)$ unknown expansion coefficients $\alpha_{c,u1}^{(i)}$, $\alpha_{c,u2}^{(i)}$ and $\alpha_{c,u3}^{(i)}$.

Finally, the crucial link between the cuboids “a” and “c,” a three-port (“b”) problem, is dealt with. The cuboid “b” possesses two interfaces. Considering one, at the time, the description of the vibrational behavior is determined by $u_1^b(x, y, z)$, $u_2^b(x, y, z)$ and $u_3^b(x, y, z)$ evaluated at the right- and back port by means of $3 \times (L+1) \times (M+1)$ known expansion coefficients. Additionally, by the $2 \times 3 \times (M+1) \times (N+1) \times (L+1) \times (N+1)$ unknown expansion coefficients $\alpha_{c,u1}^{(i)}$, $\alpha_{c,u2}^{(i)}$ and $\alpha_{c,u3}^{(i)}$ with $\alpha_{a,u1}^{(i)}$, $\alpha_{a,u2}^{(i)}$ and $\alpha_{a,u3}^{(i)}$, can be written in terms of the

cross talk terms, as:

$$\mathbf{u}_b|_{S_{2,b}^+} = \mathbf{G}_b^{(1)}(S_{2,b}^+, S_{2,b}^+) \mathbf{q}_1 + \mathbf{G}_b^{(2)}(S_{2,b}^+, S_{1,b}^+) \mathbf{q}_2 + \mathbf{G}_b^{(3)}(S_{2,b}^+, S_{3,b}^-) \mathbf{p}_b \quad (4.38a)$$

and

$$\mathbf{u}_b|_{S_{1,b}^+} = \mathbf{G}_b^{(1)}(S_{1,b}^+, S_{2,b}^+) \mathbf{q}_1 + \mathbf{G}_b^{(2)}(S_{1,b}^+, S_{1,b}^+) \mathbf{q}_2 + \mathbf{G}_b^{(3)}(S_{1,b}^+, S_{3,b}^-) \mathbf{p}_b. \quad (4.38b)$$

Matching $u_1^b(x, y, z)$, $u_2^b(x, y, z)$ and $u_3^b(x, y, z)$ with $u_1^a(x, y, z)$, $u_2^a(x, y, z)$, and $u_3^a(x, y, z)$ along with $u_1^c(x, y, z)$, $u_2^c(x, y, z)$ and $u_3^c(x, y, z)$ all simultaneously at there respective interfaces with cross talk components determines the required unknown expansion coefficients. However, prior to that consider:

$$\mathbf{G}_a^{(2)}(S_{2,a}^-, S_{3,a}^-) \mathbf{p}_a = \mathbf{H}_a(S_{2,a}^-, S_{3,a}^-), \quad (4.39a)$$

$$\mathbf{G}_c^{(2)}(S_{1,c}^-, S_{3,c}^-) \mathbf{p}_c = \mathbf{H}_c(S_{1,c}^-, S_{3,c}^-), \quad (4.39b)$$

$$\mathbf{G}_b^{(3)}(S_{2,b}^+, S_{3,b}^-) \mathbf{p}_b = \mathbf{H}_b(S_{2,b}^+, S_{3,b}^-) \quad (4.39c)$$

and

$$\mathbf{G}_b^{(3)}(S_{1,b}^+, S_{3,b}^-) \mathbf{p}_b = \mathbf{H}_b(S_{1,b}^+, S_{3,b}^-) \quad (4.39d)$$

Substituting the value of Eq. (4.39) and equating Eq. (4.36) to (4.38a), and Eq. (4.38b) to (4.37):

$$\begin{aligned} \mathbf{G}_a^{(1)}(S_{2,a}^-, S_{2,a}^-) \mathbf{q}_1 - \mathbf{G}_b^{(1)}(S_{2,b}^+, S_{2,b}^+) \mathbf{q}_1 - \mathbf{G}_b^{(2)}(S_{2,b}^+, S_{1,b}^+) \mathbf{q}_2 \\ = \mathbf{H}_b(S_{2,b}^+, S_{3,b}^-) - \mathbf{H}_a(S_{2,a}^-, S_{3,a}^-) \end{aligned} \quad (4.40a)$$

and

$$\begin{aligned} \mathbf{G}_b^{(1)}(S_{1,b}^+, S_{2,b}^+) \mathbf{q}_1 + \mathbf{G}_b^{(2)}(S_{1,b}^+, S_{1,b}^+) \mathbf{q}_2 - \mathbf{G}_c^{(1)}(S_{1,c}^-, S_{1,c}^-) \mathbf{q}_2 \\ = \mathbf{H}_c(S_{1,c}^-, S_{3,c}^-) - \mathbf{H}_b(S_{1,b}^+, S_{3,b}^-) \end{aligned} \quad (4.40b)$$

Equivalently in matrix form:

$$\begin{aligned} \left[\begin{array}{cc} \mathbf{G}_a^{(1)}(S_{2,a}^-, S_{2,a}^-) - \mathbf{G}_b^{(1)}(S_{2,b}^+, S_{2,b}^+) & -\mathbf{G}_b^{(2)}(S_{2,b}^+, S_{1,b}^+) \\ \mathbf{G}_b^{(1)}(S_{1,b}^+, S_{2,b}^+) & \mathbf{G}_b^{(2)}(S_{1,b}^+, S_{1,b}^+) - \mathbf{G}_c^{(1)}(S_{1,c}^-, S_{1,c}^-) \end{array} \right] \begin{bmatrix} \mathbf{q}_1 \\ \mathbf{q}_2 \end{bmatrix} \\ = \begin{bmatrix} \mathbf{H}_b(S_{2,b}^+, S_{3,b}^-) - \mathbf{H}_a(S_{2,a}^-, S_{3,a}^-) \\ \mathbf{H}_c(S_{1,c}^-, S_{3,c}^-) - \mathbf{H}_b(S_{1,b}^+, S_{3,b}^-) \end{bmatrix} \end{aligned} \quad (4.41)$$

This completes the discussion of determining the dynamics of composite structures in terms of their reduced (collapsed on the boundary) \mathcal{GF} s.

Remark: As it can be concluded from the above procedure, in solving the interface problem, only the displacement functions at the interface were explicitly matched. However, it should be clear that continuity of the traction forces were also implicitly required. The traction continuity conditions were satisfied by assuming equal and opposite equivalent forces at the interfaces.

The implementation of Sufficiency- and Exhaustion principles in the above mentioned fashion does not depend on the material properties of the cuboid. The numerical results for the given composite structure (Fig. 4.1), where cuboids with different material constituents, need to be interconnected utilizing proposed method. More specifically, the darker region of the composite structure to be

Lithium Niobate and lighter region to be Aluminium is considered. The material properties as given in Table 4.1. The displacement solutions $u_1(x, y, z)$, $u_2(x, y, z)$ and $u_3(x, y, z)$ are shown in Figs. (4.5), (4.6) and (4.7), respectively.

Furthermore, the interconnection scheme described above was thoroughly tested for more complex structures (an example is shown in Fig. 4.8). To account for cases which are relevant in practical cases a wall shaped enclosure structure was considered. The structure was assumed to be made of Aluminium (Table 4.1) and subject to force vector $\mathbf{F} = [0.7, 0, 0]^t$ N/m². The force was applied over the entire ‘southern’ surface of the structure, at operating frequency $\omega = 2.1$ GHz. The remaining surfaces were stress-free. The wall-shaped structure was partitioned into eight cuboids. Between any two adjacent cuboids, fictitious interfaces were introduced, due to the partitioning. The application of the interconnection method ensures the conservation of the energy throughout the wall-shaped structure is maintained in weak form.

4.6 Conclusion

Elastodynamic simulation of a composite structure utilizing a novel Green’s function method was demonstrated. The involved 3D dyadic Green’s functions were derived in response to Distributed-Elementary-Sources rather than traditionally-utilized point-like sources, giving rise to a new class of Green’s functions, termed

here as Distributed-Elementary-Source Self-regularized Dyadic Green's Functions (\mathcal{GF} s). The \mathcal{GF} s were computed and stored in a LIBRARY which was further facilitated by introducing the concept of physics-based MOR. The method employed for the construction of the \mathcal{GF} s can easily accommodate isotropic as well as fully-anisotropic elastic media. The stored \mathcal{GF} s were retrieved to solve the Neumann and Dirichlet boundary- and interface conditions, with given test problems, utilizing the Sufficiency- and Exhaustion principles. The results shown, exemplify the applicability of the proposed method to various classes of elastic media. The solution obtained for elastodynamic problem showed continuity of the mechanical displacement solution regardless of the material transition in a more complex 3D cases as well.

4.7 Summary

Focusing on the elastic properties associated with the massloading effect in SAW- and BAW devices, the ideas underlying the proposed method were outlined in this thesis. The basic features underlining the method are: (1) Reducing the dimensionality of the problem by one, and thus, considerably reducing the number of unknowns involved. (2) Pre-calculating relevant data with desired accuracy, compressing the data effectively, and storing the data compactly. (3) Maintaining the advantages offered by competing computational methods. Furthermore, the limitations of FEM and BEM were addressed, enabling the reader to compare the

proposed method with existing standard techniques. Simultaneously, appreciate the capabilities and limitations of the proposed technique. While BEM “naturally” applies to open boundary problems, and provides comparatively more accurate numerical results than alternative techniques, BEM is not easily applicable to problems with strongly varying inhomogeneities. This limitation is due to the need for calculating dyadic Green’s functions and their spatial derivatives, which are as conventionally constructed, singular or hyper-singular. Therefore, it is numerically a challenge for the algorithm designers to compute the involved Green’s Functions. The \mathcal{GF} s technique presented in this thesis, addressed this particular shortcoming of BEM more elegantly and constructively.

By appropriately selecting distributed force functions (from a complete sequence of orthonormal functions), and applying these elementary force functions to the bounding surface of the simulation domain, the notion of Distributed-Elementary-Source (DES) Self-regularized (SR) Dyadic Green’s Functions (DGFs) is introduced. Distributed sources, as opposed to localized sources, do not give rise to singularities in Green’s functions - the singularities of GFs are automatically dealt with (self-regularized). This choice of distributed forces results in well-conditioned system matrices, in contrast to conventional “impedance” matrices, which are often ill-conditioned and thus pose considerable challenges to the computational scientists. The information necessary for the construction of \mathcal{GF} s, and their spatial derivatives, evaluated at the boundary surface of an elastic cuboid

(electrodes), can be efficiently and compactly stored, and conveniently imported for frequent future applications.

The pre-calculated \mathcal{GF} s, associated for a given material with a given size and shape remains unaltered, regardless of the relative position of the cuboid considered. Essentially, all the cuboids in a given device geometry with the same size, shape and material constants only needs to be calculated once, the rest are treated as copy of original cuboid. This property has significant implications in numerical calculations. Hence, computing all possible \mathcal{GF} s for only one electrode or cuboid, suffices to characterize all identical cuboidal electrodes. The realization of this property enables to save computational resources (both time and storage space) by orders of magnitudes. In view of the fact that practical micro-acoustic devices can be assembled with only a dozen “macro-cuboids”, the implication of the above-mentioned saving of resources can fundamentally change the way how simulations are carried out. In particular, and somehow paradoxical, the savings are more prominent for the larger devices. The reason for this most favorable property is again due to the fact that the larger devices can typically be assembled from a comparatively small number of macro-cuboids. Therefore, the computational efforts which are utilized for frequent data transfer from the LIBRARY to the “WORKING MEMORY” is all the computational needs that are required to calculate the given BVPs. This feature of the proposed algorithm, once fully exploited, can accelerate computational times, and additionally allows

the computational scientists to create the required LIBRARIES, independent of the concrete geometries at hand.

Thereby, a comprehensive series of numerical tests were carried out for composite structures involving isotropic/anisotropic- and anisotropic/anisotropic interfaces. Both 2D and 3D test problems were considered. Invariably, in all experiments encouraging results were found. Here, it should be mentioned that the created LIBRARY is powerful enough to allow 2D and 3D massloading analysis in conventional, as well as more exotic SAW and BAW structures, by employing Sufficiency- and Exhaustion principles.

At this point, it needs to be mentioned that, along with all these intrinsic properties, the method also contains its drawbacks. For example, a problem has been identified while subjecting the macro-cuboid with a discontinuous source. Since the basis functions employed here are distributed over the entire macro-cuboid, the response to such a discontinuous source is prone to errors. Obviously, the shortcoming can be partially remedied by partitioning the macro-cuboid into an adequate number of cuboids. The partitioning is carried out such that each cuboid is subject to uniform and continuous sources. This proposal certainly comes at an expense of higher computational resources. Another proposed solution to the problem is to adopt the entire concept of generating \mathcal{GF} s and employing the Sufficiency- and Exhaustion principles, utilizing some other technique such as FEM. FEM can provide greater flexibilities and broader scope to the overall con-

cept, thus the future work will be dedicated to interface the current work with FEM, making the concept more versatile to other well established techniques.

References

- [1] Auld BA. *Acoustic Fields and Waves in Solids: Volume I and II*. John Wiley and Sons: New York, 1973. [4](#), [43](#), [87](#), [145](#)
- [2] Tiersten HF, Sinha BK. A perturbation analysis of the attenuation and dispersion of surface waves. *Journal of Applied Physics* 1978; **49**(1):87–95. [4](#)
- [3] Eernisse EP. Variational method for electroelastic vibration analysis. *IEEE Transaction on Sonic and Ultrasonics* 1967; **SU-14**:153–160. [4](#)
- [4] Eernisse EP, Clayton LD, Watts MH. Variational method for modeling static and dynamic stress in a resonator disc with mounts. *Annual Symposium on Frequency Control*, SU-14, USA, Denver, 1989; 377–387. [4](#)
- [5] Tiersten HF. *Linear Piezoelectric Plate Vibrations*. Plenum Press: USA, New York, 1969. [4](#)
- [6] Wright PV. Analysis and design of low-loss SAW device with internal reflections using Coupling-of-Modes theory. *IEEE Ultrasonics Symposium*, IEEE IUS, Canada, Montreal, 1989; 141–152. [4](#)

- [7] Hashimoto K. *Surface Acoustic Wave Devices in Telecommunications: Modelling and Simulation*. Springer-Verlag: Berlin Heidelberg, Germany, 2000. 4, 39, 83
- [8] Brebbia CA, Dominguez J. Boundary element methods for potential problems. *Applied Mathematical Modeling* 1977; **1**:372–378. 5, 7
- [9] Milsom RF, Reilly NHC, Renwood M. Analysis of generation and detection of surface and bulk acoustic waves by interdigital transducers. *IEEE Transaction on Sonic and Ultrasonics* 1977; **SU-24**(3):147–166. 5
- [10] Wadji ARB. *Physical Acoustics; Fundamentals and Applications*. Plenum Press: New York and London, 1991. 7, 41, 84
- [11] Baghai-Wadji AR. Theory and applications of Green's functions. *International Journal of High Speed Electronics and Systems* 2000; **10**(4):949–1015. 7, 17, 21, 40, 43, 46, 52, 58, 84, 87, 96, 145
- [12] Reichinger HP, Baghai-Wadji AR. Rigorous electrostatic field analysis of surface acoustic wave devices with closed-form formula A Two-Dimensional Representation. *IEEE Electrotechnical Conference*, Slovenia, LJubljana, 1991; 154–157. 7
- [13] Wagner KC, Visintini G. Spurious bulk wave in SAW filters with apodized transducers. *IEEE Ultrasonics Symposium*, IEEE IUS, USA, Chicago, 1988; 34–38. 7

- [14] Wagner KC, Reindl L, Manner O. Surface wave to bulk wave conversion in SAW-reflectors on strong coupling substrates. *IEEE Ultrasonics Symposium*, IEEE IUS, USA, Baltimore, 1993; 209–213. [7](#)
- [15] Baghai-Wadji AR, Penunuri D. Coordinate-free, frequency-independent universal functions for BAW analysis in SAW devices. *IEEE Ultrasonics Symposium*, IEEE IUS, USA, Seattle, 1995; 287–290. [7](#)
- [16] Laude V, Jerez-Hanckes C, Ballandras S. Surface Green's function of a piezoelectric half-space. *IEEE Transactions on Ultrasonics, Ferroelectrics, and Frequency Control* 2006; **53**(2):420. [7](#)
- [17] Zidek HP, Baghai-Wadji AR, Seifert FJ. Full-wave 3D analysis of singly- and doubly periodic SAW-structures. *IEEE Ultrasonics Symposium*, IEEE IUS, USA, Tucson, 1992; 11–14. [7](#)
- [18] Baghai-Wadji AR, Ringhofer C. A survey of numerical techniques for modeling the massloading effects in SAW devices. *IEEE Ultrasonics Symposium*, IEEE IUS, USA, San Antonio, 1996; 111–116. [7](#)
- [19] Gockenbach MS. *Understanding and Implementing the Finite Element Method*. SIAM: University City Science Center, Philadelphia, 2006. [8](#), [40](#)
- [20] Benjeddou A. Advances in piezoelectric finite element modeling of adaptive structural elements: A survey. *Computers and Structures* 2000; **76**:347–363.

- [21] Lerch R. Simulation of piezoelectric devices by two- and three-dimensional finite element. *IEEE Transactions on Ultrasonics, Ferroelectrics, and Frequency Control* 1990; **37**(2):233–247. [8](#)
- [22] Wang J, Lin J. A two-dimensional theory for surface acoustic wave propagation in finite piezoelectric solids. *Journal of Intelligent Material Systems and Structures* 2005; **16**:623–629. [8](#)
- [23] Mindlin R. High frequency vibrations of piezoelectric crystal plates. *International Journal of Solids and Structures* 1972; **8**:895–906. [9](#)
- [24] Hofer M, Finger N, Kovacs G, Schoberl J, Zaglmayr S, Langer U, Lerch R. Finite-element simulation of wave propagation in periodic piezoelectric SAW structures. *IEEE Transactions on Ultrasonics, Ferroelectrics, and Frequency Control* 2006; **53**(6):1192–1201. [9](#)
- [25] Liu GR, Dai KY, Lim KM, Gu YT. A point interpolation mesh free method for static and frequency analysis of two-dimensional piezoelectric structures. *Computational Mechanics* 2002; **29**:510–519. [9](#)
- [26] Liu GR. *Mesh Free Methods: Moving Beyond the Finite Element Methods*. CRC Press LLC: Boca Raton, Florida, 2003. [9](#), [40](#), [87](#)
- [27] Hegen D. Element-free Galerkin methods in combination with finite element approaches. *Computer Methods in Applied Mechanics and Engineering* 1996; **135**:143–166. [9](#)

- [28] Belytschko T, Lu YY, Gu L. Element-free Galerkin methods. *International Journal for Numerical Methods in Engineering* 1994; **37**:229–256. [9](#), [40](#)
- [29] Becker R, Hansbo P, Stenberg R. A finite element method for domain decomposition with non-matching grids. *Mathematical Modeling and Numerical Analysis* 2003; **37**(2):209–225. [9](#)
- [30] de Boer A, van Zuijlen AH, Bijl H. Comparison of conservative and consistent approaches for the coupling of non-matching meshes. *Computer Methods in Applied Mechanics and Engineering* 2008; **197**:4284–4297. [9](#), [42](#), [86](#)
- [31] Beer G, Lu YY, Gu L. An isoparametric joint/interface element for finite element analysis. *International Journal for Numerical Methods in Engineering* 1985; **21**:584–600. [9](#)
- [32] Pantano A, Averill RC. A penalty-based finite element interface technology. *Computers and Structures* 2002; **80**:1725–1748. [9](#), [42](#), [86](#)
- [33] Farhat C, Roux FX. A method of finite element tearing and interconnecting and its parallel solution algorithm. *International Journal for Numerical Methods in Engineering* 1991; **32**:1205–1227. [9](#), [42](#), [85](#), [86](#), [135](#)
- [34] Bouhaddi N, Fillod R. Substructuring using a linearized dynamic condensation method. *Computers and Structures* 1992; **44**:679–683. [9](#)
- [35] Leung YT. An accurate method of dynamic substructuring with simplified

- computation. *International Journal for Numerical Methods in Engineering* 1978; **14**:1241–1256. [9](#)
- [36] Aminpour MA, Ransom JB, McCleary SL. A coupled analysis method for structures with independently modelled finite element subdomains. *International Journal for Numerical Methods in Engineering* 1995; **38**:3695–3718. [9](#)
- [37] Pfeiffer HP, Kidder LE, Scheel MA, Teukolsky SA. A multidomain spectral method for solving elliptic equations. *Computer Physics Communications* 2003; **152**:253–273. [9](#), [42](#), [86](#), [135](#)
- [38] Ventura P, Hode JM, Lopes B. Rigorous analysis of finite SAW devices with arbitrary electrode geometries. *IEEE Ultrasonics Symposium*, IEEE IUS, USA, Seattle, 1995; 257–262. [10](#)
- [39] Ventura P, Steichen W. FEM/BEM analysis of a generalized periodic array. *IEEE Transactions on Ultrasonics, Ferroelectrics and Frequency Control* 2007; **54**(10):2052. [10](#), [39](#)
- [40] Ventura P, Duflie P, Boret S. The effect of the fabrication process in propagation and reflectivity in an IDT. *IEEE Ultrasonics Symposium*, IEEE IUS, USA, San Antonio, 1996; 281–284. [10](#)
- [41] Brebbia CA, Georgiou P. Combination of boundary and finite elements in elastostatic. *Applied Mathematical Modeling* 1979; **3**:212–220. [10](#)

- [42] Reichinger HP, Baghai-Wadji AR. Dynamic 2D analysis of SAW-devices including massloading. *IEEE Ultrasonics Symposium*, IEEE IUS, USA, Tucson, 1992; 07–10. [10](#)
- [43] Campbell CK. *Surface Acoustic Wave Devices for Mobile and Wireless Communications*. Academic Press: Orlando, Florida, 1998. [39](#), [83](#)
- [44] Sherwin SJ, Karniadakis GE. A new triangular and tetrahedral basis for high-order(hp)finite element methods. *International Journal for Numerical Methods in Engineering* 1995; **38**:3775–3802. [40](#)
- [45] Vagh H, Baghai-Wadji AR, Chamaly S. Ab-initio mesh-less modelling of three-dimensional massloading effect in SAW and BAW devices. *IEEE International Ultrasonics Symposium*, IUS, IEEE: Italy, Roma, 2009; 2684–2687. [74](#), [100](#)
- [46] Vagh H, Baghai-Wadji AR. On the construction of problem-specific basis functions for modelling the massloading effects in micro-acoustic devices. *IEEE International Symposium on Integrated Circuits*, ISIC, IEEE: Singapore, 2009; 260–263. [74](#), [78](#), [100](#)
- [47] Vagh H, Baghai-Wadji AR. 3D mass-loading effect of metallic electrodes with ultra-high aspect ratios in SAW devices. *IEEE International Ultrasonics Symposium*, IUS, IEEE: San Diego,USA, 2010; 1898–1902. [74](#), [128](#)
- [48] Doha ED, Bhrawy AH, Abd-Elhameed WM. Jacobi spectral Galerkin

- method for elliptic Neumann problem. *Numerical Algorithms* 2009; **50**(1):67–91. [76](#)
- [49] Warburton TC, Sherwin SJ, Karniadakis GE. Basis functions for triangular and quadrilateral high-order elements. *SIAM Journal of Scientific Computing* 1999; **20**(5):1671–1695. [76](#)
- [50] Dubiner M. Spectral methods on triangles and other domains. *Journal of Scientific Computing* 1991; **6**(4):345–390. [76](#), [78](#)
- [51] Baghai-Wadji AR, Penunuri D. Universal functions for 3D analysis of the massloading effect in SAW- and BAW devices. *IEEE Ultrasonics Symposium*, IUS, IEEE: Munich, Germany, 2002; 61–64. [84](#), [103](#), [134](#)
- [52] Klymyshyn DM, Kannan T, Kachayev A. Finite element modeling of electrode mass-loading effects in longitudinal leaky SAW resonators. *Microwave And Optical Technology Letters* 2009; **51**:390–395. [84](#)
- [53] Hamidon MN, Mousavi SA, Isa MM, Ismail A, Mahdi MA. Finite element method on mass loading effect for Gallium Phosphate surface acoustic wave resonators. *Proceedings of the world Congress on Engineering*, WCE, London, U.K, 2009. [84](#), [134](#)
- [54] Atluri SN, Zhu T. A new meshless local Petrov-Galerkin (MLPG) approach in computational mechanics. *Computational Mechanics* 1998; **22**:117–127. [84](#)

- [55] Sladek J, Sladek V, Zhang C. Stress analysis in anisotropic functionally graded materials by the MLPG method. *Engineering Analysis with Boundary Elements* 2005; **29**:597–609. [84](#)
- [56] Mukherjee YX, Mukherjee S. On boundary conditions in the Element-free Galerkin method. *Computational Mechanics* 1997; **19**:264–270. [85](#)
- [57] Gunzburger MD, Hou SL. Treating inhomogeneous essential boundary conditions in finite element methods and the calculation of boundary stresses. *SIAM Journal of Numerical Analysis* 1992; **29**(2):390–424. [85](#)
- [58] Fernandez-Mendez S, Huerta A. Imposing essential boundary conditions in mesh-free methods. *Computer Methods in Applied Mechanics and Engineering* 2004; **193**:1257–1275. [85](#)
- [59] Sharma M. Propagation of elastic energy in a general anisotropic medium. *Journal of Sound and Vibration* 2007; **302**:629–642. [85](#)
- [60] Kocak H, Yildirim A. Numerical solution of 3D Green's function for the dynamic system of anisotropic elasticity. *Physics Letters A* 2009; **373**:3145–3150. [85](#)
- [61] Langer U, Steinbach O. Coupled finite and boundary element domain decomposition methods. *Lecture Notes in Applied and Computational Mechanics* 2007; **29**:61–95. [85](#)

- [62] de Klerk D, Rixen DJ, Voormeeren SN. General framework for dynamic substructuring: History, review, and classification of techniques. *AIAA Journal* 2008; **46**(5):1169–1181. [85](#)
- [63] Raju IS, Sistla R, Krishnamurthy T. An efficient boundary element method for computing accurate stresses in two-dimensional anisotropic problems. *Computers and Structures* 1996; **59**(3):453–462. [85](#)
- [64] Rangelov T, Manolis G, Dinevac P. Elastodynamic fundamental solutions for certain families of 2D inhomogeneous anisotropic domains: Basic derivations. *European Journal of Mechanics A/Solids* 2005; **24**:820–836. [85](#)
- [65] Miller ST, Costanzo F. A numerical verification for an unconditionally stable FEM for elastodynamics. *Computational Mechanics* 2009; **43**:223–237. [87](#)
- [66] Matsuda O, Glorieux C. A Green’s function method for surface acoustic waves in functionally graded materials. *Journal of Acoustical Society of America* 2007; **121**(6):3437–3445. [131](#), [134](#)
- [67] Wapenaar K. Retrieving the elastodynamic Green’s function of an arbitrary inhomogeneous medium by cross correlation. *Physical Review Letters* 2004; **93**(254301):1–4. [131](#), [133](#)
- [68] Pan E, Tonon F. Three-dimensional Green’s function in anisotropic piezoelectric solids. *International Journal of Solids and Structures* 2000; **37**:943–958. [131](#), [133](#)

- [69] Yakhno VG, Yaslan HC. Computation of the time-dependent fundamental solution for equations of elastodynamic in general anisotropic media. *Computers and Structures* 2011; **89**:646–655. [133](#)
- [70] Ali A, Rajakumar C, Yunus SM. Advances in acoustic eigenvalue analysis using boundary element method. *Computers and Structures* 1995; **56**(5):837–847. [133](#)
- [71] Tewary VK. Computationally efficient representation for elastostatic and elastodynamic Green's functions for anisotropic solids. *Physical Review B: Condensed Matter* 1995; **51**(22):695–702. [133](#)
- [72] Wang CY, Denda M. 3D BEM for general anisotropic elasticity. *International Journal of Solids and Structures* 2007; **44**:7073–7091. [133](#)
- [73] Sharma MD. Group velocity along general direction in a general anisotropic medium. *International Journal of Solids and Structures* 2002; **39**:3277–3288. [133](#)
- [74] Niu Y, Dravinski M. Direct 3D BEM for scattering of elastic waves in a homogenous anisotropic half-space. *Wave Motion* 2003; **38**:165–175. [133](#)
- [75] Kog1 M, Gaul L. Free vibration analysis of anisotropic solids with the boundary element method. *Engineering Analysis with Boundary Elements* 2003; **27**:107–114. [133](#)

- [76] Thompson LL. A review of finite-element methods for time-harmonic acoustics. *Journal of Acoustical Society of America* 2006; **119**(3):1315–1330. [134](#)
- [77] Harari I. A survey of finite-element methods for time-harmonic acoustics. *Computer Methods in Applied Mechanics and Engineering* 2006; **195**:1594–1670. [134](#)
- [78] Garcia JMB, Bernat ARM. Coupled model for the non-linear analysis of anisotropic sections subjected to general 3D loading. part 1: Theoretical formulation. *Computers and Structures* 2006; **84**:2254–2263. [134](#)
- [79] Rungamornrat J, Mear ME. SGBEM-FEM coupling for analysis of cracks in 3D anisotropic media. *International Journal for Numerical Methods in Engineering* 2011; **86**:224–248. [134](#)
- [80] Lovane G, Nasedkin AV. Finite element dynamic analysis elastic solids with voids. *Computers and Structures* 2009; **87**:981–989. [134](#)
- [81] Fagerholm J, Friberg AT, Huttunen J, Morgan DP, Salomaa MM. SAW diffraction using the thin-element decomposition method. *IEEE Transactions on Ultrasonics, Ferroelectrics and Frequency Control* 1997; **44**(2):505–514. [134](#)
- [82] Pantano A, Averill RC. A penalty-based interface technology for coupling independently modeled 3D finite element meshes. *Finite Element in Analysis and Design* 2006; **43**(4):271–286. [135](#)

- [83] Casadei F, Gabellini E, Fotia G, Maggio F, Quarteroni A. A mortar spectral/finiteelement method for complex 2D and 3D elastodynamics problems. *Computer Methods in Applied Mechanics and Engineering* 2002; **191**(45):5119–5148. [135](#)
- [84] Araujo FC, Martins CJ, Mansur WJ. An efficient BE iterative-solver-based substructuring algorithm for 3D time-harmonic problems in elastodynamics. *Engineering Analysis with Boundary Elements* 2001; **25**(9):795–803. [135](#)